2015

KINETICS AND MECHANISMS OF CRYSTAL GROWTH INHIBITION OF INDOMETHACIN BY MODEL PRECIPITATION INHIBITORS

Dhaval D. Patel
University of Kentucky, patel.dhavald@gmail.com

STUDENT AGREEMENT:

I represent that my thesis or dissertation and abstract are my original work. Proper attribution has been given to all outside sources. I understand that I am solely responsible for obtaining any needed copyright permissions. I have obtained needed written permission statement(s) from the owner(s) of each third-party copyrighted matter to be included in my work, allowing electronic distribution (if such use is not permitted by the fair use doctrine) which will be submitted to UKnowledge as Additional File.

I hereby grant to The University of Kentucky and its agents the irrevocable, non-exclusive, and royalty-free license to archive and make accessible my work in whole or in part in all forms of media, now or hereafter known. I agree that the document mentioned above may be made available immediately for worldwide access unless an embargo applies.

I retain all other ownership rights to the copyright of my work. I also retain the right to use in future works (such as articles or books) all or part of my work. I understand that I am free to register the copyright to my work.

REVIEW, APPROVAL AND ACCEPTANCE

The document mentioned above has been reviewed and accepted by the student's advisor, on behalf of the advisory committee, and by the Director of Graduate Studies (DGS), on behalf of the program; we verify that this is the final, approved version of the student's thesis including all changes required by the advisory committee. The undersigned agree to abide by the statements above.

Dhaval D. Patel, Student

Dr. Bradley D. Anderson, Major Professor

Dr. Jim Pauly, Director of Graduate Studies

KINETICS AND MECHANISMS OF CRYSTAL GROWTH INHIBITION OF INDOMETHACIN BY MODEL PRECIPITATION INHIBITORS

DISSERTATION

A dissertation submitted in partial fulfillment of the requirements for the degree of Doctor of Philosophy in the College of Pharmacy at the University of Kentucky

By

Dhaval Patel

Lexington, Kentucky

Director: Dr. Bradley D. Anderson, Professor of Pharmaceutical Sciences

Lexington, Kentucky

2015

ABSTRACT OF DISSERTATION

KINETICS AND MECHANISMS OF CRYSTAL GROWTH INHIBITION OF INDOMETHACIN BY MODEL PRECIPITATION INHIBITORS

Supersaturating Drug Delivery Systems (SDDS) could enhance oral bioavailability of poorly water soluble drugs (PWSD). Precipitation inhibitors (PIs) in SDDS could maintain supersaturation by inhibiting nucleation, crystal growth, or both. The mechanisms by which these effects are realized are generally unknown. The goal of this dissertation was to explore the mechanisms underpinning the effects of model PIs including hydroxypropyl β-cyclodextrins (HP-β-CD), hydroxypropyl methylcellulose (HPMC), and polyvinylpyrrolidone (PVP) on the crystal growth of indomethacin, a model PWSD. At high degrees of supersaturation (S), the crystal growth kinetics of indomethacin was bulk diffusion-controlled, which was attributed to a high energy form deposited on the seed crystals. At lower S, indomethacin growth kinetics was surface integration-controlled. The effect of HP-β-CD at high S was successfully modeled using the reactive diffusion layer theory. The superior effects of PVP and HPMC as compared to HP-β-CD at high S were attributed to a change in the rate limiting step from bulk diffusion to surface integration largely due to prevention of the high energy form formation. The effects of PIs at low S were attributed to significant retardation of the surface integration rate, a phenomenon that may reflect the adsorption of PIs onto the growing surface. PVP was selected to further understand the relationship between adsorption and crystal growth inhibition. The Langmuir adsorption isotherm model fit the adsorption isotherms of PVP and N-vinylpyrrolidone well. The affinity and extent of adsorption of PVP were significantly higher than those of N-vinylpyrrolidone, which was attributed to cooperative interactions between PVP and indomethacin. The extent of PVP adsorption on a weight-basis was greater for higher molecular weight PVP but less on a molar-basis indicating an increased percentage of loops and tails for higher molecular weight PVPs. PVP significantly inhibited indomethacin crystal growth at high S as compared to N-vinylpyrrolidone, which was attributed to a change in the growth mechanism resulting in a change in the rate limiting step from bulk diffusion to surface integration. Higher molecular weight PVPs were better inhibitors than lower molecular weight PVPs, which was attributed to a greater crystal growth barrier provided by a thicker adsorption layer.

KEYWORDS:

Precipitation inhibitor, Supersaturation, Crystal growth, Indomethacin, Adsorption

Dhaval D. Patel

2015

KINETICS AND MECHANISMS OF CRYSTAL GROWTH INHIBITION OF INDOMETHACIN BY MODEL PRECIPITATION INHIBITORS

By

Dhaval Patel

Dr. Bradley D. Anderson

(DIRECTOR OF DISSERTATION)

Dr. Jim Pauly

(DIRECTOR OF GRADUATE STUDIES)

2015

Dedicated To

My Parents and My Wife

For Their Unconditional Love and Support

ACKNOWLEDGEMENTS

Above all, I would like to thank my mentor, Dr. Bradley Anderson, for his valuable guidance and comprehensive training throughout this doctoral work. His supervision and insightful discussions were essential in developing the framework of this dissertation. His mentoring has helped me grow as an independent researcher. His immense passion and enthusiasm for science will always serve as a source of motivation for me in future. Without his support and patience, this work would not have been possible. I would also like to thank my doctoral committee members, Dr. Paul Bummer, Dr. Eric Munson, Dr. Markos Leggas, Dr. Zach Hilt, and Dr. Tonglei Li for their valuable time and fruitful discussions. Special thanks to Dr. Bummer, Dr. Hilt and Dr. Li for allowing me to use scientific instruments in their laboratories. I am grateful to the Pharmaceutical Sciences graduate program at the University of Kentucky for providing me with this opportunity and overall doctoral training. I would like to acknowledge the financial support from Boehringer Ingelheim Pharmaceuticals, Inc., Ridgefield, CT. I am very grateful to Dr. Vijay Joguparthi and Dr. Zeren Wang for valuable discussions and for forging this research collaboration between Boehringer Ingelheim and the University of Kentucky. I would like to thank the University of Kentucky for a Graduate School Fellowship. Special thanks to Dr. Corinne Jankovsky and Dr. Pekka Hoppu for assistance with certain analytical techniques such as PXRD and UV spectroscopy. I am very thankful to current and past members of Dr. Anderson's laboratory including Dr. Xiang, Dr. Rane, Michael, Vijay, Sweta, and Kyle for making my tenure at the laboratory a fun-filled learning experience. I would like thank Ore, a rotation student in Dr. Anderson's Lab, for assisting me with the evaluation of various particle size

measurement techniques. I would like to thank Catina for all her help with fulfilling various requirements of the graduate program. My graduate school tenure was made special and memorable by several friends and colleagues including Mikolaj, Kamalika, Melissa, Shaoxin, Lin, Anshul, and Saurabh. Finally, the unconditional love and support from my family including my loving wife (Salin Gupta Patel), my adorable son (Dev Patel), my parents (Manjulaben and Dineshbhai Patel), my in-laws (Arti and Jagdeo Gupta), and my sisters (Preeti Shah and Krishna Patel) were critical in making this journey of doctoral training possible and enjoyable.

TABLE OF CONTENTS

LIST OF TABLES

LIST OF FIGURES

Chapter One

Statement of Aims

Oral bioavailability of poorly water soluble drugs has been successfully enhanced in pre-clinical and clinical studies through the maintenance of supersaturation (i.e., maintenance of drug concentration above its equilibrium solubility) in the gastrointestinal (GI) tract by using Supersaturating Drug Delivery Systems (SDDS).[1-6] Precipitation inhibitors (PIs) including cyclodextrins, polyvinylpyrrolidone (PVP), polyvinylpyrrolidone-vinyl acetate (PVP-VA), hydroxypropyl methylcellulose (HPMC), hydroxypropyl methylcellulose-acetate succinate (HPMC-AS), polyethylene glycol (PEG), d-α-tocopheryl polyethylene glycol 1000 succinate (TPGS or vitamin E TPGS), and polysorbate 80 have been incorporated into SDDS to maintain the supersaturation of drugs to varying degrees of effectiveness.[7-9] The PIs generally maintain the supersaturation of poorly water soluble drugs by inhibiting nucleation, crystal growth, or both.[1] The degree of effectiveness of PIs depend on their mechanisms of action and the physico-chemical properties of the PIs as well as drugs including hydrogen bonding capacity, hydrophobicity, semi-rigid structure, and amphiphilic nature.[9-13] In addition to the intermolecular interactions between PIs and drug molecules in the bulk solution,[13-16] the effects of PIs have been attributed to the adsorption on the growing crystal surface.[4,12,17-24] While the beneficial effects of PIs on the maintenance of supersaturation of poorly water soluble drugs have been demonstrated by the above-mentioned studies, the mechanistic understanding as to how PIs achieve their beneficial effects is generally lacking. Additionally, a correlation between the beneficial effects of PIs and the molecular properties of drugs and PIs is not well understood. This significantly impacts

the ability of pharmaceutical scientists to rationally select a suitable PI for the development of an SDDS. One of the reasons behind this gap in the scientific literature could be a lack of simple techniques and models to study the beneficial effects of PIs on the maintenance of supersaturation through the inhibition of nucleation, crystal growth, or both for poorly water soluble drugs. The goal of this dissertation was to develop methods and models to mechanistically explore the effects of model pharmaceutical PIs including hydroxypropyl β-cyclodextrin (HP-β-CD), HPMC, and PVP on the maintenance of aqueous supersaturation by crystal growth inhibition of indomethacin, a model poorly water soluble drug. The following aims were completed as part of this work:

a) Develop reliable methods and relevant mathematical models to study crystal growth kinetics of indomethacin, a model poorly water soluble drug

The deficiency of quantitative explorations on the crystal growth inhibitory effects of PI for poorly water soluble drugs in the literature could be attributed to a lack of simple, reliable, and robust techniques to quantify the kinetics of crystal growth that influence the maintenance of supersaturation. A non-invasive (online) technique was developed to measure the crystal growth kinetics of indomethacin using second derivative UV spectroscopy, batch crystallization, and a crystal seeding method in Chapter 3. The crystal seeding method was developed to study the crystal growth kinetics by avoiding primary nucleation at high degrees of supersaturation (S). The development of the seeding method consisted of steps to obtain narrow as well as unimodal size distributions and to determine any change in seed size and number upon mixing and crystal growth. Our hypothesis was that the second derivative UV method

would remove the interference in UV absorption from the growing seed crystals in the solution, and in turn provide accurate measurements of indomethacin concentrations in real time. The indomethacin concentration vs. time profile would be utilized in determining crystal growth rates. A mathematical model based on the two-step diffusion-reaction theory for crystal growth was developed, and the rate limiting step for the crystal growth of indomethacin at high S was identified based on the measurements of the mass transfer and crystal growth rate coefficients of indomethacin. A different high energy form was deposited on the seed crystals of indomethacin after crystal growth at high S. This high energy form probably accounted for the bulk-diffusion controlled crystal growth of indomethacin at high S.

b) Determine the effect of degree of supersaturation on the crystal growth kinetics of indomethacin

To study the effect of PI on the crystal growth kinetics of indomethacin, it would be important to derive a physical theory based model which describes the crystal growth kinetics of indomethacin. Several factors including degree of supersaturation, impurities, PI, chemical structure, physical conformation, bonds, and defects or disorder can influence the kinetics of crystal growth.[25,26] The thermodynamic driving force for crystal growth (i.e., degree of supersaturation) could influence kinetic parameters such as the rate limiting step of crystal growth.[24] The effect of degree of supersaturation on the crystal growth kinetics of indomethacin was determined in Chapter 4. The crystal growth rate coefficients of indomethacin were determined over a wide range of degree of supersaturation ($1.6 \leq S \geq 9$). An infusion-based method to measure the crystal growth rate of indomethacin at very low S of 1.6 was developed to avoid the formation of the

high energy indomethacin form on seed crystals. While the high energy form probably accounted for the rapid, bulk-diffusion controlled crystal growth of indomethacin at high S, at low S (i.e., at a solution concentration above the solubility of the high energy form) the mechanism of crystal growth was different and consistent with surface integration control. The understanding of the fundamental relationship between the degree of supersaturation and the rate limiting step for indomethacin crystal growth was further employed in understanding the effects of model PIs such as cyclodextrins on crystal growth and, in turn, the maintenance of supersaturation of indomethacin in Chapter 5.

c) Explore mechanisms and relevant mathematical models for the effect of model precipitation inhibitors on the crystal growth of indomethacin

Despite some studies in the literature that have qualitatively screened or rank ordered the effects of PIs on the maintenance of supersaturation, mechanistic explorations on the beneficial effects of PIs using mathematical models have been seldom carried out.[8,9] In this aim, a quantitative approach to explore the inhibition of crystal growth and, in turn, the maintenance of supersaturation of indomethacin by three model PIs including HP-β-CD, PVP and HPMC was developed. The effects of model PIs on the driving force and the rate determining step of the crystal growth kinetics of indomethacin were determined in Chapter 5. Our hypothesis was that after accounting for the effect of PI on the equilibrium solubility of indomethacin, two factors including the speciation in the bulk solution and the impact of PI on the surface integration rate of indomethacin due to the interactions of PI with the crystal surface of indomethacin would explain the inhibitory effect of PI on the crystal growth of indomethacin. The inhibitory effect of HP-β-CD on the crystal growth of indomethacin at high S was successfully explained by a

reactive diffusion theory based mathematical model. The retardation of crystal growth by PIs at high S was largely due to prevention of the formation of a high energy indomethacin form on seed crystals. The effects of PI on surface integration may also be a factor but that was a small effect, as surface integration was already quite slow at low S. The inhibitory effects of all three model PIs on the surface integration of indomethacin could be attributed to the adsorption of PI on the seed crystals of indomethacin.

d) Explore the relationship between the adsorption of PVP and the crystal growth inhibitory effects of PVP for indomethacin

A majority of commonly used pharmaceutical PIs including PVP, PVP-VA, HPMC, HPMC-AS, PEG, TPGS, and polysorbate 80 are polymeric in nature, which are sometimes described as polymeric PIs (PPIs).[9] Previous studies have proposed that the inhibitory effects of PPIs on the precipitation of drugs could be attributed to their adsorption on the growing drug crystal surface.[12,17,18,20] For example, the inhibitory effect of PVP on the crystal growth of bicalutamide was attributed to its adsorption onto bicalutamide crystals.[20] Despite these studies, the mechanisms of the inhibitory effects of PPIs on drug precipitation are seldom proven directly or correlated with the adsorption of PPI in a quantitative manner. Consequently, the nature of the adsorbed PPI layer as well as the key physicochemical properties of PPIs and drugs such as molecular weight, hydrogen bonding capability and hydrophobicity that could influence the adsorbed PPI layer and, in turn, the effectiveness of a given PPI are not well understood. In this aim, the effect of molecular weight and concentration of PVP, a model PPI, on its adsorption onto the crystalline surface of indomethacin, a model poorly water soluble drug was determined. Additionally, the adsorption behavior of PVP was correlated with its

effectiveness as a crystal growth inhibitor of indomethacin in Chapter 6. PVP significantly inhibited the crystal growth of indomethacin at a high degree of supersaturation, which was attributed to a change in the crystal growth mechanism of indomethacin resulting in a change in the rate limiting step from bulk diffusion to surface integration at a high S. The change in the crystal growth mechanism of indomethacin could be due to prevention of the formation of a high energy form of indomethacin on the seed crystals of indomethacin by PVP. The adsorption and the crystal growth inhibitory effects of PVP for indomethacin correlated well across different molecular weights and concentrations of PVP. The greater effectiveness of PVP as a crystal growth inhibitor of indomethacin as compared to its monomer was not only attributed to the higher surface coverage of indomethacin crystals but also to the greater barrier for the surface diffusion of indomethacin molecules provided by a thicker PVP adsorption layer.

Chapter Two

Introduction

Supersaturating drug delivery systems (SDDS) contain precipitation inhibitors (PIs), which could maintain supersaturation of poorly water soluble drugs over a prolonged period of time in the GI tract and, in turn, enhance oral bioavailability.[1-6] The beneficial effects of PIs on the maintenance of supersaturation could be due to inhibition of nucleation, crystal growth, or both for poorly water soluble drugs. While the nucleation and crystal growth of drugs could be influenced by the intermolecular interactions between PIs and drug molecules in the bulk solution,[13-16] the adsorption of PIs on the growing crystal surface has been linked to their crystal growth inhibitory effects.[4,12,17-24] The inhibition of crystal growth by the adsorbed PIs may be attributed to their effects on either bulk diffusion and/or surface integration of drug molecules.[9,10,18,27] Their effectiveness has been linked to their hydrogen bonding capacity, hydrophobicity, semi-rigid structure, and amphiphilic nature.[10-13] Despite the above-mentioned studies, a significant literature gap exists between present knowledge and for a more comprehensive, mechanistic understanding of PI effects. Since the inhibitory effects of PIs on nucleation, crystal growth, or both vary significantly with the combination of drug and PI, predictive models are required to enhance the ability of pharmaceutical scientists to rationally select suitable PIs *a priori* for the development of SDDS. A thorough understanding of the correlation between the adsorption of a given PI and its crystal growth inhibitory effect is needed to explore possible crystal growth inhibition mechanisms such as the creation of a barrier for surface diffusion of the adsorbed drug molecules or the blocking of active growth sites for the incorporation of drug molecules

into crystal lattices. The literature gap could be attributed to several reasons including: (1) a lack of simple techniques and models that would allow scientists to explore the effects of a given PI on drug precipitation kinetics by individually focusing on the kinetics of nucleation and crystal growth of drugs in aqueous media, (2) a lack of information on the solution-mediated phase transformations that could occur during drug precipitation and its application in developing models for drug precipitation kinetics, and (3) experimental difficulties encountered during robust measurements of supersaturated drug concentrations.

To develop a quantitative and mechanistic understanding of the effects of PIs on the maintenance of supersaturation by inhibiting nucleation or crystal growth, it is essential to determine parameters that govern the kinetics of nucleation or crystal growth of poorly water soluble compounds. Since nucleation is generally spontaneous and the sizes of nuclei are very small, a clear experimental distinction between nucleation and crystal growth is generally difficult.[24] In many previous supersaturation studies,[9,13] experimental methods were not well designed to study nucleation and crystal growth independently. For example, the supersaturation of danazol was studied using a turbidity method, which grossly detected the precipitation of danazol but did not differentiate it further into nucleation and crystal growth.[9] The lack of reliable methods to distinguish between nucleation and crystal growth could impact the development of kinetic models for drug precipitation in aqueous media.

The drug precipitation kinetic models could be further optimized by tracking solution-mediated phase transformations that could occur during nucleation and crystal growth and, in turn, by utilizing more specific values of the kinetic and thermodynamic

parameters of the newly detected solid phase (e.g., equilibrium solubility, dissolution rate). The solution-mediated phase transformations observed during drug precipitation could include: (1) the formation of new solid phase (amorphous or crystalline) in solution by homogeneous nucleation, and (2) the formation of new solid phase including higher energy forms such as metastable polymorphs or an amorphous form on the surface of the most stable form, and vice versa.[28-34] Epitaxial growth is defined as the growth of one molecule on another substrate with similar structural features such as similar crystallographic lattice.[28,35-37] The epitaxial growth is commonly observed in cross-seeding methods that are used to crystallize a material of choice on the surface of a different seed crystal.[35] The formation of surface disorder including lattice defects and amorphous regions has been observed for inorganic and organic materials from either precipitation at high degrees of supersaturation or mechanical activation through milling.[24,29,33-35,38-40] For example, samples of cephalothin sodium and cefamandole nafate that were crystallized from supersaturated mother liquor exhibited higher exothermic heats of solution as compared their 100% crystalline standards, which was attributed to a higher crystal disorder on the surface of cephalothin sodium and to an amorphous layer coating on the crystals of cefamandole nafate.[33] Potassium perchlorate crystals that were grown at different degrees of supersaturation and, in turn, at different growth rates were identical as detected by PXRD and DSC; however, the crystals were found to be different based on the surface density of dislocations.[40] The crystals grown at the fastest growth rate showed the highest mean dislocation density whereas the crystals with the lowest dislocation density were grown at the slowest growth rate. Amorphous indomethacin with different levels of crystallinity underwent solution-mediated phase

transformation during dissolution in aqueous media.[41] Unlike the completely amorphous indomethacin sample where only γ polymorph had formed on the surface, the amorphous indomethacin samples with partial crystallinity were covered with more than one polymorph. Grinding of anhydrous monoclinic carbamazepine produced surface disorder consisting of amorphous phases and lattice defects, which facilitated the surface nucleation of carbamazepine dihydrate.[29] During dissolution of theophylline monohydrate, a decline in the dissolution rate from a peak was observed using a combined UV imaging and Raman spectrometric technique, which was attributed to the formation of a higher energy form (i.e., a new crystalline hydrate form or a crystalline or amorphous dehydrated form on the surface of theophylline monohydrate crystals at levels below the detection limit of PXRD or Raman measurements.[31] Higher apparent solubility obtained with mechanically activated griseofulvin was attributed to the higher energy, disordered surface layer with the thickness of 40 to 50 nm, which was not detectable by DSC.[32] The stability of the higher apparent solubility of griseofulvin was explained by the slower, surface integration controlled growth of griseofulvin.

Another experimental difficulty in studying the kinetics of drug precipitation is the inability of common analytical methods to accurately measure the concentrations of supersaturated samples. Previously, supersaturated concentrations have been measured using several off-line (e.g., filtration, centrifugation) and on-line (e.g., real-time UV or Raman or IR spectroscopy) techniques.[2-6,42,43] However, the supersaturated concentrations measured using the off-line methods including filtration and centrifugation could be inaccurate in cases where drug might have precipitated due to temperature fluctuations and/or physical contact of supersaturated solutions with solid

surfaces of syringes, filter membranes, and centrifuge tubes during off-line sample collections. Recently, non-invasive and online methods consisting of spectroscopic techniques such as ATR-FTIR,[44] Raman,[17] and fluorescence[20] have been employed to measure supersaturated concentrations without the risk of off-line sampling errors.

A mechanistic understanding of the effect of pharmaceutical excipients such as precipitation inhibitors (PIs) on the maintenance of supersaturation of poorly water soluble drugs is essential to facilitate rational designs of SDDS. The objective of this dissertation was to explore mechanisms underpinning the effects of model PIs on the maintenance of supersaturation of a model poorly water soluble drug, indomethacin, via crystal growth inhibition. The specific aims were: (1) to develop robust experimental methods and models to study the crystal growth kinetics of indomethacin in water, (2) to determine the effect of degree of supersaturation on the kinetics of indomethacin crystal growth including its rate-limiting steps, (3) to explore mechanisms and develop relevant mathematical models for the effect of model PIs including HP-β-CD, PVP and HPMC on the crystal growth of indomethacin, and (4) to explore the relationship between the adsorption of PVP and the crystal growth inhibitory effects of PVP for indomethacin. The following topics are described in detail considering overall objective of this dissertation.

1. Supersaturating Drug Delivery Systems (SDDS)

Current pharmaceutical R&D pipelines are flooded with poorly water soluble drug candidates mainly due to recent advances in high throughput technologies and combinatorial chemistry for drug screening and hit identification.[45] The emerging drug candidates from these technologies generally have higher molecular weight, greater

lipophilicity and very low water solubility.[46] Most of the emerging drug candidates belong to the Class II and IV of the Biopharmaceutical Classification System (BCS)[47] indicating that the oral absorption and, in turn, oral bioavailability of these drug candidates could be limited by equilibrium solubility, dissolution rate, or both. To circumvent this issue, SDDS are specifically designed to enhance the solubility and/or dissolution rate of poorly water soluble drugs by modifying the physico-chemical properties of drugs as well as by using various formulation approaches. Some of these approaches include salt formation,[48] cocrystal formation,[49] drug-excipient complexation,[7,43] lipid-based drug delivery systems,[8,50-52] solid dispersions,[3,53] and nanoparticles.[54,55] Oral administration of SDDS may achieve higher drug concentrations than the equilibrium solubility of drug in the GI tract due to higher apparent solubility (i.e., supersaturation) and/or the maintenance of supersaturation of drugs in the GI tract resulting in higher oral bioavailability.[1-6]

The SDDS could be classified into two main classes: (1) SDDS developed through formulation approaches, and (2) SDDS developed through the modification of physico-chemical properties of drugs (Table 2.1). For both classes of SDDS, the primary goal is to provide higher apparent solubility (also defined as "kinetic solubility") and, in turn, generate supersaturation of drugs. Some SDDS, especially the Class 1 SDDS, not only generate supersaturation but also maintain or prolong supersaturation. The generation and maintenance of supersaturation by SDDS has recently been described by a "spring and parachute" approach.[56] For example, the higher energy form of drug that generates supersaturation is compared with the "spring" analogy (i.e., sudden rise in drug concentration), whereas PIs that maintain supersaturation by inhibiting drug precipitation

are compared with the “parachutes” analogy (i.e., slower decline of drug concentration). If the supersaturation of drug in the GI tract is maintained through the absorption window (i.e., the time interval for complete GI absorption), it could enhance oral bioavailability.[9] The selection of a particular SDDS for drug product development mainly depends on clinical and pharmacokinetic requirements as well as the physico-chemical properties of drug candidates. For example, a drug candidate with high log P and high solubility in lipid-based vehicles would be more suitable for lipid-based SDDSs as long as the required concentration of drug candidate in the lipid vehicle as dictated by clinical requirements (e.g., estimated human dose range) is not higher than the solubility of drug candidate in the same lipid vehicle. If the drug concentration/loading requirements are significantly higher than the solubility limit in the lipid-based SDDS), amorphous solid dispersion SDDSs could be used to circumvent the solubility limitation of lipid-based SDDSs.

Table 2.1. Classification of Supersaturating Drug Delivery Systems (SDDS)

SDDS Class	SDDS	Example	Reference
Class 1: SDDS Based on Formulation Approaches	Lipid-based drug delivery system		
	SEDDS	Paclitaxel SEDDS	5
	S-SEDDS	AMG-517 S-SEDDS	4
	SMEDDS	Piroxicam SMEDDS	57
	SNEDDS	Quercetin SNEDDS	58
	Solid dispersions		
	Spray drying	Dipyridamole solid dispersion	59
	Hot-melt extrusion	Itraconazole hot-melt extrudate	60
	Nanoparticles	Cefuroxime axetil nanoparticles	61
	Complexation	DB 67-SBE-CD complexes	7
Class 2: SDDS Based on Physico-Chemical Property Modification Approaches	Salts	Celecoxib sodium salt	56
	Cocrystals	AMG-517 benzoic acid cocrystals	62
	Amorphous forms	Atorvastatin amorphous form	63
	Metastable polymorphs	Carbamazepine anhydrous	29
	Prodrugs	Fosamprenavir	64

SEDDS: Self emulsifying drug delivery system; S-SEDDS: Supersaturating self emulsifying drug delivery system; SMEDDS: Self micro-emulsifying drug delivery system; SNEDDS: Self nano-emulsifying drug delivery system

1.1 SDDS Based on Formulation Approaches (Formulation-SDDS)

The formulation approaches utilized in the development of SDDS include spray drying,[53] hot-melt extrusion,[3,65,66] co-precipitates/nanoparticles,[54] self-emulsifying micro- & nanoemulsions,[4,52] and complexation.[7] Since the *in vivo* supersaturation generated by SDDS could lead to the precipitation of drug due to limited solubility in the highly variable local aqueous *in vivo* environment, the optimal success of SDDS in terms of ensuring higher and reproducible bioavailability depends on the maintenance of supersaturation for a sufficient period of time to allow higher drug absorption. The SDDS developed using the above-mentioned formulation approaches are specifically designed not only to generate but also to maintain the supersaturation of drugs.

One of the most commonly used formulation approaches to develop SDDS is the amorphous solid dispersions (ASD). The ASD-based SDDS are developed using techniques such as spray drying, hot-melt extrusion, and co-precipitation/co-processing, lyophilization.[7] In ASD, the drug is present in a high energy form such as amorphous form and the high energy state of the drug is stabilized using a polymeric matrix.[67] When the drug is molecularly dispersed in the polymeric matrix, the ASD is also described as a "solid solution".[68] However, it is very difficult to experimentally measure the thermodynamic equilibrium solubility of drug in a solid solution, and therefore it is challenging to determine if an ASD is truly a solid solution or not. The polymeric matrices of ASD-based SDDS are generally composed of one or more polymers such as PVP, PVP-VA, polyvinyl alcohol (PVA), HPMC, and HPMC-AS. The amorphous form of drug along with precipitation inhibitors present in ASDs provides higher dissolution rate and supersaturation (i.e., "kinetic solubility"). The ASD of itraconazole prepared by

spraying itraconazole onto a highly porous carrier such as silica generated and maintained supersaturation for about 4 hours at intestinal pH and, in turn, mitigated the negative impact of pH-dependent solubility on oral bioavailability as observed earlier with crystalline itraconazole.[55] The ASD of itraconazole with HPMC (40:60 w/w) prepared through a hot-melt extrusion technique significantly enhanced its dissolution rate as compared to crystalline itraconazole.[60] The dissolution of the itraconazole ASD and the physical mixture of crystalline itraconazole and HPMC in 0.01N HCl at 37°C showed that approximately 90% and 2% of the 200-mg dose of itraconazole dissolved after 120 minutes, respectively.

The co-precipitate-based SDDS, prepared from the co-precipitation of drug and excipients, are generally used when conventional spray drying and melt-extrusion techniques are not feasible due to process-related limitations. The drug and excipients including PIs are simultaneously precipitated from mother liquor resulting in fine particles containing the amorphous drug dispersed in an excipient matrix. The co-precipitate-based SDDS provide a high degree of supersaturation due to the amorphous nature of the drug as well as the high surface area of fine co-precipitate particles.[69,70] Celecoxib nanoparticles prepared using an emulsion method and a polymer such as ethyl cellulose provided higher exposure and faster absorption as compared to the commercial capsule dosage form containing crystalline drug.[70]

The lipid-based SDDSs do not require the dissolution of drugs since drug particles are already solubilized in the liquid vehicle. The lipid-based SDDSs include self-emulsifying drug delivery systems (SEDDS), self-microemulsifying drug delivery systems (SMEDDS), and self-nanoemulsifying drug delivery systems (SNEDDS). The

lipid-based SDDSs are commonly composed of triglycerides such as glyceryl tricaprylate/caprate, cosolvents such as PEG, and surfactants such as Cremophor® RH40. They are commonly used with lipophilic drugs with sufficiently higher solubilities in the vehicle of the lipid-based SDDS than clinical dose requirements.[52,71] For example, griseofulvin and other drugs with log P of ~2 having very low solubility in glycerides are not good candidates for lipid-based SDDS. These would require other SDDS approaches such as ASD. Drugs with high log P values (>5) including halofantrine or cinnarizine are suitable candidates for lipid-based SDD.[71] When administered orally, lipid-based SDDSs form dispersions consisting of colloidal species of varying sizes. While some formulation components of lipid-based SDDS such as surfactants and oils could enhance the solubilization capacity of the GI fluids, the solubilization capacity of the GI fluids changes over time due to continuous dispersion and digestion of the lipidic components of lipid-based SDDS leading to the generation of supersaturation.[72] The piroxicam SMEDDS containing Labrasol provided approximately 7-times higher apparent solubility than its equilibrium solubility in the same medium.[57] Precipitation of piroxicam occurred upon the dilution of the SMEDDS. This was attributed to the change in organization of Labrasol and, in turn, the conversion of microemulsion to fine emulsion upon dilution. While the maintenance of supersaturation provided by regular lipid-based SEDDS significantly depends on the dilution and digestion of the formulation components, novel supersaturable SEDDS (S-SEDDS) are designed to enhance the maintenance of supersaturation using additional PIs such as polymers.[73] For example, the supersaturated concentration of AMG 517 generated by a lipid-based S-SEDDS containing Tween 80 was effectively maintained by the addition of HPMC to the S-SEDDS.[4]

Cyclodextrins have been used to prepare solid and liquid SDDS of poorly water soluble drugs.[46,74] A parenteral SDDS of DB-67, an experimental anti-cancer drug, in the form of lyophiles was prepared using a sodium salt of the β-cyclodextrin sulfobutyl ether (SBE-CD).[7] The stable supersaturated solution of 20% w/v DB-67 was prepared by chemically converting the ring-opened DB-67 to its lactone form using an acidified SBE-CD solution, which maintained the supersaturation for at least three days.

1.2 SDDS Based on Physico-Chemical Property Modification Approaches (Physical Form-SDDS)

The SDDS developed by modifying the physico-chemical properties of drugs include salts, cocrystals, prodrugs, and other higher energy forms (e.g., amorphous forms, metastable polymorphs, and nanocrystals). The higher dissolution rate and apparent solubility provided by the Physical Form-SDDS could generate supersaturation in the GI tract. However, the main limitation of the Physical Form-SDDS, unlike the Formulation-SDDS, is their inability to maintain supersaturation for a prolonged period of time.

Crystalline salt forms are one of the most popular Physical Form-SDDSs used in drug product development.[75] The crystalline salt is preferred over an amorphous solid dispersion for the development of an oral solid dosage form for two main reasons: (1) crystalline salts provide higher purity and, in turn, more efficient drug manufacturing process as compared to the amorphous form, and (2) crystalline salts provide better physical and chemical stability during manufacturing and storage as compared to amorphous forms.[48] For the salts of weakly basic drugs, chloride is the most commonly used counter ion, whereas sodium is a popular counter ion for salts of weakly acidic drugs.[48,76] Crystalline salts often provide high supersaturation due to faster dissolution

rates and higher apparent solubilities. For example, both the sodium salt and the sodium propylene glycol salt of celecoxib provided approximately 10-fold higher apparent solubility in water as compared to free celecoxib.[56] The higher dissolution rate of salts is often attributed to an alteration in the microenvironmental pH and solubility at the surface of dissolving salt.[48,77]

Cocrystals are molecular complexes between two or more entities within a single crystal lattice, which are viable alternatives to crystalline salts when drug molecules lack ionizable functional groups.[49] Higuchi and Ikeda[78] showed in the early 1970s that cocrystal formation between digoxin and hydroquinone significantly improved the dissolution rate of digoxin. The formation of cocrystals for ionizable drug candidates is preferred if their traditional salt forms are highly unstable during manufacturing and storage. For example, AMG517, a weakly basic drug candidate, was highly sensitive to degradation at acidic pH, which was required for salt formation.[62] Several cocrystals of AMG517 were formed using coformers such as carboxylic acids and carboxamides that provided better stability and apparent solubility.[79] The apparent solubility of benzoic acid cocrystal was about 10 times higher than that of the free drug (21 µg/mL vs. 2 µg/mL). Cocrystals of itraconazole with fumaric and succinic acid generated 4 to 20-fold higher supersaturation as compared to crystalline itraconazole.[80]

Prodrugs have been used to enhance bioavailability through higher solubility, dissolution rate or both.[64] For example, a water soluble prodrug of carbamazepine, N-glycylcarbamazepine, provided higher oral bioavailability as compared to carbamazepine. It was determined that the prodrug was a peptidase substrate and rapidly cleaved to

carbamazepine *in vivo*. A phosphate ester prodrug of phenytoin, fosphenytoin, provided improved oral bioavailability over the parent drug.

The other higher energy forms of drugs that are used in SDDS are amorphous forms, solvates, metastable polymorphs, and nanocrystals. The amorphous form of atorvastatin calcium provided >3-fold higher apparent solubility than the equilibrium solubility of crystalline atorvastatin.[63] While the supersaturated concentration decreased from 460 to 200 μg/mL in 24 hours, an approximately 2-fold degree of supersaturation was maintained for about 3 hours. The generation of supersaturation was attributed to a very high dissolution rate of the amorphous atorvastatin. A significant increase in the dissolution rate and apparent solubility of amorphous atorvastatin resulted in ~3-fold higher oral bioavailability in rats.[63] Nanocrystals of a crystalline drug, due to the significant reduction of particle size to sub-micron ranges, not only enhance the dissolution rate of drug but also increase the apparent solubility of drug as predicted by the Ostwald-Freundlich or Kelvin equation.[24] The main limitation of the SDDS based on the modification of physicochemical properties is its inability to maintain supersaturation for a prolonged period of time, which could lead to drug precipitation and, in turn, lower and highly variable bioavailability. The sub-optimal bioavailability with respect to the requirements of clinical research and development programs could terminate the development of new drug candidates that are pharmacologically active for some of the most unmet needs of patients including cancer, heart diseases, and AIDS.

1.3 Impact of SDDS on Bioavailability

A significant issue with the oral bioavailability of poorly water soluble drugs is that the conditions in the GI tract including pH, amount of bile surfactant, and permeation

rate vary significantly based on the location in the GI tract. Due to the continuous changes in the local GI microenvironment and a high patient to patient variability in the local GI conditions, the aqueous solubility of poorly water soluble drugs in the GI tract could vary by several orders of magnitude. This may result in local supersaturation and rapid precipitation of solubilized/dissolving drug, which can lead to high variability in oral bioavailability of poorly water soluble compounds. For example, weakly basic drugs, due to their inherent pH-solubility profiles, are susceptible to significant precipitation when they transit from the low pH environment of the stomach to a high pH environment of the small intestine.

The benefits of supersaturation on the enhancement of *in vitro* drug transport across membranes[81,82] as well as *in vivo* drug absorption from the GI tract[6,83,84] are well documented in the scientific literature. Oral administration of SDDS could provide higher drug concentrations in the GI tract than the equilibrium solubility of drug. If the higher luminal concentration or supersaturation of drug is maintained during the GI absorption phase, it could lead to higher oral absorption and, in turn, higher oral bioavailability of poorly water soluble drugs.[2,3,5,84] However, it should be noted that, in addition to the higher drug concentration in the GI tract, oral bioavailability depends on other absorption, distribution, metabolism, and excretion (ADME) related factors such as efflux transporters, and gut wall metabolism. The beneficial effect of SDDS on oral bioavailability is only realized when oral bioavailability is mainly governed by the drug concentration gradient in the GI tract.[85] In such cases, the relationship between the drug concentration gradient and its absorption through the GI tract could be characterized by

Fick's First law. According to this law, the permeability of drug (*P*) and the drug concentration gradient contribute to the flux of drug through the GI membrane.[1]

$$J = PA(C_g - C_b) \tag{2.1}$$

where C_g and C_b are the concentrations of drug in the GI lumen and in the intestinal capillaries, respectively, and *A* is surface area. As shown in Eq. 2.1, the maintenance of supersaturation could be advantageous for drugs with the solubility-limited absorption (i.e., BCS Class II drugs). Moreover, the maintenance of supersaturation could help in enhancing the flux across the GI membrane when permeability is low.[85] The required degree of supersaturation to provide higher absorption could be estimated using the maximum absorbable dose (MAD) calculation:[86,87]

$$MAD = S \times k_{abs} \times SIWV \times SITT \tag{2.2}$$

where *S* is the solubility of drug at pH 6.5 (i.e., simulating drug solubility in the small intestine), k_{abs} is the intestinal absorption rate constant, which is related to permeability, *SIWV* is the small intestinal water volume, assumed to be ~250 mL, and *SITT* is the small intestinal transit time, assumed to be ~270 min or ~4.5 hours. Hence, from Eq. 2.2 and the clinical dose of a drug candidate, the required intestinal concentration/solubility of drug for maximum adsorption could be estimated. If the dose is low and permeability is high, the required intestinal solubility would be relatively low. However, drugs with high dose and low permeability would require higher intestinal solubility.[85]

Achieving a high degree of supersaturation from SDDS may not be sufficient to get higher oral bioavailability unless the degree of supersaturation is maintained through

the absorption window.[88] While the natural surfactants present in the intestinal milieu, food effects may be beneficial in prolonging supersaturation,[89] PIs play an important role in the maintenance of supersaturation. Since a majority of the Physical-Form SDDS could not maintain supersaturation, they are generally accompanied with PIs. Approximately 10-fold higher supersaturation generated by the sodium salt celecoxib, an anti-inflammatory poorly water soluble drug, was maintained for about 30 minutes using PIs such as HPC and TPGS or Pluronic F127, which resulted in higher oral bioavailability as compared the commercial drug product containing a free acid form (>90 vs. 30% bioavailability).[56] A cocrystal of AMG 517, a vanilloid receptor 1 antagonist, with sorbic acid when formulated as a suspension using 10% (w/v) Pluronic F108® in OraPlus® provided greater exposures in rats at a 30 mg/kg dose, which was comparable to the exposures achieved using 500 mg/g of a free base form of the drug.[62] A 20-fold greater exposure in rhesus monkeys was observed with the tartaric acid cocrystal of a phosphodiesterase-IV inhibitor, L-883555, as compared to a free base form of the drug.[90] The ASD of itraconazole with Eudragit E100 or Eudragit E100-PVPVA64 showed faster and higher in-vitro dissolution as compared to itraconazole ASD with HPMC, however the ASD with HPMC provided higher oral bioavailability as compared to the ASD Eudragit E100 or Eudragit E100-PVPVA64 due to the longer supersaturation maintenance provided by the HPMC-based ASD.[88] Dai et al.[2] observed that lower bioavailability was obtained using formulations with less precipitation resistance as compared the formulations with high precipitation resistance. Some of the SDDS that contain PIs (e.g., ASD, and lipid-based SDDS) are specifically designed to maintain drug supersaturation in the GI tract and, in turn, provide higher and less variable oral

bioavailability of poorly water soluble drugs. A more comprehensive discussion on the maintenance of supersaturation by PIs could be found in Section 3 of this chapter.

The relationship between the maintenance of supersaturation by various Formulation-SDDS and its impact on oral bioavailability has been explored in recent studies. Recent studies on lipid-based SDDS have shown that the generation and maintenance of drug supersaturation in the GI tract by lipid-based SDDS is more critical for higher and less variable oral bioavailability than the enhancement of the solubilization capacity of the GI fluids by lipid-based SDD as viewed historically.[5,8,73] The generation of supersaturation from lipid-based SDDS could be due to: (1) the dilution/dispersion of highly concentrated lipid-based SDDS in the GI fluids, (2) the digestion of lipidic components such as glyceride lipids and fatty acid ester surfactants in the GI tract, (3) the micellar transformation of lipid-rich colloids by bile, and (4) lipid depletion from the micelles by fatty acid absorption.[8,71,73] The digestion of lipidic components changes the solubilization capacity of colloids that are formed after the dilution/dispersion of lipid-based SDDS in the GI tract, which generates supersaturation.[71] The lower solubilization capacity of digested colloids is attributed to the increased water solubility of the digested lipidic components. Moreover, the lipid-rich, large, liquid crystalline structures that are formed after the dilution and digestion of lipid-based SDDS in the GI tract are converted to smaller, bile-rich mixed-micelles and micellar colloids that further reduce the solubilization capacity and therefore assists in generation of supersaturation.[73] The solubilization capacity of the micellar colloids is further reduced at the intestinal wall where the adsorption of fatty acid from the micellar colloids occurs.[73] As mentioned earlier, the Formulation-SDDS including lipid-based SDDS are formulated with PIs such

as polymers and surfactants to maintain drug supersaturation for a prolonged period of time, which allows the maximum utilization of the higher thermodynamic activity of drug for its maximum absorption. In other words, the success of SDDS in promoting higher and less variable oral bioavailability of poorly water soluble drugs has often been attributed to the generation and stabilization of supersaturated solutions in the GI tract.[1] The knowledge of fundamental relationships between the mechanisms of crystallization (i.e., nucleation and crystal growth) and the variables that govern the rate of crystallization including pH, temperature, agitation, and the number of active growth sites on the growing surface would be essential for understanding the effects of PIs on the crystallization rate and, in turn, on the maintenance of supersaturation.

2. Supersaturation and Drug Precipitation

Drug supersaturation could exist in liquid as well as solid systems. For example, the supersaturation in solid systems such as ASD can be attributed to higher drug loading than the equilibrium solubility of drug in ASD.[53] The example of supersaturation in liquid systems includes aqueous supersaturated solutions that could be produced *in vivo* or *in vitro* after the dissolution/dispersion of SDDS.[91] The liquid-state supersaturation is generally produced due to the higher apparent solubility of drug in liquid media, which could be attributed to PIs, higher energy drug forms, or both in the SDDS.

The supersaturated state is inherently thermodynamically unstable, which leads to precipitation until an equilibrium state is achieved.[92] Supersaturation, the thermodynamic driving force for precipitation or crystallization, is the difference between the chemical potentials of drug in solid phase as well as in solution phase.[24] The chemical potentials

of drug in the supersaturated solution state ($\mu_{supersaturated}$) and the saturated solid phase ($\mu_{saturated}$) may be defined in terms of the standard potential, μ_0, by[24]

$$\mu_{supersaturated} = \mu_0 + RT \ln a_{supersaturated} \tag{2.3}$$

$$\mu_{saturated} = \mu_0 + RT \ln a_{saturated} \tag{2.4}$$

where $a_{supersaturated}$ and $a_{saturated}$ are the activities of drug in the supersaturated solution state and the saturated solid state, respectively, R is the gas constant, and T is the absolute temperature. The fundamental driving force for crystallization can be described as[24]

$$\Delta\mu = \mu_{supersaturated} - \mu_{saturated} = RT \ln\left(\frac{a_{supersaturated}}{a_{saturated}}\right) = RT \ln\left(\frac{\gamma_{supersaturated} C_{supersat}}{\gamma_{saturated} C_{saturated}}\right) = RT \ln S \tag{2.5}$$

where $\gamma_{supersaturated}$ and $\gamma_{saturated}$ are the activity coefficients of drug in the supersaturated solution state and the saturated solid state, respectively, $C_{supersaturated}$ and $C_{saturated}$ are the concentrations of drug in the supersaturated solution state and the saturated solid state (i.e., equilibrium solubility), respectively, and S is the ratio-based degree of supersaturation. For practical purposes, it is assumed that the ratio of activity coefficients, $\gamma_{supersaturated}/\gamma_{saturated}$, is unity.[93] Hence, the ratio-based degree of supersaturation (S) is most commonly expressed as

$$S = \left(\frac{C_{supersat}}{C_{saturated}}\right) \tag{2.6}$$

Another commonly used expression for the degree of supersaturation, also defined as relative supersaturation (σ), is[25]

$$\sigma = S - 1 = \left(\frac{C_{supersat} - C_{saturated}}{C_{saturated}} \right) \tag{2.7}$$

The drug crystallization process could be divided into several zones.[24,93] The stable zone is the area where drug concentration is either equal or below the equilibrium solubility of drug. The crystallization of drug is impossible when the drug concentration is in this zone. The zone above the stable zone can be termed as metastable zone. In this zone, spontaneous crystallization is probable. Crystal growth occurs when the metastable system is seeded with drug crystals. The top zone is defined as labile zone, where spontaneous crystallization is probable, however it is not inevitable. Precipitation or crystallization could be divided in two steps: (1) nucleation, and (2) crystal growth (Figure 2.1). In nucleation, a new phase is separated by the birth of new nuclei or crystals, whereas in crystal growth, the new nuclei or crystals grow in size. While the maintenance of supersaturation could be achieved by inhibiting drug precipitation in the presence of PIs, the abilities of PIs to prolong supersaturation of poorly water soluble drugs could be linked to their effects on nucleation and/or crystal growth of drugs.[4,20] Therefore, a quantitative and mechanistic understanding of the nucleation and crystal growth of drugs is needed to effectively utilize PIs in maintaining the supersaturation of drugs.

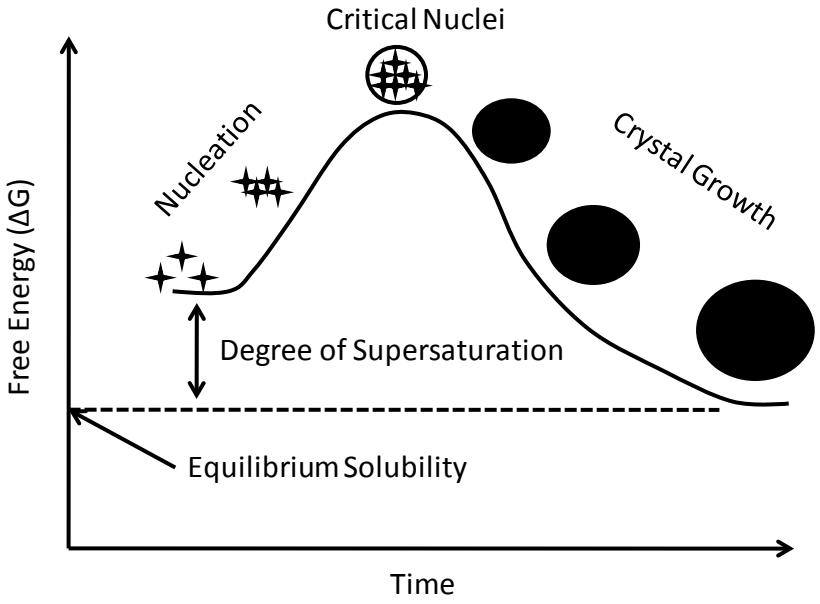

Figure 2.1. Schematic diagram illustrating the change in free energy during crystallization.[94]

2.1 Nucleation

The nucleation process consists of the formation of stable nuclei, which are also known as critical nuclei.[93,95,96] The mechanism of nucleation can be divided into two classes: 1) primary nucleation, and 2) secondary nucleation. Primary nucleation can further be classified into homogeneous and heterogeneous nucleation (Figure 2.2).[92] Homogenous nucleation occurs in clear solution and, generally, the free energy barrier is significantly higher to create a new solid phase. In the case of heterogeneous nucleation, the presence of a foreign substance or an impurity lowers the free energy barrier for nucleation. In supersaturated solutions, weak aggregates or clusters of drug molecules smaller than a critical size are unstable and redissolve. According to the classical theory of nucleation, stable aggregates, also known as critical nuclei, are formed when the size of the aggregates reaches a critical radius and the free energy barrier for the formation of critical nuclei is overcome.[92] The nucleation rate (J) which describes the number of critical nuclei formed per unit time and volume of the bulk can be expressed as

$$J = Aexp\left(\frac{-\Delta G_{critical}}{kT}\right) \tag{2.8}$$

where A is the pre-exponential factor, $\Delta G_{critical}$ is the free energy change for the formation of stable nuclei, k is the Boltzmann's constant, and T is the absolute temperature.[24] In the case of homogeneous nucleation, according to the classical theory of nucleation, the free energy change for the formation of new phase is equal to the sum of free energy change for the formation of new surface (i.e., surface excess free energy, $\Delta G_{surface}$) and the free energy change for the phase transformation into a very large particle, as known as the volume excess free energy (ΔG_{volume}).[24] Hence,

$$\Delta G = \Delta G_{surface} + \Delta G_{volume} = \beta L^2 \gamma + \alpha L^3 \Delta G_v \quad (2.9)$$

where β and α are the area and volume shape factors, respectively, L is the characteristic length, γ is the surface tension, and ΔG_v is the free energy change of the phase transformation per unit volume. For spherical nuclei, the critical radius ($r_{critical}$) can be determined by setting $d\Delta G/dr = 0$:[24]

$$\frac{d\Delta G}{dr} = 8\pi r_{critical}\gamma + 4\pi r_{critical}^2 \Delta G_v = 0 \quad (2.10)$$

$$r_{critical} = -\frac{2\gamma}{\Delta G_v} \quad (2.11)$$

From substituting for ΔG_v

$$\Delta G_{critical} = \frac{4\pi r_{critical}^2 \gamma}{3} \quad (2.12)$$

The growth of the critical nuclei is described by the Gibbs-Thompson relationship[24]

$$ln\, S = \frac{2\gamma\vartheta}{kTr_{critical}} \quad (2.13)$$

where υ is the molecular volume. Now substituting for $r_{critical}$

$$\Delta G_{critical} = \frac{16\pi\gamma^3\vartheta^2}{3(kTlnS)^2} \quad (2.14)$$

Finally, the nucleation rate (J) can be expressed as[24]

$$J = A\, exp\left(\frac{-16\pi\gamma^3\vartheta^2}{3k^3T^3(lnS)^2}\right) \quad (2.15)$$

It can be seen from Eq. 2.15 that temperature (T), degree of supersaturation (S) and surface tension (σ) are three primary variables that govern the rate of nucleation. The rate of homogeneous nucleation is difficult to measure experimentally as it is practically impossible to minimize internal and foreign impurities and particles as well as inert surfaces such as the walls of an apparatus, stirrers, and baffles.[93] While heterogeneous nucleation occurs due to the presence of foreign substances in supersaturated solution, the presence of crystals in supersaturated solution causes secondary nucleation.[92] The parent crystals may provide a catalytic effect resulting in a nucleation event at lower degrees of supersaturation than required for spontaneous homogeneous nucleation.[93] Heterogeneous nucleation and secondary nucleation may be more relevant from a biopharmaceutical perspective than homogeneous nucleation as the supersaturated solution of drug would encounter several different surfaces including gut wall, food particles, and undissolved drug and excipient particles in the GI tract.

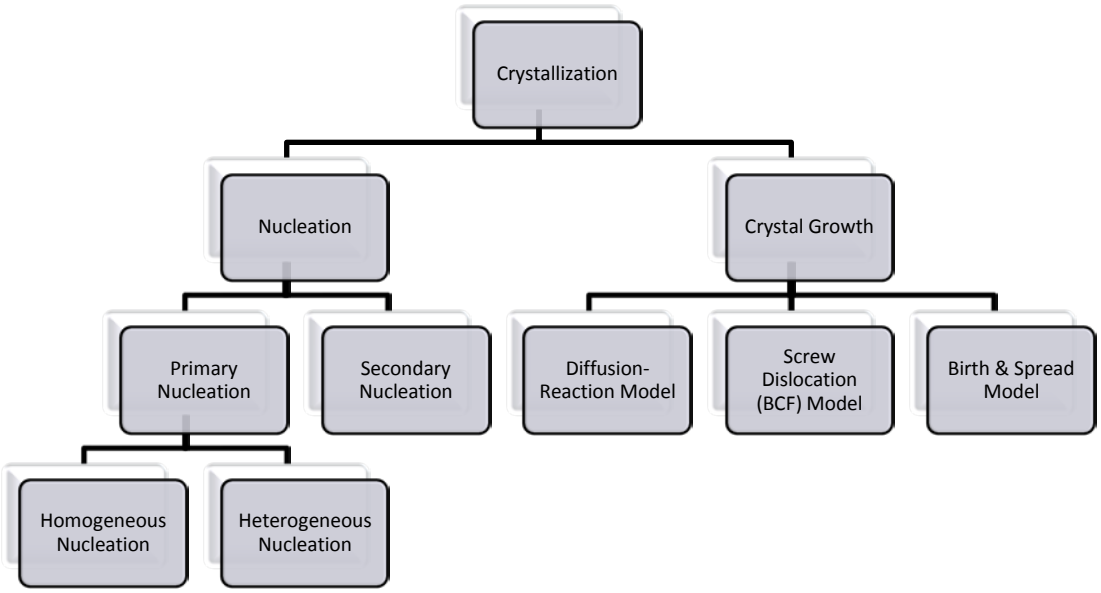

Figure 2.2. Crystallization and its sub-processes including nucleation and crystal growth.

2.2 Crystal Growth

Crystal growth process is a multistep process involving different mechanisms (Figure 2.3). Several models including the diffusion-reaction (two-step) model, screw dislocation (spiral growth) or Burton, Cabrera and Frank (BCF) model, and the surface nucleation (Birth & Spread) model have been used to study the process of crystal growth.[24,25,93,97-103] Some of the above-mentioned models are described below:

a) **Diffusion-reaction model**:

According to the diffusion-reaction theory, the major steps in the crystal growth process are: (1) the diffusion step where solute diffuses from bulk solution to the crystal/solution interface, and (2) the surface integration or surface reaction step where solute integrates into the crystal lattice.[24,92] The diffusion-reaction theory assumes that the two major steps of the crystal growth process occur in series.[24,26,92,93,101] Each step can be described by the equation shown below[24]:

Diffusion step:

$$-\frac{dc}{dt} = k_d \frac{A}{V_b}(c_b - c_i) \tag{2.16}$$

where k_d is the coefficient of mass transfer by diffusion, A/V_b is the surface area of crystals per unit volume, c_b is the solute concentration in bulk, and c_i is the solute concentration in solution at the crystal-solution interface

Surface Integration step:

$$-\frac{dc_i}{dt} = k_r \frac{A}{V_b}(c_i - c_s)^r \tag{2.17}$$

where k_r is the rate coefficient for the surface reaction (integration) process, c_s is the solute concentration in solution at equilibrium (i.e., the saturation solubility), and r is the order of the surface integration process. The driving force for the first step (i.e., bulk diffusion) is determined from the difference between the solute concentration in the bulk medium and the solute concentration in solution at the crystal-solution interface (c_i). The surface integration rate is a function of the driving force defined as the difference between c_i and the solute concentration at the solid surface (i.e., the saturation solubility). Since c_i is generally not obtainable experimentally, a simplified empirical crystal growth model is often employed that assumes the overall driving force to be equal to the difference between the bulk concentration and the equilibrium solubility.[24,104]

$$-\frac{dc_b}{dt} = k_G \frac{A}{V_b}(c_b - c_s)^g \tag{2.18}$$

where k_G is an apparent crystal growth rate coefficient, and g is the apparent order of the crystal growth process. When $k_d \ll k_r$, the crystal growth kinetics are bulk diffusion rate-limited and $k_G = k_d$, whereas when $k_r \ll k_d$, the crystal growth kinetics are surface integration (or reaction) rate-limited and $k_G = k_r$.

The surface integration process could be divided into several sub-steps.[26] Desolvation of solute occurs at the solid-liquid interface followed by the adsorption of solute on the growing crystal surface.[9] The adsorbed solute molecules diffuse on the crystal surface until active growth sites such as defects, kinks, or steps are encountered and solute molecules are incorporated into the lattice.[101] Rapid and continuous crystal growth continues until all active growth sites are occupied and a molecularly smooth crystal surface is created.[24] The crystal growth rates from molecularly smooth surfaces

are slow, which require two-dimensional nucleation to occur on the smooth surface.[96] Alternatively, crystal growth could occur through the spiral growth mechanism where screw dislocations are formed that allow continuous and faster crystal growth.[25] This process does not lead to the formation of molecularly smooth crystal surfaces upon crystal growth which, in turn, provides continuous crystal growth without the need for two-dimensional nucleation.[9]

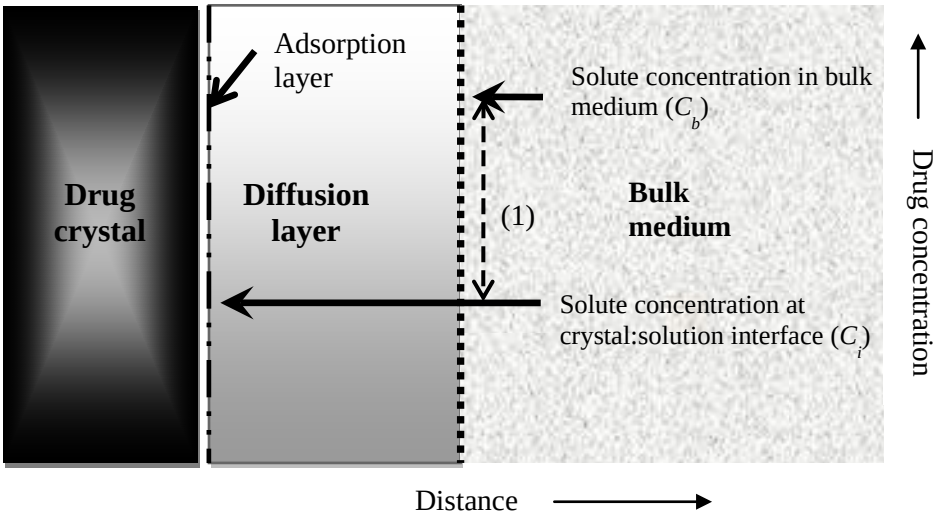

Driving force for: (1) Bulk diffusion (C_b- C_i)

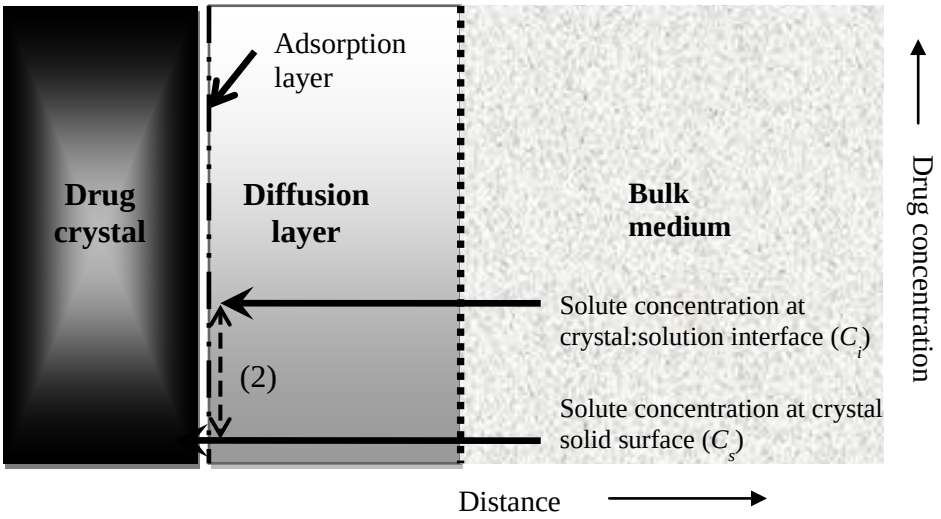

Driving force for: (2) Surface integration (C_i- C_s)

Figure 2.3. Schematic diagram illustrating the two major steps (bulk diffusion and surface integration) of a crystal growth process.

b) **Screw Dislocation or Burton, Cabrera and Frank (BCF) Model**:

The Burton, Cabrera and Frank (BCF) model is derived from the adsorption layer theories.[24,93,99,101] According to the adsorption layer theories, when solute molecules arrive at the crystal surface they are not integrated into the crystal lattice instantaneously. Rather they lose one degree of freedom and freely migrate over the crystal surface until they find active centers such as a kink or dislocation for the reaction. This process is known as surface diffusion that creates a loosely adsorbed layer of solute molecules waiting for integration.[101] In the BCF model, it is assumed that the integration occurs at a site of dislocation (i.e., imperfection).[105] One of the important types of dislocations is the screw dislocation, which renders crystals growth in a spiral fashion (spiral growth). The curvature of a spiral can reach a maximum value determined by the critical radius for a two-dimensional nucleus. The BCF model can be expressed as:[24,26,99]

$$R = A\sigma^2 tanh\left(B/\sigma\right) \tag{2.19}$$

where R is the crystal growth rate, σ is the degree of supersaturation, and A and B are system related parameters defined as:[24,26,99]

$$A = \frac{2kTD_sC_{SE}\beta\gamma_0}{19\gamma_{sl}x_s} \tag{2.20}$$

$$B = \frac{19V_m\gamma_{sl}}{2kTx_s} \tag{2.21}$$

where k is the Boltzmann constant, T is temperature (°K), D_s is the solute diffusion coefficient on the crystal surface (m^2s^{-1}), C_{SE} is the equilibrium surface concentration of the solute when σ=1 (i.e., saturation solubility), β is the retardation factor for a linear

step, γ_0 is the retardation factor for a kink, γ_{sl} is the interfacial energy between solid and liquid (Jm^{-2}), x_s is the mean diffusion distance on the surface, and V_m is the volume of solute molecule (m^3).

c) **Birth & Spread Model**:

The Birth and Spread model is based on the two-dimensional crystal surface nucleation process, which is followed by the spread of the newly formed nuclei or layer.[24,93,101,105] This mechanism is invoked when the crystal growth process requires a birth of nuclei on the crystal surface for its continuation. The model can be expressed by the equations shown below:[24,26,92,103]

$$R = E\sigma^{5/6} exp\left(F/\sigma\right) \tag{2.22}$$

$$E = 2h^{1/6} V_m^{5/6} \left(\frac{\bar{v}}{\pi}\right)^{1/3} \left(\frac{n_1 D_S C_{SE} \beta \gamma_0}{x_s}\right)^{2/3} \tag{2.23}$$

$$F = \frac{\pi h V_m \gamma_{sl}^2}{k^2 T^2} \tag{2.24}$$

where R is the crystal growth rate, E and F are the system related constants, h is the step height or lattice spacing, $\bar{v}$ is the mean rate of adsorption of molecules on the surface, and n_1 is the equilibrium number of monomers on the surface of crystal per unit area.

2.3 Techniques to characterize supersaturation

Unlike routinely executed crystallization studies that require relatively low supersaturation to precisely control and monitor growth rates during the manufacturing of active pharmaceutical ingredients, very high supersaturation (10 to 1000-fold of

equilibrium solubility) could be encountered during *in-vitro* and *in-vivo* dissolution/dispersion of SDDS. At these high degrees of supersaturation, nucleation kinetics is instantaneous and very difficult to monitor. Quantitative and mechanistic explorations of drug precipitation (i.e., nucleation and crystal growth) in aqueous systems have, in general, suffered due to a lack of simple and robust experimental techniques. Undoubtedly, understanding the effect of excipients on drug precipitation kinetics requires quantitative models describing both nucleation and crystal growth. In order to understand the mechanisms involved in the PI mediated supersaturation maintenance, it would be essential to measure the precipitation kinetics of drugs. Current methods to study precipitation kinetics involve the monitoring of concentration remaining in solution by filtration of precipitated solid at various time points and subsequently measuring solution concentration. In such off-line analysis, the crystal growth process continues while the solvent is being removed during separation, sometimes, rendering the crystal surface with high degree of imperfections. This can significantly impact the downstream analysis with other instruments. [93]

Several approaches have been described in the crystal growth literature for the measurement of crystal growth including: (1) using a single crystal vs. a population of crystals, (2) monitoring the change in the properties of crystals (i.e., mass or size) vs. a change in the properties of solution (i.e., solution concentration), and (3) varying growth conditions (e.g., isothermal vs. non-isothermal).[93] Each approach has its own advantages and limitations. For example, the single crystal measurement technique is advantageous in terms of measuring the growth rate of a specific crystal face of interest. However, it poses limitations owing to the availability of a very small surface area as compared to a

multiparticulate system. These limitations include higher sensitivity to the presence of impurities (even at very low concentrations) as well as to the primary nucleation at higher degrees of supersaturation. For our proposed studies, we have selected the multiparticulate (population of crystals) method, which is also known as batch crystallization. The advantages of this method are: (1) relevance to the GI conditions in terms of maintaining supersaturation after primary nucleation, (2) simple technique, and (3) less sensitive to small differences in crystal shapes or different number of dislocations. The limitation of this method is that it gives an average of crystal growth rates from individual faces of the crystal.[93] Since the crystal growth rate is directly proportional to the surface area, precise control over the seed number and size distribution is critical to control the available surface area for the crystal growth. Moreover, to provide a constant surface area for growth, it is important to maintain the seed number and size distribution during the crystal growth experiment. The effect of mixing using a magnetic stir on the seed number and size distribution could be determined using particle size measurement techniques. Besides the direct measurement of supersaturation from solution concentrations, the supersaturation can be measured indirectly by measuring properties such as refractive index and density. However, such methods require carefully controlled conditions in the laboratory.[24] The growth of precipitate in terms of particle size and shape has also been monitored by microscopy. However, such methods cannot be used to monitor rapid kinetics at high supersaturation.

3. Maintenance of Supersaturation and Precipitation Inhibitors

In order to achieve higher bioavailability and reduce inter-patient variability from SDDSs, it is essential to maintain the supersaturation of drug by inhibiting precipitation

(i.e., nucleation and/or crystal growth) using precipitation inhibitors (PIs).[1,8] Pharmaceutical excipients including cyclodextrins, polyvinylpyrrolidone (PVP), hydroxypropyl methylcellulose (HPMC), polyethylene glycol (PEG), and their derivatives (e.g., PVP-VA, HPMC-AS, TPGS, Cremophor RH 40, polysorbate 80) that maintain the supersaturation of drug in solid and/or liquid dispersions have been incorporated in various SDDSs as PIs.[2,9,10,12,13,15,18,42,106,107] Recent studies, as discussed in an earlier section, have clearly shown the impact of precipitation inhibitors on the enhancement of oral bioavailability of poorly water soluble drug through the maintenance of supersaturation.[1-6,9,108]

A majority of the precipitation inhibitors are polymeric in nature and hence could be defined as polymeric precipitation inhibitors (PPIs).[9] One of the most commonly used non-polymeric PIs is cyclodextrin.[46] The PPIs can be further classified as surface active PPIs and non-surface active PPIs (Figure 2.4). Some of the surface active PPIs include PEG, TPGS, Poloxamer, Pluronic F127, Cremophor EL, PG, and Carbomer. The surface active PPIs, depending on the concentration above the critical micellar concentration, could enhance the equilibrium solubility of drugs. Hence, both the supersaturation maintenance as well as the high equilibrium solubility provided by the surface-active PPIs could enhance the bioavailability of poorly water soluble drugs.[1]

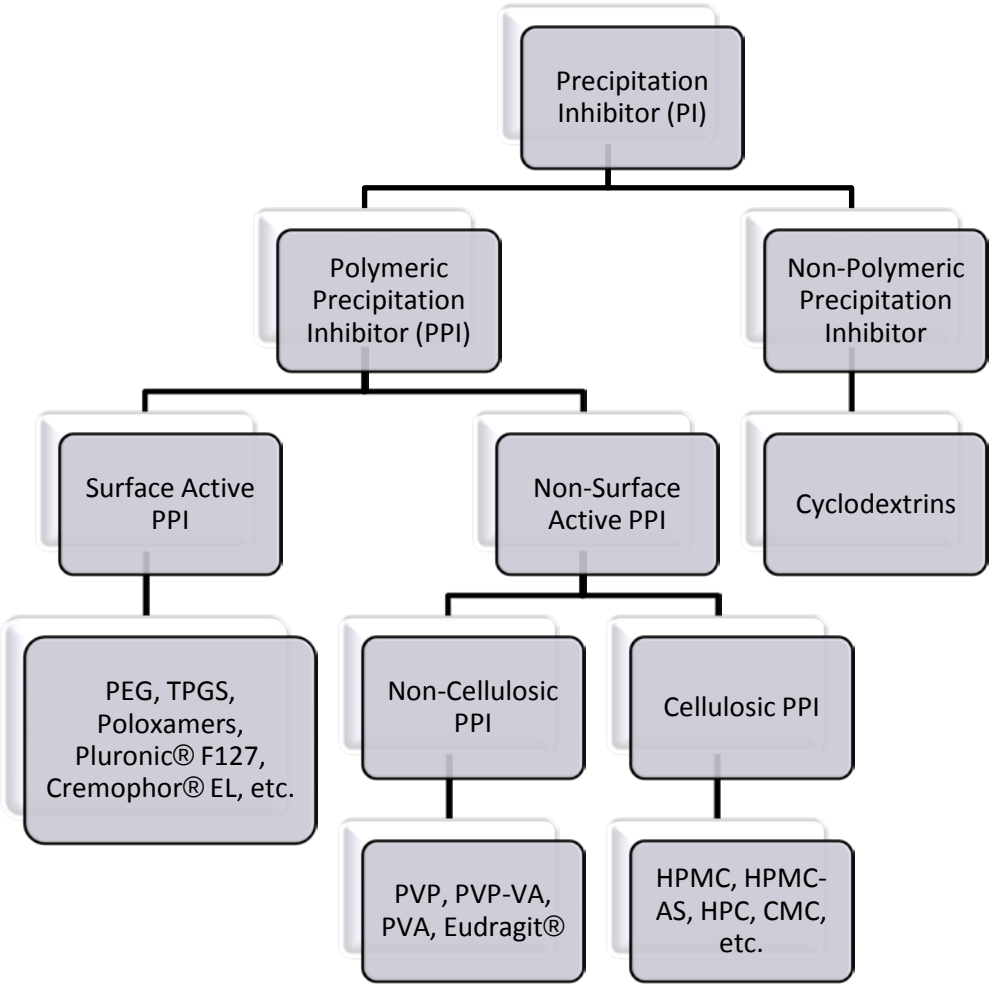

Figure 2.4. Classification of precipitation inhibitors (PIs).

The non-surface active PPIs can be further divided into two groups: 1) cellulosic PPIs and 2) non-cellulosic PPIs (Figure 2.4). PVP, PVP-VA, PVA, PAA, and Eudragit are some examples of the non-cellulosic PPIs. PVP and its derivatives have been successfully used to inhibit the precipitation of drugs in supersaturated solid as well as liquid dispersions. PVP is commonly used as a dispersant for several chemical entities such as drugs, dyes, and pesticides due to its amphiphilic nature. This property of PVP could be attributed to its structural features including the highly polar amide group and apolar methylene and methine groups. Due to the amphiphilic nature, PVP is soluble in water and several other non-aqueous solvents. The Eudragits are anionic polymers containing methacrylic acid groups. They are copolymers of methacrylic acid and acrylic acid derivatives. The cellulosic PPIs include HPMC, HPMC-AS, HPC, CMC, MC, cellulose, acetate phthalate, alginic acid, HEC, NaCMC, and gum Arabic. The selection of PPIs in the development of drug product not only depends on the properties of drug but also depends on the properties of PPIs as well as the type of SDDS.[9] For example, PPIs with high glass transition temperatures including HPMC, PVP, and their derivatives are commonly used in solid dispersions, whereas PPIs with low melting points such as vitamin E TPGS and Cremophor RH40 are frequently used in lipid-based drug delivery systems.

The inhibition of nucleation and crystal growth due to impurities and additives has been studied extensively for non-pharmaceutical systems, especially for inorganic salts.[37,109-116] The inhibitory effects of 1,2-dihydroxy-1,2-bis(dihydroxyphosphonyl)ethane and Zn on the crystal growth of hydroxyapatite were attributed to adsorption and, in turn, blocking of active growth sites on the hydroxyapatite

seed crystals. The inhibitory effect of additives on crystal growth has been successfully exploited to engineer crystals with a desired shape[117-119] (crystal habit) and size.[37,119] In the case of pharmaceutical systems, several studies have been carried out to determine the effect of PPIs on the precipitation of drugs.[2,7,11,12,17,18,20,21,43,46,120-122] Some studies have been aimed at understanding the effects of PIs on the growth of a specific crystal face, the change in the crystal lattice energy, or the modification of the crystal habit of drugs.[11,123] These PPIs are believed to be maintaining drug supersaturation by changing nucleation, crystal growth, or both.[108] As illustrated in Figure 2.5, the typical shape of the drug concentration vs. time profile observed during the crystallization of drug in the presence of PPIs depends on the mechanism of precipitation inhibition. For example, if a PPI significantly inhibits nucleation then the supersaturated drug concentration is maintained for a prolonged period of time followed by a decline in concentration due to the nucleation and crystal growth of drug. However, if a PPI is selectively inhibiting crystal growth then a significant drop in drug concentration is observed initially due to nucleation followed by a slow decline in concentration due to the inhibition of crystal growth.

Recent studies have shown that the inhibitory effects of PPIs on nucleation, crystal growth, or both vary significantly from drug molecule to drug molecule. Ozaki et al.[108] showed that, unlike Eudragit, HPMC and PVP significantly inhibited the nucleation and crystal growth of griseofulvin and danazol. While HPMC was a more effective nucleation inhibitor of griseofulvin, it significantly inhibited the nucleation and crystal growth of danazol. Lindfors et al.[20] observed that PVP was a better crystal growth inhibitor than a nucleation inhibitor of bicalutamide. Vandecruys et al.[43] observed that

PPIs such as PVP & HPMC were more effective at prolonging supersaturation than providing higher degrees of supersaturation, whereas the PPIs such as surfactants and cyclodextrins provided higher degrees of supersaturation. These observations clearly indicate that the inhibition of nucleation and crystal growth of drugs by PPIs is complex, involving multiple mechanisms that could vary depending on the drug-PPI combination.

The effects of PPIs on the inhibition of nucleation are mainly associated with the interactions of PPIs with drug molecules in the bulk solution.[13-16] For example, the effectiveness of PPIs in inhibiting the formation of carbamazepine dihydrate was related to the intermolecular hydrogen bonding and hydrophobic interactions between PPIs and carbamazepine. However, their relative impact on the effectiveness of a given PPI could not be determined due to experimental limitations.[14] The superiority of HPMC-AS HF over HPMC-AS LF, two different grades of HPMC-AS containing different ratios of acetate and succinate substituents, in inhibiting the precipitation of carbamazepine from supersaturated aqueous solutions was attributed to stronger hydrophobic interactions between HPMC-AS HF and carbamazepine in the bulk solution.[13] Similarly, the inhibitory effects of cellulosic PPIs on the nucleation of three model drugs, celecoxib, efavirenz, and ritonavir, from supersaturated aqueous solutions correlated well with the hydrophobicity of the cellulosic PPI relative to that of the model drugs.[15]

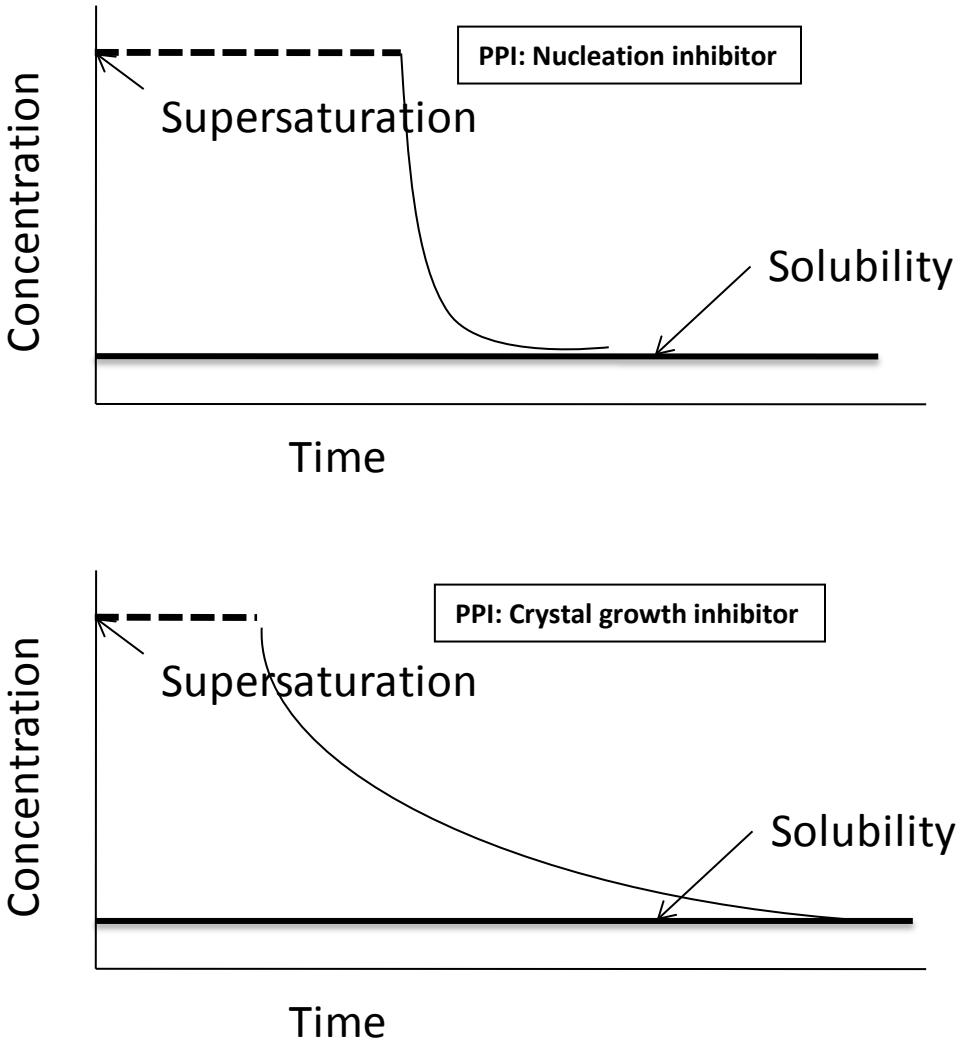

Figure 2.5. Schematic diagram illustrating desupersaturation profiles in the presence of PPIs as nucleation or crystal growth inhibitors.

The inhibitory effects of PPIs on the crystal growth of a drug have been associated with the adsorption of PPIs on the growing crystal surface.[4,12,17-24] The adsorption of polymers[9] or impurities[124] on the growing crystal surface has been linked to their crystal growth inhibitory effects. The inhibitory effect of PVP on the crystal growth of bicalutamide was attributed to the adsorption of PVP onto bicalutamide crystals.[20] The habit modification of hydrocortisone acetate crystal by HPMC was attributed to the preferential adsorption of HPMC to the crystal faces.[12] It has been proposed that the adsorbed polymer could inhibit crystal growth by blocking the active growth site, increasing the diffusive barrier at the solid-liquid interface, or both.[12,21] Raghavan et al.[12] proposed that the inhibition of hydrocortisone acetate crystal growth by HPMC could be attributed to: (1) an increase in the diffusional barrier in the hydrodynamic boundary layer by HPMC, and (2) the adsorption of HPMC on the growing crystal surface. The inhibition of the crystal growth of sulfathiazole by PVP was attributed to the formation of a possible net like structure on the crystal surface by the adsorbed PVP. It was proposed that the pore size of the net like structure would be smaller when the relative transport rate of PVP to sulfathiazole is higher, which in turn would provide greater inhibition of the crystal growth.[18]

The adsorption of PPIs on the growing surface could be attributed to the intermolecular interactions such as hydrogen bonding, and hydrophobic interactions between the PPI and surface.[4,10-12] Raghavan et al[12] proposed that the stronger inhibitory effects of HPMC as compared to PVP and PEG 400 on the crystal growth of hydrocortisone acetate may be attributed to hydrogen bonding interactions between HPMC and the drug. Moreover, the extent of HPMC adsorption was correlated with the

hydrogen bonding capacity of different faces of the HA crystal.[12] Ilevbare et al.[22] found that cellulosic polymers with moderate levels of hydrophobicity, semi-rigid structure, and amphiphilic nature were more effective crystal growth inhibitors of a highly lipophilic and poorly water soluble drug, ritonavir, in aqueous suspensions. It was proposed that these properties of PPIs could likely promote adsorption onto the crystal surface of ritonavir.[10] Gao et al.[4] observed that HPMC was a better PPI than PVP for AMG 517, a poorly water soluble drug candidate, which was attributed to the greater hydrophobicity of HPMC than that of PVP. Tian et al.[14] observed that both the hydrogen bonding and hydrophobicity of PPIs were important for the inhibition of the form conversion of carbamazepine anhydrous to carbamazepine dihydrate. However, a complete inhibition of carbamazepine dehydrate formation was achieved only with more hydrophobic polymers such as HPMC, methylcellulose (MC), and hydroxypropyl cellulose (HPC) and not with less hydrophobic polymers such as HEC indicating that hydrogen bonding interactions between the drug and polymers did not play a significant role here as all the above-mentioned polymers had a similar cellulosic backbone.

The mobility of the functional group of PPIs involved in the interaction with the surface and, in turn, the adsorption process also affects the precipitation inhibitory effects of PPIs.[19,125] The crystal growth inhibitory effects of PPIs have been associated with the molecular weight and chain length of PPIs as both PPI properties could influence the ability of PPI to make greater number of contacts with the crystalline surface and, in turn, reduce the mobility of the adsorbed PPI.[9,107,125] Unlike PVA and PEG, the stronger crystallization inhibitory effect of PVP for acetaminophen was attributed to the lower flexibility of PVP chains as compared to PVA and PEG chains.[19] In a molecular

dynamics simulation study, the superior inhibitory effect of PVP as compared to HPMC on the crystal growth of salbutamol sulfate was attributed to the higher interaction energy and greater number of contacts with the salbutamol sulfate crystal by PVP as compared to HPMC, which in turn reduced the movement of PVP chains.[125] Gift et al.[107] determined that, unlike hydroxyl group containing small molecules such as glycerol, glucose, adipic acid, and methanol, only polymers such as PVA and PAA were able to inhibit the precipitation of caffeine indicating that the hydrogen bond formation was not enough to inhibit caffeine precipitation. The inhibitory effect of PPI on caffeine precipitation was greater at higher molecular weights of PPI, which was attributed to probably a greater number of hydrogen bonding interactions provided by higher molecular weight PPIs.

While a few recent studies[1,20,43] have attempted to discern the mechanism of action for PPIs, the supersaturation maintenance effects of PPIs are still not well understood due in part to a paucity of systematic and quantitative explorations.[104,108] Most of the existing literature studies on the inhibition of drug precipitation are of screening types where the PPIs are rank ordered based on their inhibitory effects.[2,17,43,46,122] The proposed mechanisms of PPI effects including the adsorption of PPI on the growing crystal surface are rarely correlated with the sub-processes of drug precipitation (i.e., nucleation and crystal growth) and their specific mechanisms such as bulk diffusion or surface integration. Specifically, the mechanism of the inhibitory effects of PPIs on drug crystal growth is seldom proven directly and/or correlated with the adsorption of PPIs in a quantitative manner. Consequently, the nature of the adsorbed PPI layer as well as the key physicochemical properties of PPIs and drugs such as molecular weight, hydrogen bonding capability and hydrophobicity that could influence

the adsorbed PPI layer and, in turn, the effectiveness of PPI are not well understood. A thorough understanding of the correlation between the adsorption of a given PPI and its crystal growth inhibitory effect is still required. The identification of a specific mechanism such as the blocking of growth sites or the diffusional resistance for drug molecules underpinning the effectiveness of PPI is absent in many previous studies. The knowledge of the adsorption behavior of PPIs would help in exploring the mechanisms of crystal growth inhibition by PPIs. A thorough understanding of how the adsorbed PPIs inhibit the crystal growth of poorly water soluble drugs would be essential in a rationale selection of PPIs for the development SDDS.

Finally, the overall lack of thorough understanding of the effects of PIs on drug supersaturation maintenance makes *a priori* predictions of their beneficial effects very challenging. The mechanism by which a given PPI achieves its beneficial effect is unknown and what combination of properties of the drug and PPI provides an optimal benefit is unclear. In general, good correlations between the effects of PPIs and the physico-chemical properties of PPIs as well as drugs have not been established. The supersaturation maintenance effects of PPIs vary extensively between drug molecules rendering the development of predictive tools for a rational and efficient PPI selection process more difficult. There are no reliable quantitative models that would allow a formulator to predict *a priori* the most suitable PPIs and the amounts that should be used for a given dose of a new poorly water soluble drug candidate to achieve the desired prolongation in supersaturation. It is currently impossible to rapidly select (without performing screening studies for each drug candidate) suitable PPIs that can inhibit

precipitation to improve oral absorption and, in turn, oral bioavailability of poorly water soluble drugs.

4. Indomethacin, a Model Poorly Water Soluble Drug

Indomethacin is an anti-inflammatory, antipyretic, and analgesic drug.[126] Indomethacin was chosen as the model compound in the present study due to its low intrinsic solubility (~1 μg/mL) and the availability of physical characterization data in the existing literature.[127-129] It is a suitable model compound for the studies aimed at understanding the abilities of certain excipients or PIs to prolong drug supersaturation after oral administration of drug products that produce supersaturated solutions in the GI tract. The physicochemical properties of indomethacin including stability,[130,131] physical forms,[126] and solubility[132,133] in aqueous solutions have been characterized previously. Indomethacin decomposes in aqueous solutions by hydrolysis.[130] The rate of hydrolysis is significantly slower at low pH.[131]

Indomethacin exists in several polymorphic forms including the γ, α, and δ forms.[128,134] The two major polymorphs of indomethacin are the γ and α polymorphs. The γ-form used in these crystal growth studies is thermodynamically most stable.[126] The metastable α-form of indomethacin has a lower heat of fusion and lower melting point.[135] The melting points of γ and α polymorphs are 160°C and 154°C, respectively.[127] While it is metastable, the α-form has remained stable for longer than 18 months at room temperature.[128] The experimental densities of the γ and α polymorphs are 1.38 g/cm^3 and 1.40 g/cm^3, respectively.[134] The unit cell of the α-polymorph consists of three indomethacin molecules, whereas the unit cell of the γ-polymorph has two molecules forming a dimer.[126] The unit cell of α-polymorph provides more conformational

arrangements as compared to the same for the γ-polymorph.[126] A recent study found that the amorphous form of indomethacin had lower dissolution rate as compared to the crystalline γ and α polymorphs, which was in contrast to the thermodynamic predictions.[126] The α polymorph showed the highest rate of dissolution amongst the amorphous and crystalline γ polymorph.[126] Hancock et al.[132] reported the solubility of γ-indomethacin in deionized water at 25ºC as ~5 µg/mL (~1.4×10^{-5} M). Wassvik et al.[133] reported an intrinsic solubility of $1.12 \pm 0.03 \times 10^{-6}$ M for γ-indomethacin. The higher indomethacin solubility reported by Hancock et al. is in accordance with the solubility enhancement provided by indomethacin ionization at higher pH (>pKa) that would result from dissolution in deionized water.

Chapter Three

Maintenance of supersaturation: 1. Indomethacin crystal growth kinetic Modeling using an online second derivative UV spectroscopic method

INTRODUCTION

The risk of clinical failure associated with poorly water soluble drug candidates due to their low and variable oral bioavailability remains a significant concern in current drug development. For poorly water soluble drugs, oral bioavailability enhancement may be possible by achieving and maintaining supersaturated drug concentrations in the gastrointestinal (GI) tract.[1-6] Salts,[48] cyclodextrin complexes,[7,43] lipid-based delivery systems,[4,5,136] high energy amorphous solid dispersions,[3] and nanoparticles[6,137] are among the types of strategies that may produce high, supersaturated drug concentrations in the GI tract facilitated by the local GI environment, which is constantly changing in pH, food effects, and natural surfactant concentrations. However, prolonged maintenance of supersaturation in the GI tract may be difficult to achieve due to the inherent thermodynamic instability of the supersaturated state, which may lead to precipitation or crystallization (nucleation and crystal growth) of poorly water soluble drugs and variable, sub-optimal oral bioavailability.

Formulation excipients can play an important role in maintaining supersaturation and may provide better control from patient to patient independent of variability in the local GI environment. Literature studies have shown that excipients such as cyclodextrins,[7,43] polyethylene glycol (PEG) and PEG containing derivatives,[2,4,43] as well as other polymers such as hydroxypropylmethyl cellulose (HPMC)[4,5,12,43,138] and polyvinylpyrrolidone (PVP)[4,12,18,42,43,138] have the potential to prolong drug supersaturation to varying degrees depending on the properties of the drug and excipient.

The effectiveness of such excipients in maintaining supersaturation may be attributable to their ability to inhibit nucleation, crystal growth, or both.

Inhibition of nucleation and crystal growth due to the presence of impurities or additives has been widely studied for non-pharmaceutical systems,[37,110,112,113,115-117,119,139,140] especially for inorganic salts,[37,110,112,113,115,116] and in some cases the kinetics and mechanisms of nucleation and crystal growth inhibition have been rationalized. For example, based on the kinetics observed, the crystal growth of hydroxyapatite was attributed to a surface controlled spiral growth mechanism.[113] The inhibitory effects of 1,2-dihydroxy-1,2-bis(dihydroxyphosphonyl)ethane and Zn on the crystal growth of hydroxyapatite were attributed to adsorption and, in turn, blocking of active growth sites on the hydroxyapatite seed crystals. The inhibitory effect of additives on crystal growth has been successfully exploited to engineer crystals with a desired shape[117-119] (crystal habit) and size.[37,119] Effects of additives on polymorphic transformation[141,142] and lattice energy[139,143] have also been determined. Several studies have also been carried out to determine the effects of excipients on drug crystallization.[1-6,12,17-20,42,43,138,144] The inhibitory effect of polymers on drug crystallization has been attributed to their adsorption on to the crystal surface.[12,17-19] Raghavan et al.[12] proposed that the inhibition of hydrocortisone acetate crystal growth by PVP could be attributed to an increase in the diffusional barrier around the growing crystal due to the presence of high molecular weight PVP and its adsorption on the growing crystal surface. However, most of the above-mentioned studies on drug crystallization have been screening studies in which the excipients were simply rank ordered based on their inhibitory effects. Generally, the mechanism by which a given excipient achieves its beneficial effect is unknown and what

combination of properties of the drug and excipient molecules provides an optimal benefit is unclear. Consequently, there are no reliable quantitative models that would allow a formulator to predict *a priori* the most suitable excipient(s) and the amounts that should be used for a given dose of a new poorly water soluble drug candidate to achieve the desired prolongation in supersaturation.

Undoubtedly, understanding the effect of excipients on precipitation kinetics will require quantitative models describing both nucleation and crystal growth. One of the reasons for the deficiency of such quantitative models could be the lack of simple, robust, and reliable techniques to separately quantify the kinetics of nucleation and crystal growth that influence the maintenance of supersaturation. The aims of this study were twofold: (1) to develop and test a non-invasive (online) technique to measure crystal growth kinetics using second derivative UV spectroscopy; and (2) to use this technique to determine the reaction order and rate-limiting step for the crystal growth kinetics of a model poorly water soluble drug, indomethacin (Figure 3.1). Indomethacin appears to be a suitable model compound for future studies aimed at understanding the abilities of certain excipients to prolong supersaturation after oral administration of drug products that produce supersaturated solutions in the GI tract.

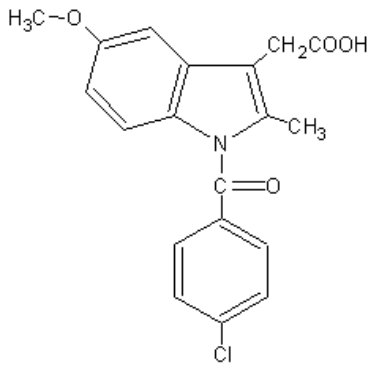

Figure 3.1. Chemical structure of indomethacin.

THEORY

Classical Diffusion-Reaction Model for Crystal Growth

Crystal growth processes are classically described by a two-step diffusion-reaction model (Figure 2.3)[24,26,92,93,101] involving (1) solute diffusion from the bulk solution to the crystal/solution interface and (2) a surface integration reaction whereby the solute is incorporated into the crystal lattice. These two processes are assumed to occur in series. The equation for solute diffusion to the crystal/solution interface is:

$$-\frac{dc_b}{dt} = k_d A(c_b - c_i) \tag{3.1}$$

where k_d is the coefficient of mass transfer by diffusion, A is the crystalline surface area per unit volume of the bulk medium, c_b is the solute concentration in the bulk medium, and c_i is the solute concentration in solution at the crystal-solution interface.

The second step is the surface integration step:

$$-\frac{dc_i}{dt} = k_r A(c_i - c_s)^r + k_d A(c_b - c_i) \tag{3.2}$$

where k_r is a rate coefficient for surface integration, r is the order of the surface integration process, and c_s is the solute concentration in solution at equilibrium (i.e., the saturation solubility).

Since c_i is generally not obtainable experimentally, a simplified empirical crystal growth model is often employed that assumes the overall driving force to be equal to the

difference between the bulk concentration and the equilibrium solubility, $(c_b - c_s)$, as in Eq. (3.3):

$$-\frac{dc_b}{dt} = k_G A(c_b - c_s)^g \tag{3.3}$$

where k_G is an apparent crystal growth rate coefficient, A, c_b, and c_s are as defined previously, and g is the apparent order of the crystal growth process. If $g = 1$, then k_G can be expressed as

$$\frac{1}{k_G} = \frac{1}{k_d} + \frac{1}{k_r} \tag{3.4}$$

When $k_d \ll k_r$, the crystal growth kinetics are bulk diffusion rate-limited and $k_G \approx k_d$, whereas when $k_r \ll k_d$, the crystal growth kinetics are surface integration (or reaction) rate-limited and $k_G \approx k_r$.

Classical Diffusion Layer Model for Drug Dissolution

The rate of dissolution of drug particles in aqueous media is generally treated as a bulk diffusion controlled process wherein the rate-limiting step is the diffusion of solute molecules through an aqueous boundary layer surrounding the solid particles.[24] Noyes & Whitney[145] as well as Nernst[146] & Brunner[147] modeled the bulk diffusion controlled dissolution process from planar surfaces using Eq. 3.5:

$$\frac{dc_b}{dt} = \frac{DA_t}{V_b h}(c_s - c_b) \tag{3.5}$$

where D is the diffusion coefficient of solute, h is the thickness of the diffusion layer, A_t is the total surface area of dissolving solid, V_b is the volume of bulk medium, c_s is the equilibrium solubility of solute, and c_b is the solute concentration in the bulk medium at time t. The quantity D/h in Eq. 3.5 is analogous to the coefficient of mass transfer (k_d) in Eq. 3.1.

Mass-Balance Relationship in Crystal Growth Processes

A mass balance relationship can be used to predict the change in seed crystal size upon crystal growth at a specific degree of supersaturation. The mass-balance relationship[24,92,93] assumes that the change in bulk solution concentration is proportional to the mass deposition on seed crystals, i.e., $dm = -V_b dC_b$. Here, m is the mass of seed crystals (moles), V_b is the volume of bulk medium in liters, and c_b is the molar solute concentration in the bulk medium. The relationship between the apparent crystal growth rate or mass deposition rate, R_G (moles/cm^{2}time), and the apparent linear growth rate, G (cm/time), can be expressed as:

$$R_G = \frac{1}{A_t}\frac{dm}{dt} = -\frac{V_b}{A_t}\frac{dc_b}{dt} = k_G\left(c_b - c_s\right)^g = G\left(\frac{3\alpha\rho_c}{\beta}\right) = \frac{dL}{dt}\left(\frac{3\alpha\rho_c}{\beta}\right) \qquad (3.6)$$

where A_t is the total surface area (cm^2) of seed crystals, k_G is the apparent crystal growth rate coefficient, g is the apparent order of crystal growth, α and β are the volume and surface shape factors of seed crystals, respectively, ρ_c is the seed crystal density, L is the characteristic size of seed crystals (e.g., volume based diameter), and t is time. The change in seed crystal diameter, ΔL, can be expressed as:

$$\Delta L = \frac{M_F^{1/3} - M_B^{1/3}}{(\alpha \rho_c N)^{1/3}} \tag{3.7}$$

where M_B and M_F are the mass of seed crystals before and after growth, respectively, and N is the total number of seed crystals.

For a population of seed crystals with a specific size distribution, the entire population can be divided into size classes containing collections of particles in a size range represented by each class. A change in size distribution after growth for the entire seed crystal population can be determined from the changes in the number of particles in each size class. When crystal growth is bulk diffusion controlled, k_G and g in Eq. 3.6 are equal to D/h and 1, respectively. Consequently, the mass of the seed crystals in the i^{th} size class after bulk diffusion controlled crystal growth (M_{Fi}) can be predicted using Eq. 3.6 as follows:

$$R_G = -\frac{V_b}{A_t}\frac{dc_b}{dt} = \sum_i \frac{1}{A_i}\frac{dm_i}{dt} = \sum_i \frac{D}{h_i}\left(c_b - c_s\right) \tag{3.8}$$

where m_i, A_i, and h_i are the mass, total surface area, and thickness of the diffusion layer for the seed crystals in the i^{th} size class using a characteristic size L_i. The change in diameter (ΔL_i) for the seed crystals in the i^{th} size class can be described as

$$\Delta L_i = \frac{M_{F_i}^{1/3} - M_{B_i}^{1/3}}{(\alpha \rho_c n_i)^{1/3}} \tag{3.9}$$

where M_{Bi} and n_i are the mass (before growth) and number of seed crystals in the i^{th} size class. Therefore, the apparent crystal growth rate (R_G) and the surface area A_i can be

used to estimate the change in seed crystal diameter (ΔL_i) for each *i*, and in turn the size distribution of an entire seed crystal population after growth.

MATERIALS AND METHODS

Materials

Indomethacin (1-(*p*-chlorobenzoyl)-5-methoxy-2-methylindole-3-acetic acid, 99+%, γ-polymorph, molecular weight =357.8 g/mole, pK_a=4.17[148]) was purchased from Sigma-Aldrich, Inc. (St. Louis, MO, USA). Nylon net filters (30 µ) and polycarbonate membrane filters (3 µ) were purchased from Millipore Inc., (Milford, MA, USA). Nylon membrane filters (0.2 µ) and 13 mm PTFE syringe filters (0.45 µ) were purchased from Whatman Int. Ltd. (Maidstone, England). Deionized water was obtained from a Milli-Q water purification apparatus (Milli-Q Synthesis, Millipore Inc., Milford, MA, USA) and pre-filtered through a 0.22 µ filter (Millipak Express 20, Millipore Inc., Milford, MA, USA). All other reagents and materials were of an analytical grade.

Preparation of Indomethacin Seed Crystal Suspension

A technique to obtain a narrow and unimodal size distribution of indomethacin seed crystals was developed. A pre-weighed quantity of indomethacin solid powder was dispersed (0.1% w/w) in 50 mM phosphate buffer (pH 2.15, ionic strength of 0.1 M using NaCl) in a glass bottle with a polypropylene cap. The mixture was vigorously mixed for about 2 minutes using a vortex mixer to ensure a uniform dispersion. The suspension was equilibrated for about 72 hours at 25ºC in a shaker water bath to ensure complete saturation of indomethacin. The saturated suspension was vacuum filtered through a 30

μ nylon net filter using a stainless steel vacuum filtration device containing a stainless steel mesh to support the filter followed by a second filtration through a 3 μ polycarbonate filter. The seed crystals retained on the top of the 3 μ filters were redispersed in a saturated solution of indomethacin in a glass bottle. The final suspension was stored at 25ºC before being used in a crystal growth experiment. The particle size distribution, total surface area, and the mass median diameter of indomethacin seed crystals were determined before their use in a crystal growth experiment.

UV Spectroscopic Analysis

Indomethacin concentrations in clear solutions as well as in suspension samples were determined using 1-cm matched quartz cells (Starna Cells Inc., Atascadero, CA, USA) and a dual beam UV-Visible spectrophotometer (Lambda 40P, Perkin-Elmer Inc., USA). The indomethacin concentration in clear solutions was determined from the absorbance at 321 nm. The indomethacin concentration in suspensions was measured from the second derivative absorbance ($d^2A/d\lambda^2$ or A") at 295 nm. The second derivative UV absorbance was obtained by taking a second derivative of the original indomethacin UV absorption spectrum (wavelength range: 400 to 210 nm) with respect to the absorption wavelength. More detailed results obtained during the development of this method are provided in the Results section.

Indomethacin Phase Solubility Study

The intrinsic solubility of indomethacin was determined using the phase solubility method described by Higuchi and Connors.[149] An amount of indomethacin solid powder in excess of its saturation solubility was added to a glass vial with a PTFE lined screw cap containing pH 2.15 phosphate buffer to produce a 0.1% w/w suspension. The

mixture was shaken end-to-end at 25ºC in a rotary shaker. An aliquot (~9 mL) of the suspension was withdrawn at regular time intervals (1, 2, 3, and 5 days) and filtered through a 0.45 µ PTFE syringe filter, discarding the initial ~6 mL of filtrate to ensure saturation of the filter. Indomethacin concentration was determined by UV spectrophotometry. All measurements were determined at least in triplicate. The experiment was repeated using a higher suspension concentration (0.2% w/w) to determine the effect of amount of excess solid on the indomethacin intrinsic solubility value.

Indomethacin Seed Crystal Particle Size Distribution and Number Concentration

The particle size distribution of indomethacin seed crystals in suspensions was determined using a Coulter counter (Multisizer Z2, Beckman Coulter Inc., Miami, FL, USA) fitted with a 50 µ glass aperture tube and filled with clear indomethacin saturated solution, obtained by filtering the indomethacin saturated suspension through a 0.2 µ nylon membrane filter. Since the coincidence error in the Coulter counter measurement depended on the seed crystal concentration, the indomethacin seed crystal suspension samples were diluted as needed using the clear indomethacin saturated solution to maintain the coincidence error in the manufacturer recommended optimum range (~ 5%). The raw data obtained from the Coulter counter included the number of particles (per 1 mL of suspension) in 256 different size classes. Each size class contains a collection of particles in a size range represented by that class. The indomethacin seed crystal size distribution in the size range of 2 to 25 µ was determined by obtaining two Coulter counter measurements (each with 256 size classes) in the size ranges of 2 to 8 and 8 to 25 µ for each suspension sample. The seed crystal number concentration (# of seed crystals

per mL of suspension) was calculated by summing the number of particles in each size class in the range of 2 to 25 µ. Each size class represented the volume based diameter of the representative indomethacin seed crystal. Calibration of the Coulter counter was performed using 3 and 10 µ particle size standards (Beckman Coulter Inc., Miami, FL, USA).

Physical Form of Indomethacin Seed Crystals

Powder X-ray diffraction (PXRD) was used to determine the physical form of indomethacin seed crystals before and after crystal growth. Indomethacin seed crystal suspensions (before and after growth) were centrifuged for about 5 minutes at 12000 RPM. The clear supernatant solution was discarded and the solid collected in the bottom of the centrifuge tubes was air dried before PXRD analysis. PXRD patterns were obtained using an X-ray diffractometer (Bruker D8 Advance, Bruker AXS, Inc., Madison, WI, USA). The X-ray copper anode (1.54A) was operated at 40 kV and 40 mA. The scans were performed from 3 to 35º 2θ with 0.05° step size and 4 or 0.6 seconds step time.

Microscopic Evaluation of Indomethacin Seed Crystals

The shape and size of the indomethacin seed crystals were also characterized using a scanning electron microscope (Hitachi S4300) and a polarized light microscope. For scanning electron microscopy (SEM), the samples were prepared by filtering the indomethacin seed crystal suspension through a 0.2 µ nylon membrane filter. The seed crystals retained on the filter were air dried. A section of the filter membrane was cut and mounted on a scanning electron microscopy sample holder using graphite tape. In the case of polarized light microscopic analysis (PLM), the slide sample was prepared by

placing a small aliquot of indomethacin seed crystal suspension between a glass slide and a glass cover slip.

Indomethacin Crystal Growth Rate Measurement

Indomethacin crystal growth kinetics was measured at 25ºC in aqueous supersaturated suspensions of indomethacin seed crystals (pH 2.15) by determining the decline in indomethacin concentration (desupersaturation) at different time intervals online in a UV spectrophotometer (Figure 3.2). Supersaturation was attained by the controlled addition of approximately 100-150 µl of freshly prepared, highly concentrated (~120 µg/mL), high pH (6.8) indomethacin solution to 3 mL of the low pH indomethacin saturated suspension (pH 2.15) using a micro-syringe pump at an addition rate of 150 µl/min. The high pH indomethacin solution was in 50 mM phosphate buffer (pH 6.8, ionic strength of 0.1 M using NaCl). The bulk pH of the supersaturated indomethacin suspensions after the addition of a small amount of high pH (6.8) indomethacin solution remained below pH 2.2. The higher pH indomethacin stock solution was held in a gas tight syringe and the tip of the tubing from the syringe was immersed in the suspension to minimize possible entry of carbon dioxide into the high pH solution during its addition, thereby avoiding micro-bubble formation. The change in indomethacin concentration at different time intervals was measured by taking a second derivative of the original UV absorbance spectrum with respect to the absorption wavelength between 210 to 400 nm (λ_{max} =295 nm) to minimize the variability in indomethacin solution concentration measurements by removing the error from UV light scattering by indomethacin seed crystals in the sample. The homogeneity of the indomethacin concentration in the bulk solution was maintained via magnetic stirring using a pivoted rod-shaped magnetic stir

bar (400 RPM). Indomethacin crystal growth rates were measured at a degree of supersaturation *(S)* of 6, where *S*, also known as the supersaturation ratio, is defined by Eq. 3.10.

$$S = \frac{C}{C_s} \tag{3.10}$$

where c is indomethacin concentration immediately after supersaturation and c_s is the equilibrium solubility of indomethacin.

Indomethacin Dissolution Rate Measurement

Indomethacin seed crystal dissolution rates were measured to determine indomethacin mass transfer (diffusion) rate coefficients. The mass transfer rate coefficient from indomethacin dissolution was compared with the same from indomethacin crystal growth at a high degree of supersaturation (S=6) to verify the rate-limiting step in the indomethacin crystal growth process. Indomethacin seed crystal dissolution experiments were performed at 25ºC by two different experimental methods to compare their hydrodynamic conditions: (1) the USP Dissolution Apparatus II; and (2) the online UV assembly with a quartz cuvette and magnetic stirring. In both cases, a specific amount of indomethacin solid powder was added to the dissolution medium (50 mM phosphate buffer, pH 5.8, 130 RPM). The volumes of the bulk dissolution medium for method (1) and (2) were 250 mL and 3 mL, respectively. For method (1), ~3 mL of sample suspension was withdrawn at regular time intervals to measure indomethacin concentration using second derivative UV spectroscopy. For method (2), online measurements of indomethacin concentrations were obtained at regular time intervals.

Subsequently, indomethacin dissolution rates and, in turn, the mass transfer coefficients (Eq. 3.5) were also measured at pH 2.15 and 6.5 using method (2) at ~400 RPM. Here, dissolution was initiated by diluting indomethacin seed crystal suspensions (pH 2.15) with a specific volume of either pH 2.15 phosphate buffer or 0.1N NaOH to attain the final pH of 2.15 or 6.5, respectively. The final volume of the bulk dissolution medium was 3 mL.

Data Analyses

Non-linear least-squares analyses were performed using a software program, Scientist (Micromath Inc., St. Louis, MO, USA). The other statistical tests including the Student t-test and ANOVA were performed using Microsoft Excel. The lack-of-fit test analysis was performed using Scientist and Microsoft Excel.

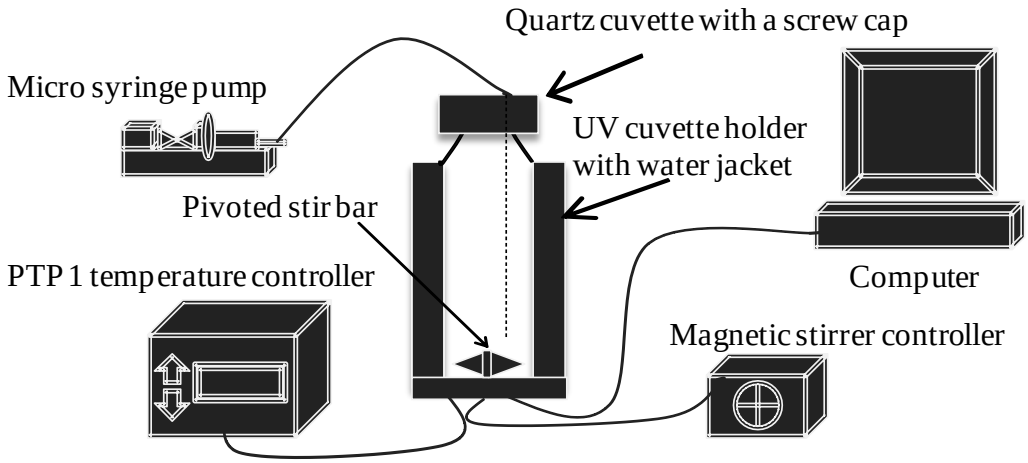

Figure 3.2. Schematic diagram describing the typical experimental assembly for the newly developed non-invasive (online) UV method to determine crystal growth kinetics of poorly water soluble drugs using second derivative UV spectroscopy and a crystal seeding technique.

RESULTS

Development of a Second Derivative UV Spectroscopic Method

Indomethacin crystal growth kinetics was determined by monitoring the change in indomethacin concentration (i.e., desupersaturation) versus time from its supersaturated seed crystal suspensions. While the precise measurement of indomethacin solution concentration was essential for obtaining reliable crystal growth rates, the presence of seed crystals in the supersaturated suspensions caused scattering of the incident UV light which in turn introduced variability in indomethacin concentration measurements. Second derivative UV spectroscopy was employed to alleviate the undesirable effect of the spectral interference on indomethacin concentration measurements. Figure 3.3 shows a representative spectrum of the indomethacin UV absorbance between 400 to 210 nm ($\lambda_{max} = 321\ nm$) and its second derivative with respect to the wavelength ($\lambda_{max} = 295\ nm$). Representative second derivative UV spectra of indomethacin at various concentrations are also shown in Figure 3.3 (inset). Effectiveness of the second-derivative UV method was tested by comparing indomethacin standard curves obtained from two different indomethacin standard solutions at varying concentrations: (1) clear indomethacin standard solutions, and (2) indomethacin standard solutions with added polystyrene latex particles (4.0×10^4 particles/mL). As shown in Figure 3.3, linear standard curves with correlation coefficients of 0.995 and 0.999 were obtained for indomethacin standard solutions with and without the scattering effect of polystyrene latex particles, respectively. The indomethacin response factors determined from the slopes of the linear standard curves (with and without scattering effect) were 42.4 and 43 ($abs \times nm^{-2} \times M^{-1}$),

respectively. This clearly indicated that the second derivative UV technique successfully eliminated the spectral interference (i.e., UV light scattering) caused by the presence of solid polystyrene latex spheres.

The robustness of the second derivative method was further validated by comparing the second derivative UV response factors obtained from the indomethacin standard curves containing varying concentrations of indomethacin seed crystals. Figure 3.3 (inset) the second derivative UV response factors at four different indomethacin seed crystal concentrations. The response factors were similar at different indomethacin seed crystal concentrations, which is indicative of the robustness of the method within the given range of solid particle concentrations.

Indomethacin Phase Solubility Study

The indomethacin intrinsic equilibrium solubility at 25ºC (pH 2.15; ionic strength: 0.1 M using NaCl) was determined to be $3.4 \pm 0.1 \times 10^{-6}$ M (95% CI). The equilibration time (i.e., time to attain saturation solubility) was determined by statistically comparing indomethacin concentrations of the samples drawn at 24, 48, 72, and 120 hour time intervals. As shown in Figure 3.4, the equilibration time for the indomethacin intrinsic solubility was 72 hours or 3 days ($p < 0.05$). At earlier time intervals (24 and 48 hours), samples with a higher amount of excess solid had higher indomethacin concentrations. However, the effect of the amount of excess solid on indomethacin intrinsic solubility was not statistically significant at the 72 and 120 hour time intervals ($p < 0.1$).

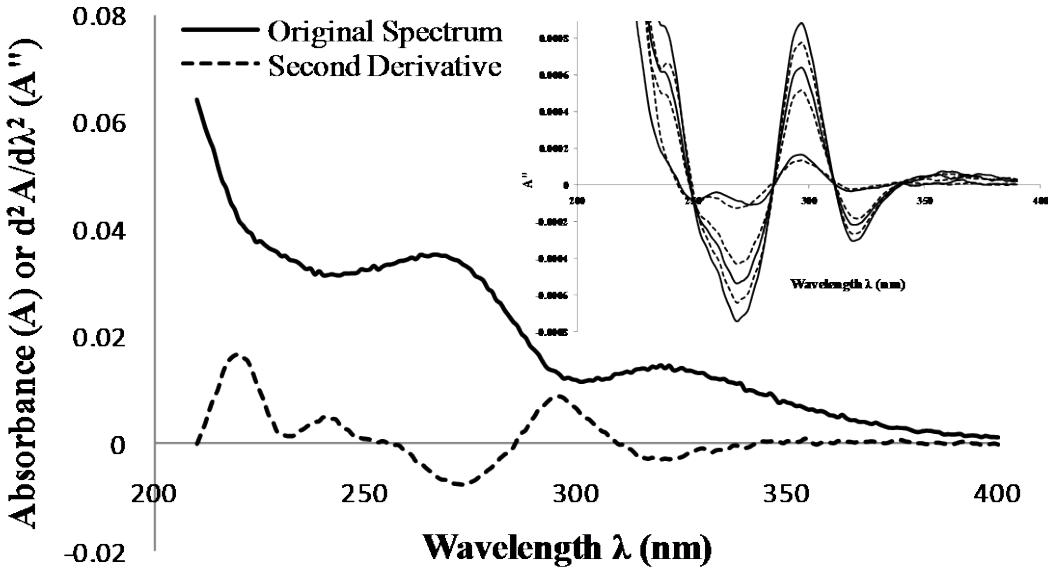

Figure 3.3. Representative indomethacin UV absorption spectra before and after second derivatization of absorbance with respect to wavelength. Inset: Representative indomethacin second derivative UV spectra at varying indomethacin concentrations.

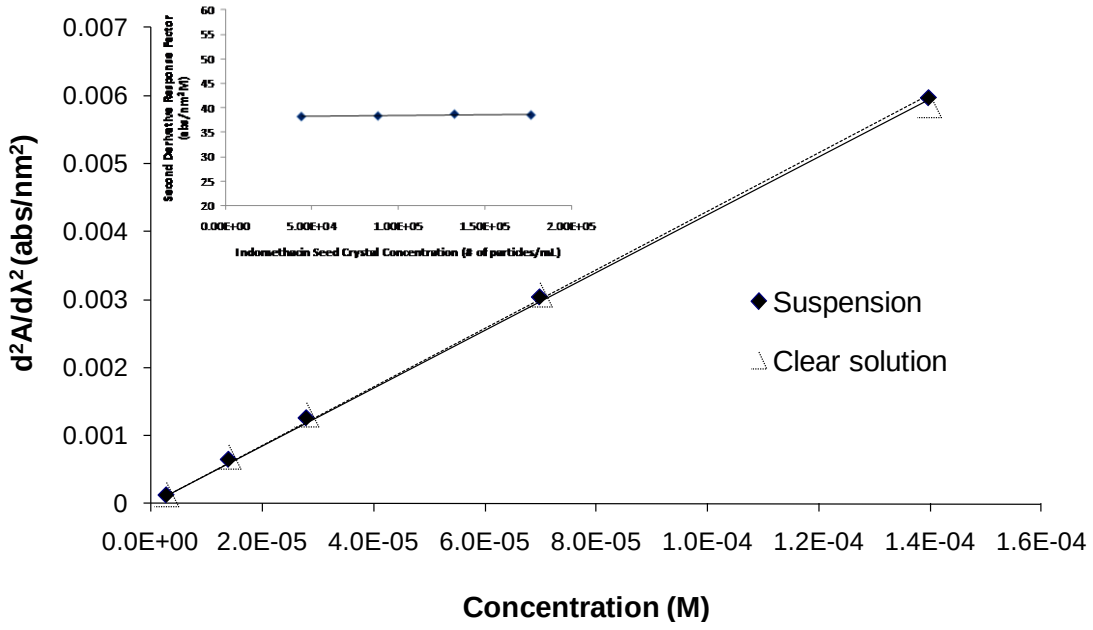

Figure 3.4. Second derivative UV absorbance standard curves of indomethacin clear solutions (Δ) and (♦) with added polystyrene latex spheres. Inset: Indomethacin second derivative response factors at different seed crystal concentrations.

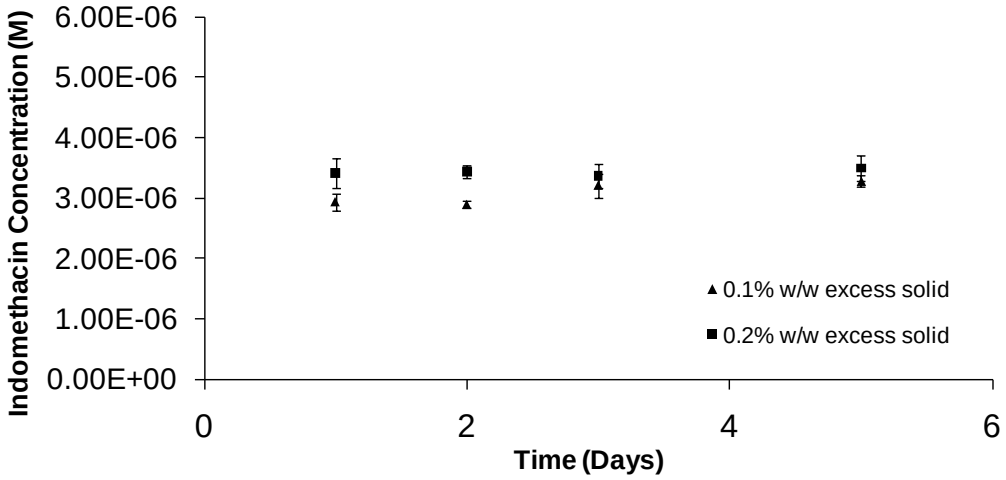

Figure 3.5. Effect of the amount of excess solid on indomethacin intrinsic equilibrium solubility. Error bars represent 95% confidence intervals (CI).

Indomethacin Seed Crystal Suspension Characterization Before and After Crystal Growth

Indomethacin seed crystal suspensions were characterized before and after crystal growth by determining their physical characteristics including size distribution, number concentration, morphology, and physical form. Raw particle size distribution data (number of particles in each volume based diameter size class) obtained from a Coulter counter measurement were converted into total volume of seed crystals in each size class. Indomethacin seed crystals were assumed to be spherical, and hence the values of the surface shape factor (β) and the volume shape factor (α) were chosen to be equal to π and $\pi/6$, respectively. Typical indomethacin seed crystal size distribution profiles (% volume vs. seed crystal diameter) are shown in Figure 3.6. The mass-median diameter (D_m) of indomethacin seed crystals was calculated using Eq. 3.11.

$$D_m = \frac{\sum n_i d_i^3}{\sum n_i d_i^2} \tag{3.11}$$

where n_i is the number of seed crystals in the i^{th} size class using a volume based diameter d. The typical mass median diameter of the indomethacin seed crystals was 11.1 ± 0.3 (95% CI) μ. The surface area of indomethacin seed crystals per unit volume (mL) of suspension was calculated using Eq. 3.12.

$$S_t = \beta \sum n_i d_i^2 \tag{3.12}$$

where β is the surface shape factor (3.14 based on the spherical shape assumption). The typical surface area of indomethacin seed crystals was $4.5 \pm 0.3 \times 10^{-2}$ (95% CI) cm^2 per mL of suspension. The number of indomethacin seed crystals per mL of

indomethacin suspension was $4.1 \pm 0.6 \times 10^4$ (95% CI). The typical seed crystal density in indomethacin suspension samples was ~50 µg/mL. In a typical crystal growth experiment (S=6), ~24 µg of indomethacin was deposited on the surface of ~160 µg of indomethacin seed crystals upon the completion of crystal growth.

A significant change in indomethacin seed crystal size characteristics including total surface area, total volume, and the mass median diameter could change the indomethacin crystal growth rate. Since the suspensions were mixed by magnetic stirring during crystal growth studies, the effect of magnetic stirring (e.g., attrition or agglomeration) on indomethacin seed crystal size distributions was evaluated by mixing the suspensions in the same manner as that employed in a typical growth study. As shown in Figure 3.6, the indomethacin seed crystal size distribution profiles before growth and after magnetic stirring with no growth were similar. There were no significant differences ($p < 0.05$) between the seed crystal size characteristics of the two indomethacin suspensions before growth vs. after magnetic stirring with no growth including total surface area ($4.6 \pm 0.8 \times 10^{-2}$ vs. $4.7 \pm 0.2 \times 10^{-2}$ cm^2/mL), total volume ($8.9 \pm 1.9 \times 10^{-6}$ vs. $8.7 \pm 0.6 \times 10^{-6}$ cm^3/mL), mass median diameter (11.3 ± 0.6 vs. 11.1 ± 0.7 µ), and the seed crystal concentration ($4.1 \pm 0.6 \times 10^4$ vs. $4.6 \pm 1.1 \times 10^4$ seed crystals/mL of suspension).

A comparison of the indomethacin seed crystal size distribution and seed crystal concentration after crystal growth (S=6) with those before growth indicated no significant change in the size distribution (Figure 3.6) or the seed crystal concentration after growth ($4.1 \pm 0.6 \times 10^4$ vs. $4.6 \pm 0.2 \times 10^4$ seed crystals/mL of suspension).

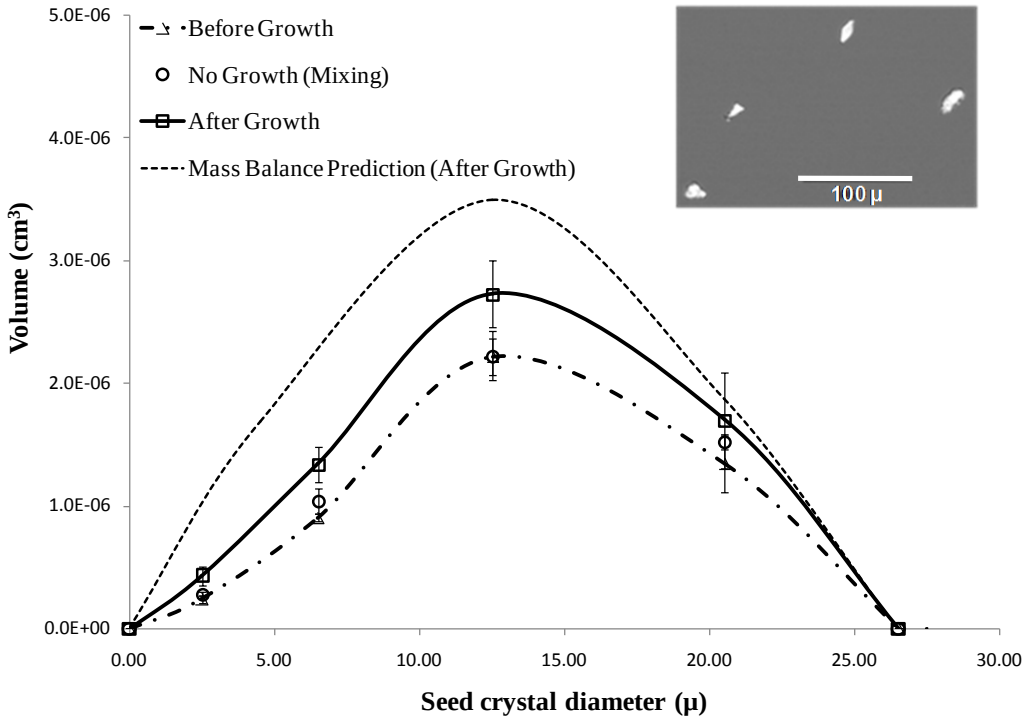

Figure 3.6. Representative indomethacin seed crystal particle size distributions from suspension samples before growth (Δ), only mixing by magnetic stirring with no growth (○) and after growth (□) as well as the predicted size distribution (broken line) after crystal growth (S=6) using the mass balance relationship (Eq. 3.8 & 3.9). Error bars represent SEM (n=3). Inset: A representative polarized optical micrograph of indomethacin seed crystals.

The absence of a significant difference between the seed crystal concentration before and after growth ($p < 0.05$) seems to rule out significant primary nucleation of indomethacin seed crystals.

The shape characteristics of indomethacin seed crystals were analyzed by microscopy (PLM & SEM). Representative micrographs of indomethacin seed crystals from PLM and SEM are shown in Figure 3.6 (inset) and Figure 3.7, respectively. The polarized light micrograph qualitatively confirmed the crystalline nature of indomethacin seed crystals. The SEM analysis of indomethacin seed crystals indicated that the crystals were of cuboid shape. Furthermore, no particles with significantly different geometry (e.g., needles) could be detected from comparisons of several SEM micrographs of indomethacin seed crystals before and after crystal growth, which again suggests the absence of primary nucleation of different indomethacin forms.

The physical form of indomethacin seed crystals before and after crystal growth was determined by PXRD. PXRD patterns of three different indomethacin seed crystal samples including original indomethacin powder as received (γ polymorph) and indomethacin seed crystals before and after growth are shown in Figure 3.8. The PXRD patterns of indomethacin seed crystals before and after crystal growth matched the PXRD patterns of original indomethacin powder, indicating that no change in the crystalline nature or polymorphic form of indomethacin seed crystals could be detected after crystal growth.

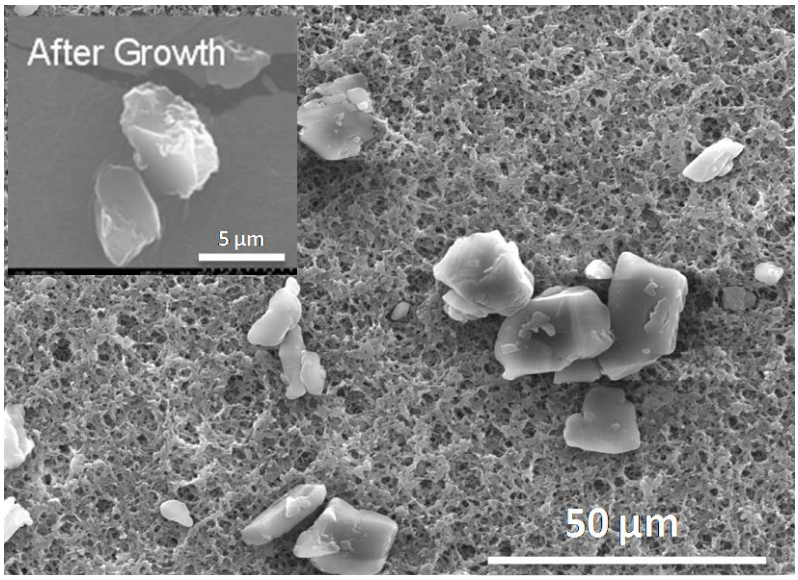

Figure 3.7. Representative scanning electron micrographs of indomethacin seed crystals before and after crystal growth (inset).

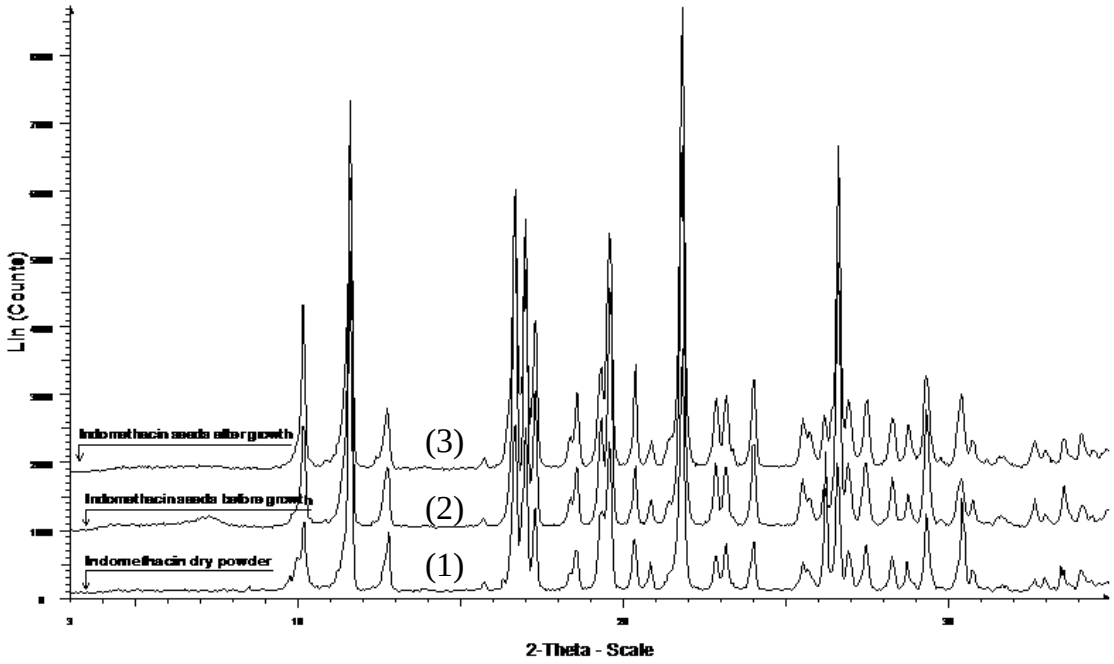

Figure 3.8. Comparison of PXRD patterns of various indomethacin seed crystals samples: (1) indomethacin powder (as received), (2) indomethacin seed crystals before crystal growth, and (3) indomethacin seed crystals after crystal growth.

Indomethacin Crystal Growth Kinetic Modeling

Representative indomethacin desupersaturation kinetic profiles (n=5) at the degree of supersaturation of 6 are shown in Figure 3.9 (solid circles). The desupersaturation kinetic profiles were fitted to the empirical crystal growth kinetic model (Eq. 3.3) with the apparent order of crystal growth *(g)* set equal to 1. The apparent crystal growth rate coefficient *(k_G)* and the equilibrium solubility *(c_s)* were used as fitting parameters. As shown in Figure 3.9 (solid line), the crystal growth profiles were fit well using the first order empirical crystal growth kinetic model. The apparent equilibrium solubility after crystal growth, henceforth defined as the apparent solubility, was 5.2 ± 0.6 × 10^{-6} M (95% CI). The apparent solubility of indomethacin seed crystals after crystal growth was significantly higher ($p < 0.05$) than the equilibrium solubility before growth (3.4 ± 0.2 × 10^{-6} M). Here, the equilibrium solubility before growth represents the indomethacin concentration in saturated indomethacin seed crystal suspensions before their use in crystal growth experiments. It should also be noted that the solubility before growth was similar to the indomethacin equilibrium solubility determined from the phase solubility studies (3.4 ± 0.1 × 10^{-6} M).

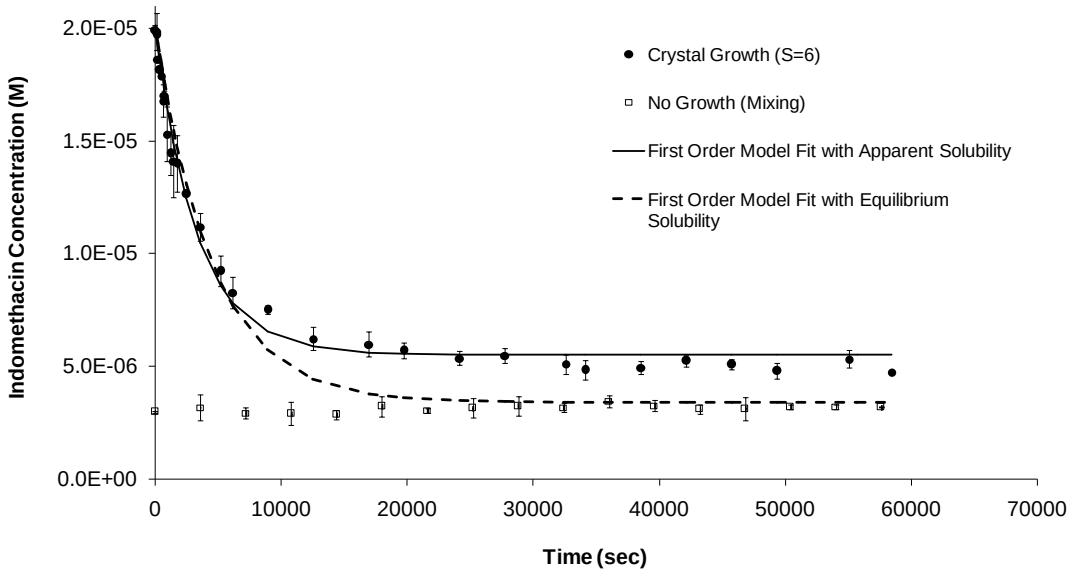

Figure 3.9. A representative desupersaturation profile (●) from indomethacin crystal growth experiments (S=6). The broken line represents the first order empirical crystal growth model (Eq. 3.3) fit using the initial equilibrium solubility value measured before crystal growth; the solid line represents the first order empirical crystal growth model fit using the apparent equilibrium solubility value measured after crystal growth. The open squares (□) represent the effect of only mixing (magnetic stirring) without any crystal growth on indomethacin equilibrium solubility. Error bars represent 95% confidence intervals.

Indomethacin Apparent Solubility and the Apparent Order of the Crystal Growth Process

The apparent indomethacin solubility after crystal growth was about 55% higher than the equilibrium solubility before growth. The value chosen for the equilibrium solubility can affect the kinetic model that best fits the desupersaturation profiles. As shown in Figure 3.9 (solid line), the crystal growth kinetic profiles were fit well by a first order crystal growth model when the value of solubility at infinity was fixed at the higher apparent solubility found after crystal growth. However, the first order model gave a poor fit (Figure 3.9; dashed line) when the equilibrium solubility before growth was selected. The kinetic profiles were re-analyzed using the same model but with the apparent order of crystal growth process *(g)* included as a fitted parameter. This approach provided a value for *g* of 1 when the higher apparent solubility was employed whereas the value of *g* increased from 1 to 1.5 when the equilibrium solubility before growth was selected. These results clearly indicated that the apparent order of the crystal growth process depends critically on the indomethacin solubility value employed. Hence, additional experiments were conducted to verify the change in indomethacin solubility after crystal growth.

During the crystal growth experiment, the homogeneity of indomethacin concentration in the bulk solution was maintained by magnetic stirring. One hypothesis for the change in indomethacin solubility considered was that the surface energy of the indomethacin seed crystals could be altered by the mechanical shear forces created by magnetic stirring during crystal growth experiments. The higher surface energy could in turn provide a higher apparent solubility after crystal growth. Hence, the effect of magnetic stirring on indomethacin solubility was determined by measuring indomethacin

concentration in stirred suspensions over time. The results indicated that magnetic stirring did not change the solubility (Figure 3.9, open squares). The solubility measured from this study ($3.2 \pm 0.1 \times 10^{-6}$ M) was similar to the solubility obtained from the phase-solubility studies ($3.4 \pm 0.1 \times 10^{-6}$ M). This clearly indicated that magnetic stirring during a crystal growth experiment does not produce the higher apparent solubility values of indomethacin observed after crystal growth.

Since the indomethacin apparent solubility after approximately 0.67 day (16-hour) crystal growth experiments (Figure 3.9, solid circle) was ~55% higher than the equilibrium solubility before growth, it was essential to explore the length of time this higher apparent solubility remained constant after growth. Multiple crystal growth experiments with durations of greater than 0.67 day were performed. A representative desupersaturation profile from a 7 day long crystal growth experiment is shown in Figure 3.10 indicating that the higher apparent solubility remained constant at around 5 μM even after 7 days. A comparison of indomethacin apparent solubility after 0.67, 1, 3, 5, and 7 day long crystal growth experiments is shown in Figure 3.10 (inset). The apparent indomethacin solubility after 0.67 day was similar to those obtained after 1, 3, 5 and 7 days indicating that the crystal growth process had reached an equilibrium (or pseudo-equilibrium) concentration after 0.67 day (16 hours) of crystal growth.

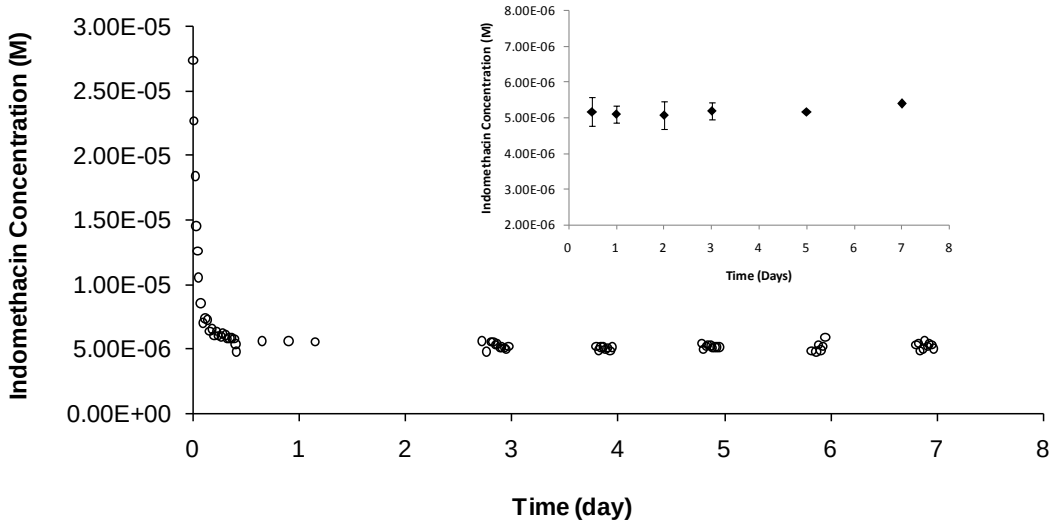

Figure 3.10. Indomethacin concentration vs. time (day) profile from a 7-day long indomethacin crystal growth study to verify the apparent indomethacin solubility after crystal growth. Inset: Comparison of indomethacin equilibrium concentrations after crystal growth at different time intervals to verify the apparent indomethacin solubility after crystal growth.

After verifying the long-term stability of the higher indomethacin apparent solubility after crystal growth, the apparent order of the overall indomethacin crystal growth process at higher degrees of supersaturation (S=6) was determined by conducting a lack-of-fit analysis using different values of g. The crystal growth kinetic profiles were fit to the empirical crystal growth model (Eq. 3.3) with varying apparent order of the crystal growth process (g = 0, 1, 2, and 3). A statistical lack-of-fit test analysis was performed for the model fits and the results from the analysis are shown in Table 3.1. The calculated F value was the smallest for the first order model (g = 1). The rank ordering of the models based on their calculated F values was first order < second order < third order < zero order. The rank ordering clearly indicated that the first order model provided the best fit for indomethacin crystal growth profiles at a degree of supersaturation of S = 6. Moreover, only the first order model successfully met the requirements of the lack-of-fit test analysis ($p < 0.05$) out of all four kinetic models.

Indomethacin Crystal Growth Rate-limiting Step

After determining the apparent order (g = 1) from the indomethacin crystal growth kinetics, the indomethacin mass transfer coefficients from its crystal growth and dissolution were compared using similar conditions including similar seed crystal suspensions. The hypothesis was that in the case of bulk diffusion rate limited indomethacin crystal growth, the mass transfer coefficients determined from indomethacin crystal growth would be similar to the same obtained from its dissolution, which is known to reflect a bulk diffusion rate limited process.[150]

Table 3.1. Statistical (Lack-of-Fit) Analysis of Fitting of Indomethacin Crystal Growth Kinetic Data using Empirical Crystal Growth Model (Eq. 3.3) with Varying Apparent Order of Crystal Growth Process.

Apparent Order of Crystal Growth Process (*g*)	Sum of Squares (Residual)	Sum of Squares (Lack of Fit)	*F* value (Calculated)	*F* value (Critical; α=0.05)
0	1.88×10^{-09}	1.87×10^{-09}	320	
1	2.27×10^{-11}	9.28×10^{-12}	1.59	1.72
2	8.33×10^{-11}	6.99×10^{-11}	12	
3	2.39×10^{-10}	2.25×10^{-10}	39	

The indomethacin mass transfer coefficient from powder dissolution was determined using the online UV method that included a quartz cuvette and magnetic stirring. Since the hydrodynamic conditions were not pre-defined for the online UV method, the indomethacin dissolution profile from the online UV method was compared with that from the standardized USP Dissolution Apparatus II method, which uses well defined hydrodynamic conditions. The dissolution profiles (pH 5.8) generated by the two different methods using the same indomethacin seed crystal suspension were similar (Figure 3.11 (inset)), indicating that the hydrodynamic conditions in both methods are similar. Subsequently, indomethacin dissolution profiles at two different pH values (2.15 and 6.5) were determined using the online UV method. A representative indomethacin dissolution kinetic profile at pH 6.5 is shown in Figure 3.11. The indomethacin mass transfer coefficients *(k_d)* were estimated from fitting the dissolution profile to the diffusion layer model (Eq. 3.5). The indomethacin mass transfer coefficients determined from the dissolution (pH 6.5 and 2.15) of indomethacin (Table 3.2) indicate that the bulk pH of the dissolution medium did not affect the indomethacin mass transfer coefficient significantly. This was attributed to the presence of 50 mM phosphate buffer in the dissolution medium at pH 2.15 as well as 6.5, which resisted the formation of pH gradients in the diffusion layer. Moreover, the mass transfer coefficients determined from indomethacin crystal growth kinetic profiles (pH 2.15) at a degree of supersaturation of $S = 6$ were similar to the same obtained from indomethacin dissolution (Table 3.2), a further indication that indomethacin crystal growth at this degree of

supersaturation is a bulk diffusion rate limited process. As shown in Eq. 3.5, from the indomethacin mass transfer coefficients, the diffusion layer thickness for the indomethacin seed crystals was estimated. The diffusion coefficient of indomethacin used in the calculation was 5.6×10^{-6} cm^2/sec.[148] The diffusion layer thicknesses estimated from indomethacin dissolution and crystal growth were 11.5 ± 4.0 and 11.5 ± 2.1 (95% CI) μ, respectively. The estimated diffusion layer thicknesses were similar to the mass median diameter of the indomethacin seed crystals (11.1 ± 0.3 (95% CI) μ) used in the dissolution and crystal growth experiments. This was in good agreement with previously published measurements of the diffusion layer thickness from bulk diffusion controlled dissolution studies.[151,152]

Prediction of Seed Crystal Size Distribution after Growth

The change in indomethacin seed crystal size distribution upon crystal growth at a high degree of supersaturation of S=6 was predicted using the mass balance relationship (Eq. 3.8 & 3.9) for bulk diffusion controlled crystal growth of a population of seed crystals. In the size prediction modeling, the diffusion layer thickness (h_i) of the seed crystals in the i^{th} size class was assumed to equal the mass-median diameter (D_{mi}). The seed crystal density (ρ_c) of indomethacin[135] was 1.37 g/cm^3. The size predictions using Eq. 3.8 & 3.9 were obtained from the numerical simulations provided by the software program, Scientist.

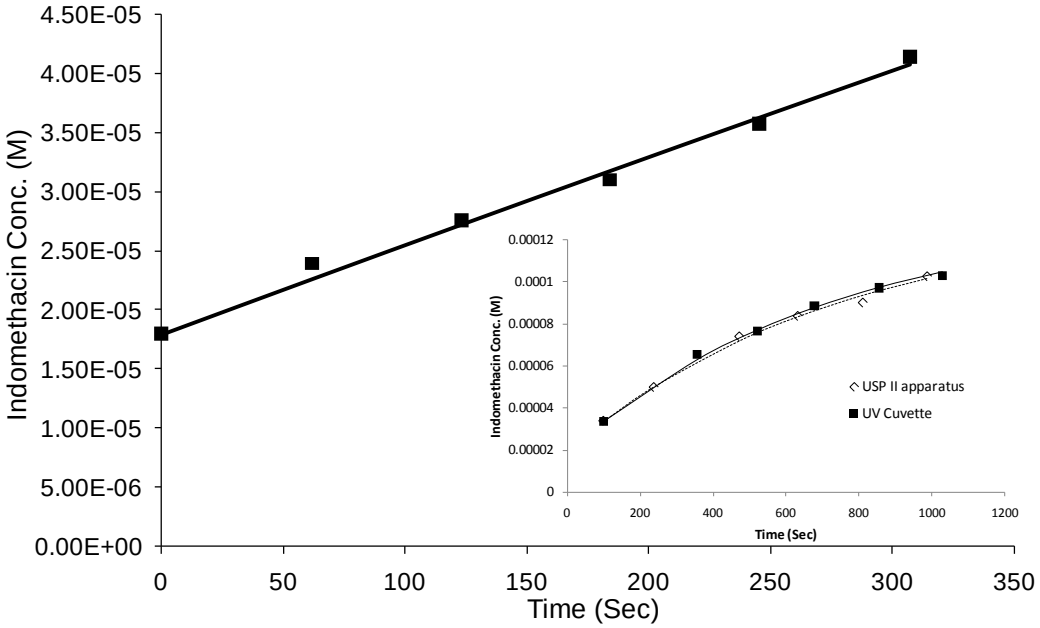

Figure 3.11. A representative indomethacin powder dissolution kinetic profile (bulk pH 6.5). The solid line represents the first-order diffusion layer (or thin layer) model fit (Eq. 3.5). Inset: A comparison of indomethacin dissolution profiles determined using the USP Dissolution Apparatus II method as well as the online UV method (quartz cuvette and magnetic stirring).

Table 3.2. Comparison of Mass Transfer Coefficients (± 95% CI) Determined from Indomethacin Dissolution and Crystal Growth (S = 6) Studies.

pH	Mass Transfer Coefficient (cm/sec)	
	Dissolution (k_d)	**Crystal Growth (k_G)**
pH 2.15	$4.6 \pm 2.0 \times 10^{-03}$	$4.7 \pm 0.7 \times 10^{-03}$
pH 6.5	$4.8 \pm 1.7 \times 10^{-03}$	

As shown in Figure 3.6, the size predictions in the larger particle size range (>15 μ) were in excellent agreement with the experimentally measured sizes but there was overall a greater increase in particle volume predicted than obtained. The predicted sizes after growth for the smaller seed crystals (<15 μ) were larger than those measured. These differences were mainly attributed to the fact that sample dilutions for the Coulter counter size measurements employed diluent solutions that were saturated using the "before" growth indomethacin crystals. Indomethacin concentrations of the after growth suspension and the saturated diluent were $5.2 \pm 0.6 \times 10^{-6}$ M (95% CI) and $3.4 \pm 0.1 \times 10^{-6}$ M, respectively. This indomethacin concentration difference provided a driving force for some re-dissolution, which would have preferentially re-dissolved seed crystals in the smaller size range.

DISCUSSION

Development of Techniques to Study Indomethacin Crystal Growth Kinetics

Supersaturation of poorly water soluble compounds can be prolonged by the presence of suitable excipients in the system. The beneficial effects of excipients on the maintenance of supersaturation may be attributable either to the inhibition of nucleation or crystal growth or both. To develop a quantitative and mechanistic understanding of excipient effects on the maintenance of supersaturation by nucleation or crystal growth inhibition, it is essential to determine the parameters that govern nucleation or crystal growth kinetics of poorly water soluble compounds. Previous kinetic studies have monitored solute concentration vs. time (i.e., desupersaturation) profiles during nucleation or crystal growth.[2-6,42,43] However, some of the sampling methods including syringe filtration and centrifugation used to determine solute concentrations in

supersaturated systems could easily lead to erroneous results mainly due to unwanted loss of solute concentration during sampling. When supersaturated samples come into contact with solid surfaces such as syringes, filter membranes, and centrifuge tubes nucleation and/or solute adsorption may occur. Recently, non-invasive and online methods consisting of spectroscopic techniques such as ATR-FTIR,[144] Raman,[17] and fluorescence[20] have been employed to measure desupersaturation profiles without the risk of sampling errors. The present study describes an online second derivative UV spectroscopic method to monitor crystal growth kinetics of the poorly water soluble drug indomethacin. The second derivative technique provided robust measurements at varying seed crystal concentrations (4.41×10^4 - 1.76×10^5 particles/mL).

The newly developed online UV assembly utilized magnetic stirring. The development and validation of the seeding method involved not only the steps to obtain narrow, unimodal seed size distributions but also the determination of any change in seed size and number upon mixing by magnetic stirring. A pivoted magnetic stir bar was selected from a range of stir bars with different shapes and characteristics to minimize any effect of stirring on seed crystal size distribution (data not shown). Since desupersaturation can occur due to primary nucleation at high degrees of supersaturation, a fine balance existed between the number of seed crystals (i.e., total available surface area for growth) and the highest possible degree of supersaturation that could be achieved. The seed crystal concentration range was limited by the ability of the second derivative technique to reliably measure indomethacin concentrations near its intrinsic solubility range, whereas higher degrees of supersaturation were limited by spontaneous primary nucleation manifested by a sharp increase (close to an order of magnitude) in

seed crystal concentrations. The prevention of primary nucleation using the seeding technique was tested by comparing the seed crystal concentrations before and after a crystal growth experiment. In a systematic study (data not shown), the optimum range of seed crystal concentrations and the degree of supersaturation was determined. The maximum achievable degree of supersaturation without any primary nucleation was about 6 for the seed crystal concentration range of 4.41×10^4 - 1.76×10^5 particles/mL. Therefore, the crystal growth experiments were conducted at an S of 6 or below.

Indomethacin Phase Solubility Study

Indomethacin was chosen as the model compound in the present study due to its low intrinsic solubility (~1 µg/mL) and the availability of physical characterization data in the existing literature. Indomethacin physicochemical properties including solubility[132,133] and stability[130] in aqueous solutions have been characterized previously. Indomethacin decomposes in aqueous solution by hydrolysis. Since indomethacin hydrolysis is significantly slower at low pH and the degradation half life is significantly longer than the equilibration time for solubility and crystal growth experiments, its effect on indomethacin intrinsic solubility and crystal growth rate determinations at pH 2.15 was considered negligible. The intrinsic solubility of indomethacin determined in the present study is $3.4 \pm 0.1 \times 10^{-6}$ (95% CI) M. Hancock et al.[132] reported the solubility of indomethacin in deionized water at 25ºC as ~5 µg/mL (~1.4×10^{-5} M). Wassvik et al.[133] reported an intrinsic solubility of $1.12 \pm 0.03 \times 10^{-6}$ M. The higher indomethacin solubility reported by Hancock et al. is in accordance with the solubility enhancement provided by indomethacin ionization at the higher pH (>pKa) that would result from dissolution in deionized water. The lower indomethacin solubility reported by Wassvik

et al.[133] reflects a lower equilibration temperature (21ºC) and shorter equilibration time (24 hr) as compared to the present study.

Relationship between Indomethacin Crystal Growth Kinetics and its Equilibrium Solubility

Several methods have been described in the crystal growth literature[24,92,93] for crystal growth rate measurement including the use of a single crystal vs. a population of crystals (multiparticulate), growth rate determination from the change in crystal properties (e.g., mass or size) vs. change in solution properties (e.g., solution concentration), and isothermal vs. non-isothermal conditions. Each technique has its own advantages and limitations. For example, the single crystal measurement technique is advantageous in terms of measuring the growth rate of a specific crystal face of interest. However, the availability of a very small surface area limits the ability to achieve high degrees of supersaturation in comparison to multiparticulate systems and results in a higher sensitivity to the presence of impurities (even at very low concentrations). The advantages of the multiparticulate method, also known as batch crystallization, chosen for this study are: (1) its relevance to the in-vivo GI conditions in terms of maintaining supersaturation after primary nucleation, (2) its simplicity, and (3) a low sensitivity to small differences in crystal shapes or to non-uniformity of the number of dislocations on crystal surfaces. A limitation of this method is that it gives an average of crystal growth rates from individual faces of the crystal.[93]

The apparent solubility of indomethacin after crystal growth was approximately 55% higher as compared to before growth. Since the solubility of a solute defines its thermodynamic activity at the solid-liquid interface in a crystal growth process, it is

essential to know its exact value to determine the true thermodynamic driving force for a crystal growth process (Figure 2.3). An array of validation studies confirmed that the equilibrium solubility was altered after crystal growth. Possibly, the apparent equilibrium after crystal growth reflects a metastable state and after a long equilibration time the system would re-establish a true equilibrium (same as before growth). However, a comparison of indomethacin equilibrium concentrations after 0.67, 1, 3, 5, and 7 day crystal growth experiments showed that the apparent equilibrium concentration did not change significantly indicating that the crystal growth process had reached an apparent equilibrium (or pseudo-equilibrium). It was therefore hypothesized that the newly grown surface could be of higher energy either due to the presence of higher disorder (i.e., higher density of high energy sites such as kinks) or due to the secondary nucleation of a metastable polymorph such as the α-polymorph of indomethacin on the existing seed crystals of the more stable γ-polymorph. While the absence of a change in the seed crystal polymorphic form detected by PXRD indicated that the primary nucleation of any new indomethacin polymorph did not occur during crystal growth, the inability of the PXRD technique to detect small crystal packing or conformational differences at the surfaces of seed crystals before and after growth is worth noting. The diffraction pattern measured by the PXRD technique is dominated by the signal from the core or bulk of the material, and hence the contributions from small differences on the surface are undetectable.[139,153,154] Theoretical calculations, described below, were performed to explore the possibility that the α polymorph formed on the surface of seed crystals.

As mentioned earlier, the two major polymorphs of indomethacin are the γ and α polymorphs. The γ-polymorph used in these crystal growth studies is thermodynamically

more stable. The metastable α-polymorph of indomethacin has a lower heat of fusion and lower melting point[135]. The heat of fusion (ΔH_m) and the melting point (T_m) of the two polymorphs were obtained from the literature[127,132,135,155] and are compared in Table 3.3. The ideal solubility of indomethacin at 25 ºC can be calculated using the following ideal solubility equation (Eq. 3.13).[156]

$$\ln X = -\frac{\Delta H_m (T_m - T)}{RTT_m} + \frac{\Delta C_p}{R}\left[\frac{(T_m - T)}{T} + \ln\frac{T_m}{T}\right] \tag{3.13}$$

where X is the ideal mole fraction solubility, ΔC_p is the heat capacity difference between the liquid and solid phases of the solute and T is temperature. If it is assumed that the heat capacity for both phases is similar, the following equation can be derived from Eq. 3.13:

$$\ln X = -\frac{\Delta H_m (T_m - T)}{RTT_m} \tag{3.14}$$

In the above equation, the calculation of the free energy difference between two phases (i.e., solid and liquid) assumes that the enthalpy and entropy differences are temperature independent and equal to ΔH_m and $\Delta H_m/T_m$, respectively. Eq. 3.14 is more suitable for calculating the mole fraction solubility at higher temperatures close to T_m. Alternatively, an extended form of Eq. 3.14 was derived by Hoffman[157] (Eq. 3.15) to predict solubility at temperatures well below T_m.

$$\ln X = -\frac{\Delta H_m (T_m - T)}{RT_m^2} \tag{3.15}$$

Using Eq. 3.14 and 3.15, the mole fraction solubilities of the two indomethacin polymorphs were calculated at 25ºC (Table 3.4). Since the values of the heat of fusion and melting point of indomethacin polymorphs, especially for α-polymorph, varied significantly in the literature (Table 3.3), averages of the predicted solubilities with 95% CI are shown in Table 3.4. The Hoffman equation (Eq. 3.15) predicted significantly higher solubilities for indomethacin polymorphs as compared to the ideal solubility equation (Eq. 3.14). Ratios of the calculated solubilities (α-polymorph/ γ-polymorph) were compared with the ratio of experimentally determined solubilities of indomethacin seed crystals after and before crystal growth (Table 3.4). There was no significant difference between the two theoretical solubility ratios and the experimental solubility ratio. Moreover, the experimental solubility ratio was very similar to the theoretically predicted solubility ratio using the Hoffman equation (Eq. 3.15). These results suggest that a metastable α-polymorph may be growing on the seed crystals of γ-polymorph during indomethacin crystal growth, which in turn could explain the higher apparent solubility of indomethacin seed crystals after crystal growth.

Table 3.3. Heat of Fusion and Melting Point of Indomethacin Polymorphs

Literature Reference	Heat of Fusion (ΔH_m, J/g)		Melting Point (T_m, °C)	
	γ-polymorph	α-polymorph	γ-polymorph	α-polymorph
Legendre et al.[127]	103	92	159.1	153
Andronis et al.[135]	110	91	161	155
Hancock et al.[132]	102	101	162	156
Urakami et al.[155]	102[a]	98.9[b]	163	157

[a] 36.5 kJ/mol
[b] 35.4 kJ/mol

Table 3.4. Comparison of Theoretical Solubility (± 95% CI) of Indomethacin Polymorphs with Experimental Indomethacin Solubility (Before and After Crystal Growth, ± 95% CI)

Indomethacin Solid Form	Solubility[a,b]	Solubility Ratio
γ-polymorph[c]	$9.0 \pm 1.4^{a} \times 10^{-3}$	1.8 ± 0.7
α-polymorph[c]	$1.5 \pm 0.4^{a} \times 10^{-2}$	
γ-polymorph[d]	$3.9 \pm 0.4^{a} \times 10^{-2}$	1.4 ± 0.4
α-polymorph[d]	$5.4 \pm 0.9^{a} \times 10^{-2}$	
Seed crystal before growth	$3.4 \pm 0.2^{b} \times 10^{-6}$	1.5 ± 0.1
Seed crystals after growth (S = 6)	$5.2 \pm 0.6^{b} \times 10^{-6}$	

[a] Mole fraction
[b] Moles/liter
[c] An average of indomethacin solubilities calculated using the ideal solubility equation (Eq. 3.14) and the physical property values listed in Table 3.3
[d] An average of indomethacin solubilities calculated using the Hoffman equation (Eq. 3.15) and the physical property values listed in Table 3.3

As shown in Figure 3.9, the first order empirical crystal growth model did not fit the indomethacin crystal growth kinetic experimental data when the driving force was calculated using the original indomethacin equilibrium solubility. A value for the apparent order of crystal growth process as high as 1.5 was required to fit the data. Since the saturated indomethacin seed crystal suspension reached a different equilibrium concentration after a crystal growth experiment, it is obvious that assuming the original indomethacin equilibrium solubility throughout the experiment could lead to an overestimation of the driving force for crystal growth. The first-order empirical crystal growth kinetic model fit the experimental data well when the apparent (or observed) equilibrium solubility value was used to determine the driving force for crystal growth.

Rate-limiting Step of Indomethacin Crystal Growth Kinetics at a High Degree of Supersaturation

The similarity between the indomethacin mass transfer coefficients from its crystal growth and dissolution indicated that the crystal growth of indomethacin at a high degree of supersaturation of S=6 was a bulk diffusion rate limited process. The indomethacin mass transfer coefficients were initially determined at higher pH (~6.5) as the higher indomethacin solubility at pH 6.5 would provide higher driving force, and in turn, faster dissolution. However, the pH at the dissolving solid surface may be lower than the bulk pH during the dissolution of weak acids in higher pH (> pKa) dissolution media.[148,158] Since a pH gradient in the diffusion layer could result in an overestimated mass transfer coefficient if not taken into account, the pH at the dissolving solid surface of indomethacin (pKa[148] 4.17) particles was estimated using the reactive diffusion layer model described in detail by Mooney et al.[148] and Ozturk et al.[158] These calculations

gave a solid surface pH of 6.44, not significantly different from the measured bulk pH (6.46). This lack of difference was attributed to the presence of 50 mM phosphate buffer in the dissolution medium. Moreover, the similarity between the mass transfer coefficients determined at pH 6.5 and 2.15 confirmed the absence of pH gradient effects (at pH 2.15, which is below the pKa of indomethacin, one would not expect a pH gradient in the diffusion layer since indomethacin would not ionize upon dissolution). Therefore, the mass transfer coefficient, and in turn, the thickness of the diffusion layer were calculated by fitting the experimental dissolution profiles (pH 6.5) to the diffusion layer model (Eq. 3.5). The value for the diffusion coefficient of indomethacin used in the calculation of the diffusion layer thickness was 5.6×10^{-6} cm^2/sec.[148] Mooney et al.[148] compared indomethacin diffusivity values that were derived from various sources including the Levich plot (dissolution by the rotating disc method at 25ºC, pH 2, μ 0.5), the Stokes-Einstein equation, and the square root of molecular weight relationship. The indomethacin diffusivity values from these sources were 5.6×10^{-6}, 4.8×10^{-6}, and 5.6×10^{-6} cm^2/sec, respectively. The similarity between the estimated diffusion layer thickness and the mass median diameter of indomethacin seed crystals was in good agreement with the widely accepted tenet in the dissolution literature stating that the diffusion layer thickness of spherical particles below a specific size is generally equal to the particle mass median diameter or radius.[150-152,159] In earlier studies, investigators including Hixson and Crowell[160] as well as Higuchi and Hiestand[150] assumed that diffusion layer thickness correlated with particle size for all size ranges. For example, Higuchi and Hiestand[150] employed the diffusion layer thickness as approximately equal to or larger than the particle radius. Later, Hintz and Johnson[161] introduced the concept of a diffusion

layer thickness that matches the particle size for particles up to 30 µ, while remaining constant at 30 µ for larger particles. Recently, De Almeida et al.[151] have shown that the thickness of the diffusion layer for ibuprofen particles below 22 µ was linearly proportional to the particle diameter. Simoes et al.[162] found the diffusion layer thickness equal to the particle diameter from the dissolution of 5-15 µ indomethacin particles. Galli[152] reported diffusion layer thicknesses of 0.3 to 8.5 µ for particles with diameters in the range of 0.5 to 5.9 µ. Sheng et al.[159] determined the diffusion layer thickness from fenofibrate powder dissolution to be equal to 1.71 and 1.59 times the particle radius for particles below 37.7 µ (50 RPM) and 23.7 µ (100 RPM), respectively. The similarity between the estimated thickness of the diffusion layer and the mass median diameter of indomethacin seed crystals in the present study also verified that the indomethacin crystal growth kinetics at higher degrees of supersaturation were bulk diffusion rate controlled.

CONCLUSIONS

A non-invasive, online, simple and reliable method to determine crystal growth rates using a batch crystallization technique and second derivative UV spectroscopy has been developed. The second derivative UV spectroscopy successfully removed the spectral interference due to the presence of seed crystals in the crystal growth samples during indomethacin concentration measurements. The presence of seed crystals obviated primary nucleation of indomethacin at higher degrees of supersaturation during crystal growth. The apparent equilibrium solubility of indomethacin after crystal growth was about 55% higher than its equilibrium solubility, which could be attributed to the growth of a higher energy indomethacin form on seed crystals of the thermodynamically most stable form. The first order desupersaturation kinetic profiles and the similarity

between the mass transfer coefficients determined from indomethacin powder dissolution and crystal growth clearly indicated that the indomethacin crystal growth at a high degree of supersaturation of S=6 is bulk diffusion rate limited. Currently, studies are underway to determine the effect of model excipients on bulk diffusion rate limited indomethacin crystal growth using the techniques and models developed in this study. The long term goal of this project is to develop a quantitative and mechanistic understanding of model excipient effects on the maintenance of supersaturation by crystal growth inhibition of poorly water soluble drugs after the administration of drug products that produce supersaturated solutions. The long term impact of this project would be the creation of a framework for rational and efficient decision making leading to the rapid selection of excipient(s) or excipient combinations specific to the drug candidate under evaluation that provide high oral bioavailability for compounds that otherwise might exhibit solubility-limited absorption or undergo extensive precipitation/recrystallization after dissolution.

Chapter Four

Maintenance of Supersaturation II: Indomethacin Crystal Growth Kinetics Versus Degree of Supersaturation

INTRODUCTION

The success of certain types of high energy formulations (e.g., amorphous dispersions) in promoting higher and less variable oral bioavailability of poorly water soluble drugs has often been attributed to the generation and stabilization of supersaturated solutions in the gastrointestinal tract.[1] The abilities of various pharmaceutical excipients to prolong supersaturation of poorly water soluble drug may be linked to their effects on nucleation and/or crystal growth of these compounds.[4,20] Quantitative, mechanistic studies of drug nucleation and crystal growth are therefore needed to fully understand how to most effectively utilize pharmaceutical excipients to maintain drug supersaturation.

Because supersaturated solutions are thermodynamically unstable, processes such as nucleation and crystal growth allow them to reach a more stable equilibrium state (Figure 2.1).[92] The nucleation process consists of the formation of stable nuclei, which are also known as critical nuclei.[93,95,96] The critical nuclei grow in size to form larger crystals during the crystal growth process.[24] The crystal growth process is a multistep process involving several mechanisms. According to the diffusion-reaction theory, the major steps in the crystal growth process are[96]: (1) diffusion of the solute molecules from bulk to the growing interface, and (2) incorporation of the solute into the crystal lattice.[24,92] The latter step is generally defined as a “surface integration” or “surface reaction” step.

The surface integration process could be divided into several sub-steps.[26] Desolvation of the solute occurs at the solid-liquid interface followed by the adsorption of the solute on the growing crystal surface.[9] The adsorbed solute molecules diffuse on the crystal surface until active growth sites such as defects, kinks, or steps are encountered upon which the molecules get incorporated into the lattice.[101] Rapid and continuous crystal growth continues until all the active growth sites are occupied and a molecularly smooth crystal surface is created. The crystal growth rates from molecularly smooth surfaces are slow, which require two-dimensional nucleation to occur on the smooth surface.[96] Alternatively, crystal growth could occur through the spiral growth mechanism where screw dislocations are formed that allow continuous and faster crystal growth.[25] This process does not lead to the formation of molecularly smooth crystal surfaces upon crystal growth which, in turn, provides continuous crystal growth without the need for two-dimensional nucleation.[9]

The diffusion-reaction theory of crystal growth assumes that the two major steps of the crystal growth process occur in series.[24,26,92,93,101] The driving force for the first step (i.e., bulk diffusion) is determined from the difference between the solute concentration in the bulk medium and the solute concentration in solution at the crystal-solution interface (c_i). The surface integration rate is a function of the driving force defined as the difference between c_i and the solute concentration at the solid surface (i.e., the saturation solubility). Since c_i is generally not obtainable experimentally, a simplified empirical crystal growth model is often employed that assumes the overall driving force to be equal to the difference between the bulk concentration and the equilibrium solubility.[24,104]

Knowledge of the fundamental relationships between the mechanisms of crystallization (i.e. nucleation and crystal growth) and the variables that govern the crystallization rate including pH, temperature, agitation, and the number of active growth sites on the growing surface would be essential for understanding the effects of pharmaceutical excipients on the crystallization rate and, in turn, the maintenance of supersaturation. Additionally, the relationship between the nucleation and crystal growth rates and the degree of supersaturation could be further employed in modeling the effects of excipients in maintaining supersaturation. Quantitative and mechanistic explorations of nucleation and crystal growth of poorly water soluble drug candidates in aqueous systems have, in general, suffered due to the lack of simple and robust experimental techniques. Recently, we have developed a non-invasive (online) method to study crystal growth of poorly water soluble compounds from supersaturated aqueous suspensions using second derivative UV spectroscopy and a controlled seeding technique.[104] Using this method, the crystal growth kinetics of indomethacin, a poorly water soluble model drug, were found to follow bulk diffusion controlled first-order kinetics at a high degree of supersaturation (S~6). The aim of this study was to determine indomethacin crystal growth kinetics in aqueous suspensions over a wide range of S to compare to the previously determined indomethacin crystal growth kinetics at high S. This kinetic information may be useful in quantitative and mechanistic treatments of indomethacin crystal growth inhibition and in turn, supersaturation maintenance by pharmaceutical excipients.

MATERIALS AND METHODS

Materials

The γ-polymorph of indomethacin (99+ %) was obtained from Sigma-Aldrich, Inc. (St. Louis, MO, USA). The chemical name of indomethacin is 1-(*p*-chlorobenzoyl)-5-methoxy-2-methylindole-3-acetic acid. The molecular weight and pK_a of indomethacin are 357.8 g/mole and 4.17,[148] respectively. Filters including 30 µm nylon net filters and 3 µm polycarbonate membrane filters were acquired from Millipore Inc. (Milford, MA, USA) whereas 0.2 µm nylon membrane filters and 0.45 µm (13 mm) PTFE syringe filters were purchased from Whatman Int. Ltd. (Maidstone, England). A MilliQ water purification apparatus (Milli-Q Synthesis, Millipore Inc., Milford, MA, USA) with a 0.22 µm pre-filter (Millipak Express 20, Millipore Inc., Milford, MA, USA) was used to obtain deionized water. All other reagents were of an analytical grade.

Preparation of Indomethacin Seed Crystal Suspensions

Indomethacin seed crystal suspensions were prepared using a previously published method.[104] Briefly, indomethacin powder (~0.1% w/w) was mixed with 50 mM phosphate buffer (pH 2.15) for about 3 days using a mechanical shaker. The temperature was controlled at 25°C using a water bath. The equilibrated suspensions were first passed through 30 µm nylon filters, and filtrates from this step were further filtered through 3 µm filters. The solids retained on the 3 µm filters were re-suspended in saturated indomethacin solutions (pH 2.15) to obtain final suspensions with a narrow and unimodal particle size distribution.

Indomethacin Crystal Growth Rate Measurement

1. Batch Method (S>1.6)

Indomethacin crystal growth rates at different S between 2 and 9 were measured using a previously published second derivative online UV method.[104] Briefly, indomethacin crystal growth rate coefficients were estimated from indomethacin desupersaturation (concentration vs. time) profiles. Indomethacin concentration vs. time profiles were determined using the second derivative UV spectroscopic method (wavelength range: 210 to 400 nm, λ_{max} =295 nm). The suspensions were supersaturated by adding 100-150 µl of a highly concentrated (~120 µg/mL) indomethacin solution (pH 6.8) at a specific addition rate using a micro-syringe pump. The final pH of supersaturated indomethacin suspensions was below 2.2. During desupersaturation, indomethacin suspensions (pH 2.15) were mixed in 1-cm matched UV quartz cells using pivoted magnetic stirrers at 400 RPM.

2. Infusion Method (S<1.6)

Indomethacin solution (5 µg/mL, pH 6.8) was infused into 3 ml of indomethacin seed crystal suspension (pH 2.15) for about 4 hours at 2.5 µl/min infusion rate using a micro-syringe pump. The total infusion volume of the indomethacin solution added was about 0.6 ml. The pH of the final supersaturated suspension after infusion remained below 2.8. Indomethacin concentrations were measured at regular time intervals using the second derivative UV method. The infusion was stopped after about 4 hours and the supersaturated indomethacin suspension (S~1.4) was allowed to reach a stable equilibrium state. Indomethacin apparent solubility after crystal growth was determined after around 24 hours using the same method as described in an earlier section.

3. High Energy Seed Crystals

Indomethacin crystal growth rates at low S (< 6) were also measured using high energy indomethacin seed crystals. High energy indomethacin seed crystals, unlike the low energy seed crystals, had higher energy surface that, in turn, provided higher apparent solubility.[104] Specifically, the low energy seed crystals from saturated indomethacin suspensions at pH 2.15 were converted into the high energy seed crystals by depositing higher energy thin surface layers of indomethacin on the low energy seed crystals. The deposition of high energy thin surface layers of indomethacin was achieved using a typical crystal growth experiment at high S (S~6). The indomethacin suspensions containing higher energy seed crystals were then utilized to determine indomethacin crystal growth rates by the batch method described in an earlier section.

Indomethacin Solubility Measurements (Before and After Crystal Growth)

The intrinsic solubility of indomethacin before crystal growth was measured using a method described previously.[104] Briefly, indomethacin was mixed with 50 mM phosphate buffer (pH 2.15) in a rotary shaker. The temperature was maintained at 25ºC using a water bath. At regular time intervals, indomethacin concentrations were measured using syringe filtration (0.45 μ PTFE syringe filter) and an UV spectrophotometer (λ_{max} =321 nm). The method for determining indomethacin apparent solubility after crystal growth, henceforth defined as the apparent solubility, was described in detail in a previous publication.[104] Briefly, the apparently solubility was measured from equilibrated indomethacin suspensions after crystal growth. Indomethacin concentrations from these suspensions were measured by UV spectrophotometry in two different ways: (1) online concentration measurements from

indomethacin suspensions using the second derivative UV spectroscopic method (λ_{max} =295 nm), and (2) off-line concentration measurements from clear indomethacin solutions by regular UV spectroscopy (λ_{max} =321 nm). The clear solutions were obtained by filtration of indomethacin suspensions through a 0.45 µ PTFE syringe filter.

Indomethacin Seed Crystal Characterization

Indomethacin seed crystals were characterized for their number and size distributions, mass median diameter, total surface area, morphology, and crystalline polymorphic form before and after crystal growth. The methods used in characterizing indomethacin seed crystals were described previously.[104] The number and size distributions per unit volume of indomethacin suspension were determined using a Coulter counter ((Multisizer Z2, Beckman Coulter Inc., Miami, FL, USA). The Coulter counter measurements were made in two size ranges: (1) 2-8 µm and 8-25 µm. Powder X-ray diffraction (PXRD) profiles were obtained using an X-ray diffractometer (Bruker D8 Advance, Bruker AXS, Inc., Madison, WI, USA). The scan settings were 3 to 35º 2θ with 0.05° step size and 4 or 0.6 seconds step time (operating conditions for the x-ray copper anode (1.54A): 40 kV and 40 mA). Analyses of the shape and size of indomethacin seed crystals utilized a polarized light microscope (PLM) and a scanning electron microscope (SEM, Hitachi S4300).

Statistical Analyses

Scientist® software (Micromath Inc., St. Louis, MO, USA) was used to perform non-linear least-squares analyses of indomethacin concentration vs. time profiles. Microsoft Excel was used to conduct the Student t-test and ANOVA.

RESULTS

Indomethacin Seed Crystal Characterization Before and After Crystal Growth

Indomethacin seed crystals were characterized in suspensions before and after crystal growth by determining their physical characteristics including size distribution, number concentration, morphology, and physical form. The typical mass median diameter of the indomethacin seed crystals was 11.1 ± 0.3 (95% CI) μm. The typical surface area of indomethacin seed crystals was $4.5 \pm 0.3 \times 10^{-2}$ (95% CI) cm^2 per mL of suspension. The number of indomethacin seed crystals per mL of indomethacin suspension was $4.1 \pm 0.6 \times 10^4$ (95% CI). The shape characteristics of indomethacin seed crystals were analyzed by PLM & SEM (data not shown). The crystalline nature of the indomethacin seed crystals was confirmed by polarized light microscopy. The SEM analysis of indomethacin seed crystals indicated that the crystals were cuboidal, a characteristic morphology of the γ-polymorph of indomethacin.[128] Furthermore, no particles with significantly different geometry (e.g., long needles or spherulites characteristic of the α-polymorph of indomethacin[128]) could be detected from comparisons of several SEM micrographs of indomethacin seed crystals before and after crystal growth, which again indicated the absence of primary nucleation of other indomethacin forms.[128] The physical form of indomethacin seed crystals before and after crystal growth was determined by PXRD. The PXRD patterns of indomethacin seed crystals before and after crystal growth matched the PXRD patterns of original indomethacin powder, indicating that there was no significant change in crystallinity or polymorphic form of the indomethacin seed crystals after crystal growth that could be detected by PXRD (data not shown). The theoretically estimated thicknesses of the

newly grown indomethacin surface layer after crystal growth at S values of 6 and 2 were approximately 0.3 µm and 0.9 µm, respectively. Considering the very small thicknesses of the newly grown surface layers, it is unlikely that surface changes on the seed crystals would have been detected by PXRD.[104,139,153,154]

Indomethacin Solubility Before and After Crystal Growth

The intrinsic solubility of indomethacin (before crystal growth) was determined previously as $3.4 \pm 0.1 \times 10^{-6}$ M (pH 2.15; 0.1 M ionic strength, 25ºC).[104] In the same earlier study,[104] we showed that the apparent solubility of indomethacin after crystal growth at a high S of 6 was about 55% higher than its equilibrium solubility (Table 4.1). The higher apparent solubility was attributed to the deposition of a thin surface layer of higher energy on the existing lower energy indomethacin seed crystal surfaces. One of the objectives of this study was to compare indomethacin apparent solubilities after crystal growth at a wide range of S and, in turn, determine if the higher energy surface was also formed after crystal growth at low S. Indomethacin apparent solubilities after crystal growth were determined at various S ranging from 2 to 9. Representative indomethacin apparent solubilities after crystal growth at a high S of 6 and a low S of 2 are compared in Table 4.1. The indomethacin apparent solubilities after crystal growth at different S from 2 to 9 were significantly higher than the indomethacin equilibrium solubility ($p < 0.05$). For example, the apparent solubility of indomethacin after crystal growth at an S of 9 was $5.3 \pm 0.3 \times 10^{-6}$ M whereas the equilibrium solubility of indomethacin was $3.4 \pm 0.2 \times 10^{-6}$ M. Moreover, there was no significant difference between the apparent solubilities after growth at low ($2 < S < 6$) and high S ($6 \leq S \leq 9$) ($p < 0.05$). Finally, the higher apparent solubility observed after crystal growth at high and

low S clearly indicated that the higher energy surface was formed on indomethacin seed crystals after crystal growth (Refer to the "Discussion" section in this report for more details on this topic).[30,104]

Indomethacin Crystal Growth Kinetics at High & Low Degrees of Supersaturation

Indomethacin crystal growth kinetic (or desupersaturation) profiles were obtained at different degrees of supersaturation between 2 and 9. Representative indomethacin desupersaturation profiles determined at high (S=6) and low (S=3) degrees of supersaturation using seed crystals with similar surface areas are shown in Figure 4.1. The indomethacin desupersaturation rate was much slower when the desupersaturation was initiated at a low S of 3 as compared to that at a high S of 6. To compare the indomethacin crystal growth rate coefficients (k_G) at a high and low S, the k_Gs at various S were determined by fitting indomethacin desupersaturation profiles to an empirical crystal growth model (Eq. 4.1).[24] More detailed discussion on the derivation of this model can be found elsewhere.[104]

$$-\frac{dc_b}{dt} = k_G A(c_b - c_s)^g \qquad (4.1)$$

where c_b is the solute concentration in the bulk medium, k_G is an apparent crystal growth rate coefficient, A is the crystalline surface area per unit volume of the bulk medium, c_s is the solute concentration in solution at equilibrium (i.e., the saturation solubility), and g is the apparent order of the crystal growth process. In our previous study,[104] we had determined that the value of g for indomethacin crystal growth kinetics (S=6) from its supersaturated aqueous suspension was equal to 1. This determination was carried out by comparing the empirical crystal growth model (Eq. 4.1) fits of

indomethacin desupersaturation profiles using three different values of g (i.e., 0, 1, 2, and 3) and the lack of fit test. The lack of fit analysis clearly showed that the crystal growth model with g=1 (Eq. 4.1) fit the indomethacin desupersaturation profiles (S=6) best. Here, the driving force for crystal growth was calculated as the difference between c_b and the apparent solubility i.e. $5.2 \pm 0.6 \times 10^{-6}$ M (Table 4.1). Since the objective of the present study was to compare indomethacin crystal growth rate coefficients (k_G) at different S including the previously studied high S of 6, we further evaluated the application of the first-order empirical crystal growth kinetic model at different S. As shown in Figure 4.1, the first-order crystal growth model fit the indomethacin desupersaturation profiles at high and low S very well and hence the first-order model was used in the present study to determine k_Gs at different S. It should also be noted that since g is an empirical parameter, the value of g used in Eq. 4.1 may not have any fundamental significance.[24]

Indomethacin crystal growth rate coefficients (k_G) were determined at various S between 2 and 9 (Figure 4.2). The k_Gs were significantly smaller at low S as compared to those at high S indicating much slower crystal growth rates at low S. For example, as shown in Table 4.1, indomethacin k_Gs at S=6 and S=2 were $5.0 \pm 0.7 \times 10^{-3}$ cm/sec and $5.5 \pm 1.3 \times 10^{-4}$ cm/sec, respectively. The indomethacin k_G increased with S between 2 and 6, while between S values of 6 and 9, the k_G did not change significantly and appeared to be reaching a plateau. The indomethacin k_G between the S= 6-9 was similar to the theoretically predicted k_G (Figure 4.2, broken line) assuming bulk diffusion controlled crystal growth ($5.0 \pm 0.3 \times 10^{-3}$ cm/sec (±95% CI)).[104] This indicated that the crystal growth kinetics of indomethacin is bulk diffusion controlled for S>6. The

indomethacin k_Gs at S <6 were significantly smaller than the theoretically predicted (bulk diffusion controlled) indomethacin k_G (Figure 4.2, broken line). The indomethacin k_G at a low S of 2 was approximately nine times smaller than the theoretically predicted k_G assuming bulk diffusion control. This could indicate a change in the rate limiting step for indomethacin crystal growth with decreasing values of S from bulk diffusion controlled crystal growth kinetics at S>6 to surface integration control at lower S values.

Indomethacin Crystal Growth Kinetics using High Energy Seed Crystals

To determine the relationship between indomethacin seed crystal surface energetics and its crystal growth kinetics (growth rates and rate limiting steps), indomethacin crystal growth rates were measured at a low S of 2 using high and low energy indomethacin seed crystals. The high energy indomethacin seed crystals were obtained from previously completed indomethacin crystal growth experiments in supersaturated aqueous suspensions at high S ($6 \leq S \leq 9$). As shown in Table 4.1, the indomethacin crystal growth rate coefficient determined at a low S of 2 using high energy seed crystals was $5.6 \pm 0.7 \times 10^{-3}$ cm/sec, which was approximately ten times higher than the k_G determined at the low S of 2 using low energy seed crystals ($5.5 \pm 1.3 \times 10^{-4}$ cm/sec). Moreover, the k_G determined from high energy seed crystals at low S was similar to the theoretically predicted k_G assuming bulk-diffusion controlled crystal growth ($5.0 \pm 0.3 \times 10^{-3}$ cm/sec). This indicated that the surface energetics of indomethacin seed crystals clearly influenced the indomethacin crystal growth rate and, in turn, its rate limiting step.

Table 4.1. Effects of degree of supersaturation and seed crystal surface energetics on indomethacin solubility and crystal growth rate coefficient (± 95% CI)

Indomethacin Seed Crystals	Degree of Supersaturation (S)	Equilibrium/ Apparent Solubility (M)	Indomethacin Crystal Growth Rate Coefficient, k_G (cm/sec)
Before Crystal Growth	6	$3.4 \pm 0.2 \times 10^{-6}$	$5.0 \pm 0.7 \times 10^{-3}$
	2	$3.4 \pm 0.2 \times 10^{-6}$	$5.5 \pm 1.3 \times 10^{-4}$
	<1.6	$3.4 \pm 0.2 \times 10^{-6}$	$6.4 \pm 1.8 \times 10^{-4}$
After Crystal Growth	6	$5.2 \pm 0.6 \times 10^{-6}$	-
	2	$6.3 \pm 0.7 \times 10^{-6}$	$5.6 \pm 0.7 \times 10^{-3}$
	<1.6	$3.9 \pm 0.5 \times 10^{-6}$	-

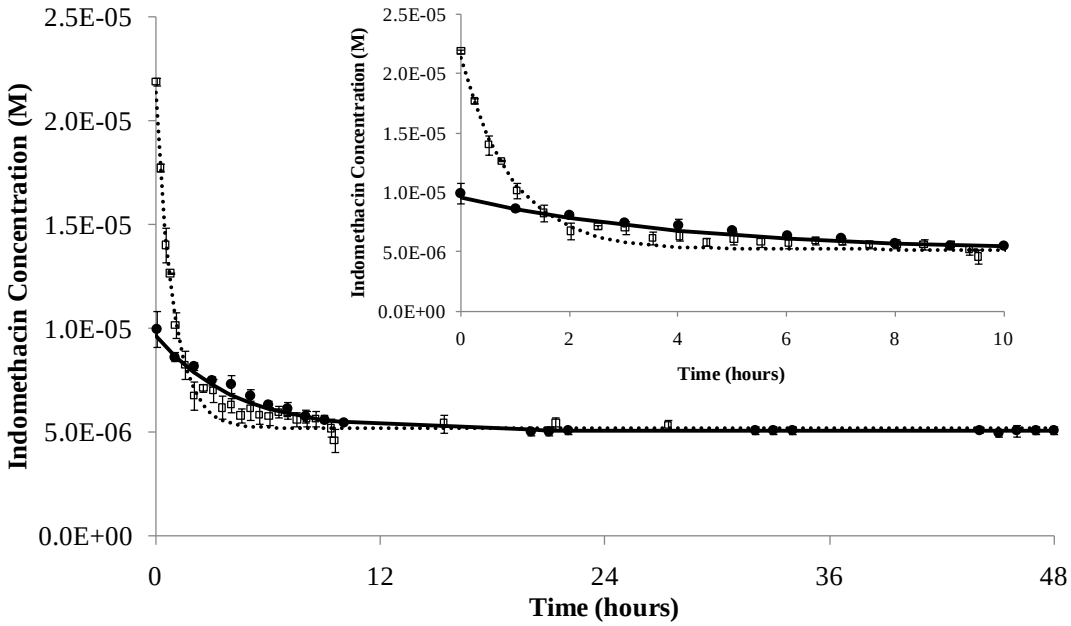

Figure 4.1. Representative indomethacin crystal growth kinetic profiles at high (S=6, □) and low (S=3, ●) degrees of supersaturation (S). The lines represent first-order empirical crystal growth model (Eq. 4.1) fits. Error bars represent 95% confidence intervals (CI).

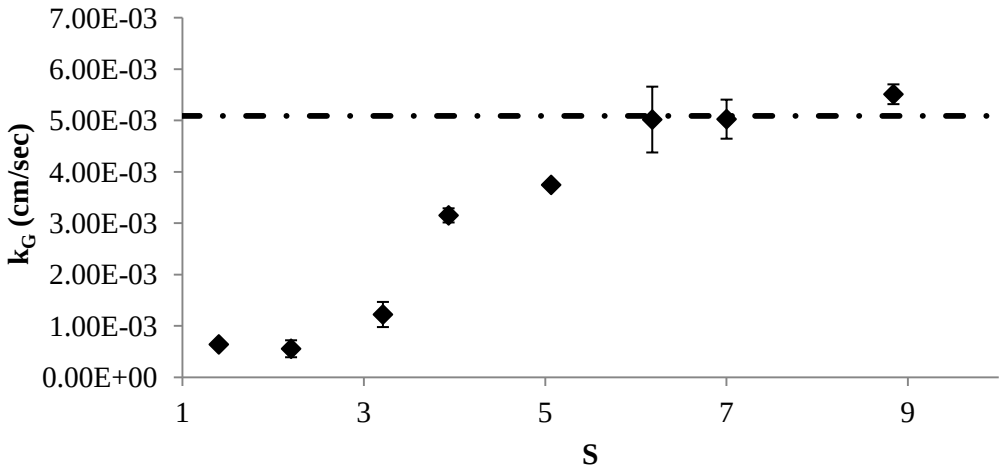

Figure 4.2. Effect of the degree of supersaturation (S) on indomethacin crystal growth rate coefficients (k_G). The broken line represents theoretically predicted indomethacin k_G for bulk diffusion controlled crystal growth. Error bars represent 95% confidence intervals (CI).

Indomethacin Crystal Growth using the Infusion Method (S<1.6)

Indomethacin crystal growth experiments at S < 1.6 were carried out using an infusion method. The purpose of this experiment was to measure indomethacin crystal growth rates at very low S without converting the initial lower energy indomethacin seed crystal surface to a higher energy surface. It was assumed that if the crystal growth of indomethacin occurred at S below the indomethacin apparent solubility (i.e., S < 1.6) then the higher energy surface would not be formed on the initial low energy seed crystal surface. Therefore, indomethacin crystal growth rates measured at S < 1.6 could be directly attributed to deposition on the lower energy indomethacin seed crystal surface. The batch method used to study crystal growth at S between 2 and 9 was limited by severe difficulties in achieving and maintaining very low degrees of supersaturation (S < 1.6). A modified crystal growth measurement method was therefore developed using an infusion technique. A detailed description of this method is provided in the Materials and Methods section.

A representative indomethacin crystal growth profile determined using the infusion method is shown in Figure 4.3. The open squares denote experimentally measured indomethacin concentrations at regular time intervals. The infusion was continued for about 4 hours after which the supersaturated indomethacin suspension was allowed to equilibrate for about 24 hours. The apparent solubility of indomethacin after crystal growth at S< 1.6 ($3.9 \pm 0.5 \times 10^{-6}$ M) was similar to its equilibrium solubility ($3.4 \pm 0.2 \times 10^{-6}$ M) (Table 4.1). This indicated that the higher energy surface did not form on

the initial lower energy seed crystal surface after crystal growth at very low S <1.6. The indomethacin crystal growth profile was fit to an infusion-based crystal growth model (Eq. 4.2), which was derived from the first-order empirical crystal growth model (Eq. 4.1).

$$c_b = \frac{R + k_{app} c_s}{k_{app}} \left(1 - e^{-k_{app}\tau}\right) e^{-k_{app} t} + c_s \left(1 - e^{-k_{app} t}\right) \tag{4.2}$$

Here, the rate constant, $k_{app} = k_G \times A$ where k_G is an apparent crystal growth rate coefficient, A is the crystalline surface area per unit volume of the bulk medium, R is the indomethacin infusion rate ($moles.liter^{-1}.sec^{-1}$), τ is the total duration of infusion (sec), c_b is the indomethacin concentration in the bulk at time t ($moles.liter^{-1}$), and c_s is the indomethacin concentration at the crystal surface (i.e., the equilibrium solubility of indomethacin). The experimentally measured indomethacin crystal growth profile using the infusion method was in good agreement with the predicted profile (solid line, Figure 4.3). The broken line (Figure 4.3) represents the predicted indomethacin concentrations assuming no crystal growth had occurred during the entire infusion period. The indomethacin crystal growth rate coefficient (k_G) estimated from the infusion method using Eq. 4.2 was $6.4 \pm 1.8 \times 10^{-4}$ cm/sec. This was in good agreement with the indomethacin k_G ($5.7 \pm 0.7 \times 10^{-4}$ cm/sec) previously estimated from the crystal growth experiments at a low S of 2 (Table 4.1), indicating that the slower indomethacin crystal growth at low S (<6) could be associated with the low energy seed crystal surface available for growth.

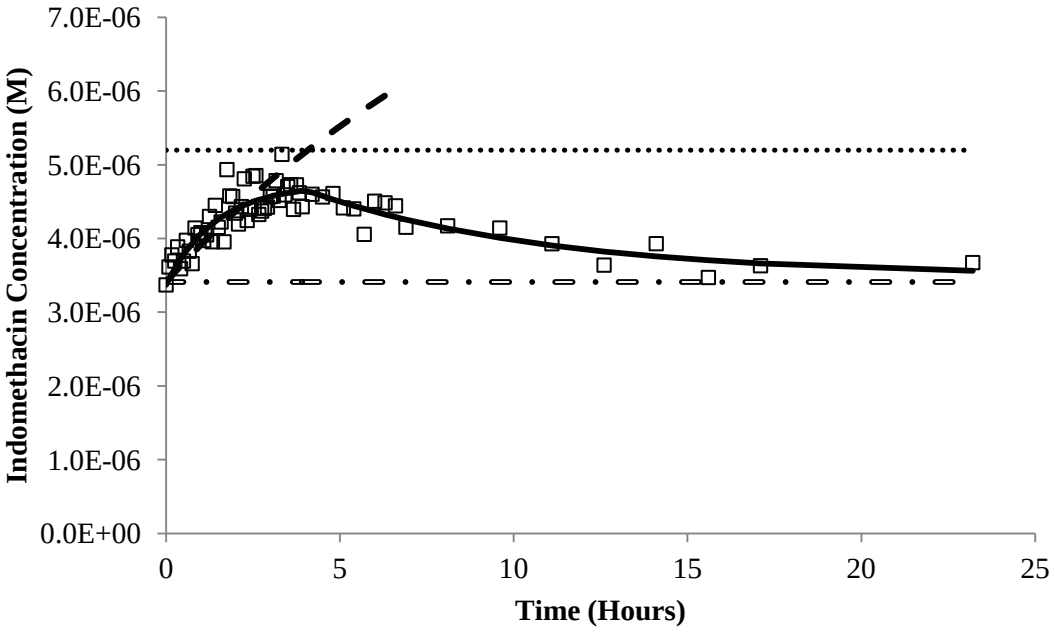

Figure 4.3. A representative indomethacin desupersaturation profile from an infusion-based crystal growth experiment at a degree of supersaturation (S) below 1.6. (Legends: □ bulk concentration, —•—•— equilibrium solubility line, …… apparent solubility line, ─ ─ ─ predicted bulk concentration in the absence of crystal growth, ——— infusion-based crystal growth model fit (Eq. 4.2))

DISCUSSION

Indomethacin Apparent Solubility after Crystal Growth

The apparent solubility of indomethacin after crystal growth at a low S of 2 was higher than the saturation solubility before growth (Table 4.1). Similar observations were made for the apparent solubilities after growth at S between 2 and 9 (data not shown). We have previously shown that the apparent solubility could be different from the equilibrium solubility depending on the nature of the newly grown surface layer.[104] If the newly grown layer is of higher energy, then the apparent solubility would be higher than the equilibrium solubility before growth.[32] Similar to our previous observation for indomethacin crystal growth at S=6,[104] we found in the present study that a higher energy indomethacin crystal surface was also formed after crystal growth at low S ($2 < S < 6$). The higher energy of the newly grown surface layer could be attributed to higher disorder[30] or the growth of a higher energy polymorphic form (e.g., the α-form of indomethacin).[104] The higher disorder could range from smaller lattice defects to larger amorphous regions depending on the degree of disorder.[29] Several previous studies have linked a higher apparent solubility or dissolution rate to higher disorder (higher energy sites) of the solid surface.[29,30,32]

Since the higher energy indomethacin surface provided an apparent solubility that was approximately 1.6 times higher than the equilibrium solubility, we determined the apparent solubility at $S < 1.6$. It was reasoned that if the S remained below 1.6 during crystal growth then the higher energy surface would not be formed. This would result in similar indomethacin solubilities before and after crystal growth. Here the equilibrium solubility represented the lower energy surface of indomethacin seed crystals. The

apparent solubility of indomethacin after growth at S < 1.6 was similar to the equilibrium solubility (Table 4.1), indicating that the lower energy indomethacin seed crystal surface was retained after growth at low S < 1.6.

Indomethacin Crystal Growth Kinetic Modeling at High & Low Degrees of Supersaturation

Several external (e.g., degree of supersaturation, impurities, and excipients) and internal (structure, bonds, and defects or disorder) factors influence the kinetics of a typical crystal growth process.[25,26] The degree of supersaturation, being the driving force for the crystal growth process, could significantly change the crystal growth kinetics and related growth parameters such as the crystal growth rate coefficient (k_G) and the order of the crystal growth process (g) (Eq. 4.1). As mentioned earlier, the term g used in crystallization studies (Eq. 4.1) is an empirical parameter, which is different from the "reaction order" term used in chemical kinetics. It does not illustrate the number of species involved in the crystal growth process and hence it may have no fundamental significance.[24] Nevertheless, several empirical correlations have been made between the value of g and the mechanism of crystal growth.[24,103,163] A g value of 1 is associated with high energy (high disorder or roughness) surface-based continuous growth at high and low S as well as screw dislocation or spiral growth mechanisms at high S.[24,103] A g value of 2 is associated with the screw dislocation mechanism-based growth at low S, whereas a $g > 2.5$ is associated with two-dimensional nucleation mechanism-based growth.[103] Li and Rodriguez-Hornedo[103] experimentally determined the values of g for two different faces of the glycine crystal. The values of g were 1.3 ± 0.2 and 1.5 ± 0.2 for 010 and 011 faces, respectively. Based on the values of g, the growth of 010 and 011 faces of glycine

was attributed to the screw dislocation mechanism. Moreno et al.[163] observed that the values of *g* were erratic and higher than 1 at low degrees of supersaturation during the crystal growth of hydroxyapatite. In our previous study,[104] we observed that when the indomethacin desupersaturation profiles were fitted to the empirical crystal growth model (Eq. 4.1) where the driving force was calculated as the difference between indomethacin bulk concentration and the apparent solubility, the value of *g* was 1. However, when the driving force for crystal growth was calculated using the equilibrium indomethacin solubility (~55% lower than the apparent solubility), the value of *g* increased from 1 to approximately 1.5. Since the higher apparent indomethacin solubility was stable up to 7 days as described in our previous study,[104] it was used to calculate the driving force for crystal growth. In the present study, we used the same method to calculate the driving force for crystal growth. As shown in Figure 4.1, the first-order empirical crystal growth model fit the desupersaturation profiles very well when the driving force was calculated using the apparent solubility. This indicated that the indomethacin crystal growth could be associated with the high energy (high disorder or roughness) surface-based continuous growth mechanism at high and low S.

The indomethacin crystal growth rate coefficient in aqueous supersaturated suspensions increased with S between 2 and 6 whereas it reached a plateau at S>6. Since the faster indomethacin crystal growth at $S \geq 6$ was bulk diffusion controlled,[104] the slower crystal growth at S<6 was associated with a change in rate limiting step from bulk diffusion to surface integration. The rate limiting steps of crystal growth have previously been correlated with the degree of supersaturation.[37] Scholl et al.[44] observed that the crystal growth rate of PDI 747, a phosphodiesterase type 4 inhibitor, was at least one

order of magnitude slower than the theoretically predicted diffusion-limited growth rates at low S between 2 and 3. The slower growth of PDI 747 was determined to be surface integration controlled. Nancollas et al.[111] observed that the crystal growth of calcium sulfate dehydrate in aqueous solutions was also surface integration controlled at low S.

Relationship between Indomethacin Crystal Surface Energetics and the Rate Limiting Steps of Indomethacin Crystal Growth

Highly disordered or molecularly smooth surfaces could be formed during crystal growth depending on high or low degrees of supersaturation, respectively.[9] Properties of the newly grown surface such as the degree of surface disorder or defects or roughness (i.e., surface energetics) significantly influence the rate limiting step of the crystal growth process. Besides surface energetics, the rate limiting step of a crystal growth process also depends on factors such as degree of supersaturation, solvent type, temperature, and the nature of the growing crystal surface.[25] The crystal surface with higher energy due to higher active growth sites such as defects or kinks is associated with faster crystal growth rates.[24,30] When the growing surface is molecularly smooth (e.g., perfect crystals), the crystal growth is significantly slower. While the bulk diffusion controlled crystal growth rate coefficient has been directly correlated with the diffusion coefficient of the solute and the diffusion layer thickness,[104] the relationship between the degree of supersaturation and surface integration rate depends on the nature of the growing crystal surface.[96]

The higher indomethacin apparent solubility at low S ($2 < S < 6$) indicated that the higher energy seed crystal surface was formed when the growth was initiated at low S. However, despite the formation of a higher energy surface, the indomethacin crystal

growth rate coefficient was significantly smaller indicating surface integration control. Hence it was hypothesized that a longer lag time existed for the conversion of the initial low energy seed crystal surface to a high energy surface when crystal growth occurred at low S (Figure 4.4). The longer lag time and, in turn, slower rate of conversion from the initial lower energy seed crystal surface to the higher energy surface at low S could be attributed to the smaller thermodynamic driving force available for crystal growth at low S. To confirm this hypothesis, the indomethacin crystal growth rate was determined at very low $S < 1.6$ using the infusion method. It was expected that the higher energy surface would not be formed at $S < 1.6$, which was later experimentally confirmed from the indomethacin apparent solubility measurements after crystal growth at $S < 1.6$. The indomethacin crystal growth rate coefficient measured at low $S < 1.6$ was similar to that measured at low S of 2 confirming the fact that the slower indomethacin crystal growth rate was associated with the lower energy surface (Table 4.1). The effect of seed crystal surface energetics on the indomethacin crystal growth rate at low S was further studied using the high energy seed crystals. Since the slower indomethacin crystal growth rate at low S was associated with the lower energy seed crystal surface, it was assumed that indomethacin crystal growth at low S would be faster when higher energy seed crystals were used. As shown in Table 4.1, the indomethacin crystal growth rate coefficient (k_G) measured at S=2 using the higher energy seed crystals was about 10 times higher than that obtained using the lower energy seed crystals at the same S. This result further supported the hypothesis that the slower indomethacin crystal growth rate at low S was associated with the lower energy surface of the seed crystals. Finally, the faster indomethacin crystal growth k at S between 6 and 9 was bulk diffusion controlled

whereas the slower crystal growth at $S < 6$ could be surface integration controlled. The change in the rate limiting step from bulk diffusion to surface integration for indomethacin crystal growth at low S could be attributed to the lower energy seed crystal surface and the longer lag time for its conversion to higher energy surface.

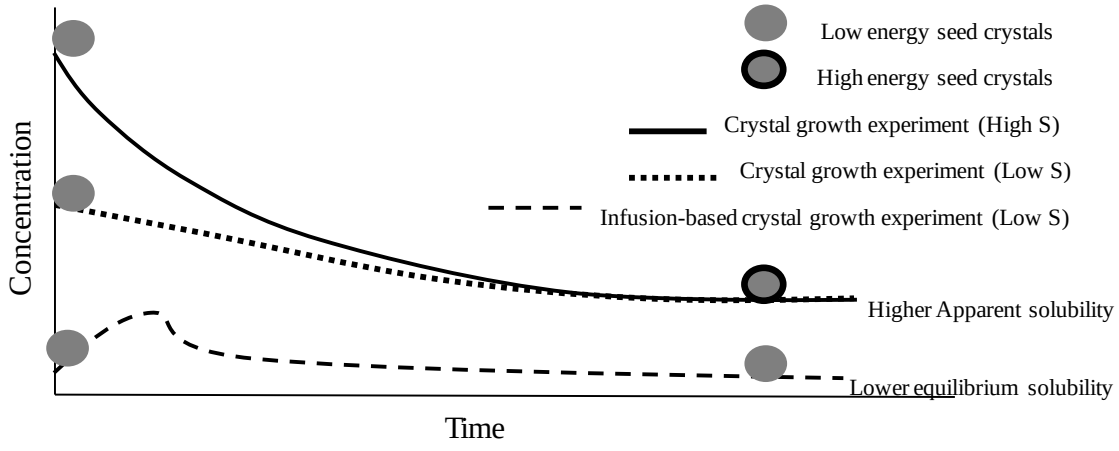

Figure 4.4. Schematic diagram illustrating a proposed hypothesis for varying indomethacin seed crystal surface energetics at different degrees of supersaturation (S) during crystal growth from supersaturated aqueous suspensions.

CONCLUSIONS

Indomethacin crystal growth kinetics from supersaturated aqueous suspensions was compared at varying degrees of supersaturation ($2 \leq S \leq 9$). The higher indomethacin apparent solubility after crystal growth at S between 2 and 9 indicated that a higher energy surface was formed on the seed crystals initially having a lower energy surface. The indomethacin crystal growth rate coefficient (k_G) increased with S between an S of 2-6. At high S ($6 \leq S \leq 9$), the k_G reached a plateau value that was similar to the theoretically predicted k_G assuming bulk diffusion controlled crystal growth. The indomethacin k_G at a low S of 2 was ~10 times smaller than the theoretically predicted k_G assuming bulk diffusion controlled crystal growth. The smaller indomethacin k_G at S=2 could be due to a change in the rate limiting step from bulk diffusion to surface integration. The change in rate-limiting step from bulk diffusion to surface integration for the indomethacin crystal growth at a low S of 2 was attributed to a longer lag time for the conversion of initial lower energy indomethacin seed crystal surface to a high energy surface due to reduced thermodynamic driving force for crystal growth at the low S of 2. The k_G determined at a low S of 2 using higher energy seed crystals was similar to that predicted assuming bulk diffusion controlled crystal growth. This result further verified the hypothesis that the higher energy surface provided faster bulk diffusion controlled crystal growth. Using an infusion-based method, the indomethacin k_G at very low S (<1.6) was determined without transforming the initial lower energy surface to the higher energy surface. The indomethacin apparent solubility after crystal growth at S<1.6 was lower and similar to the equilibrium solubility indicating that crystal growth at S below the higher indomethacin apparent solubility (i.e., $S < 1.6$) did not form the higher energy

surface. The k_G at S < 1.6 was similar to that determined at an S of 2 supporting the hypothesis that the smaller k_G at low S could be attributed to the lower energy indomethacin seed crystal surface. Finally, the higher energy surface provided faster, bulk diffusion controlled indomethacin crystal growth at high and low S, whereas the lower energy surface was associated with significantly slower surface integration controlled crystal growth rate at low S. The quantitative mechanistic understanding derived from the indomethacin crystal growth kinetics at high and low S may be useful in exploring the inhibitory effects of model pharmaceutical excipients on indomethacin crystal growth and, in turn, on its supersaturation maintenance.

Chapter Five

Effect of Precipitation Inhibitors on Indomethacin Supersaturation Maintenance: Mechanisms & Modeling

INTRODUCTION

Supersaturation is commonly encountered when high energy drug delivery technologies such as amorphous solid dispersions,[3] lipid-based delivery systems,[50] and nanoparticles[1] are utilized to enhance bioavailability of poorly water soluble drugs. Supersaturation in the solid-state can be attributed to higher drug loadings in drug delivery system matrices than the equilibrium solubilities in the same matrices.[53] Solution-state (e.g., aqueous) supersaturation could be produced in vivo after the administration of high energy drug delivery technologies to patients.[91] The in vivo aqueous supersaturation generally occurs due to higher apparent solubilities provided by the high energy states of drugs in biological media.

While the solid-state supersaturation has been an active topic of research for the past several decades, a thorough understanding of the solution-state (or aqueous) supersaturation and its maintenance is also critical for the development of robust drug delivery technologies for two main reasons: (1) the solution-state understanding could serve as a foundation for understanding supersaturation in the solid-state with the aim of improving physical stability of drugs in high energy formulations and (2) optimal in vivo supersaturation maintenance could provide higher & less variable bioavailability,[1,91] which in turn could reduce the requirements of higher and frequent dosing as well as wider safety margins for drug candidates under clinical development. Pharmaceutical polymeric precipitation inhibitors (PPIs) such as cyclodextrins,[7] surfactants,[43] polyvinylpyrrolidone (PVP),[108,164] and hydroxypropyl methylcellulose (HPMC)[108,164]

have effectively maintained aqueous supersaturation of a number of pharmaceutical compounds. The supersaturation maintenance effect of these PPIs varies extensively depending on the drug, rendering the development of predictive tools for a rational and efficient pharmaceutical PPI selection process more difficult. For example, Vandecruys et al.[43] observed in a recent screening study with several drug candidates that PPIs such as PVP & HPMC were more effective at prolonging supersaturation than providing higher degrees of supersaturation, whereas PPIs such as surfactants and cyclodextrins provided higher degrees of supersaturation. These PPIs are believed to maintain supersaturation by inhibiting drug nucleation, crystal growth, or both.[1,108] Lindfors et al.[20] recently determined that PVP was more effective at inhibiting the crystal growth of bicalutamide than its nucleation. The inhibitory effects of polymers such as PVP and HPMC were attributed to their adsorption on to the growing crystal surface. Moreover, it was proposed that the adsorbed polymer could inhibit the crystal growth process by blocking the active growth site, increasing the diffusive barrier at the solid-liquid interface, or both.[12,21] While a few recent studies[1,20,43] have attempted to discern the mechanisms of action for the above-mentioned PPIs, the supersaturation maintenance effects of these PPIs are still not well understood due in part to a paucity of systematic and quantitative explorations. Moreover, the proposed mechanisms of PPIs' actions are rarely correlated with the sub-processes of amorphous precipitation or crystallization processes including nucleation and crystal growth and their specific mechanisms such as bulk diffusion or surface integration. The overall lack of a thorough understanding of PPIs' effects on aqueous supersaturation maintenance also makes *a priori* predictions of their beneficial effects very challenging.

The objective of this study was to develop a quantitative approach to explore the crystal growth inhibition and, in turn, maintenance of supersaturation of indomethacin, a model poorly water soluble drug, by three model PPIs including hydroxypropyl β-cyclodextrin (HP-β-CD), PVP, and HPMC and to begin the process of understanding these effects mechanistically (Figure 5.1). In this report, using a recently developed second-derivative UV spectroscopy method,[104] we have shown that PVP and HPMC have more dramatic effects than HP-β-CD on the crystal growth of indomethacin, particularly at high degrees of supersaturation. HP-β-CD is a better indomethacin crystal growth inhibitor at low ($S<3$) than at high ($S>3$) degrees of supersaturation. A mathematical model based on reactive diffusion theory has been developed to rationalize the modest effect of HP-β-CD on indomethacin crystal growth at high S.

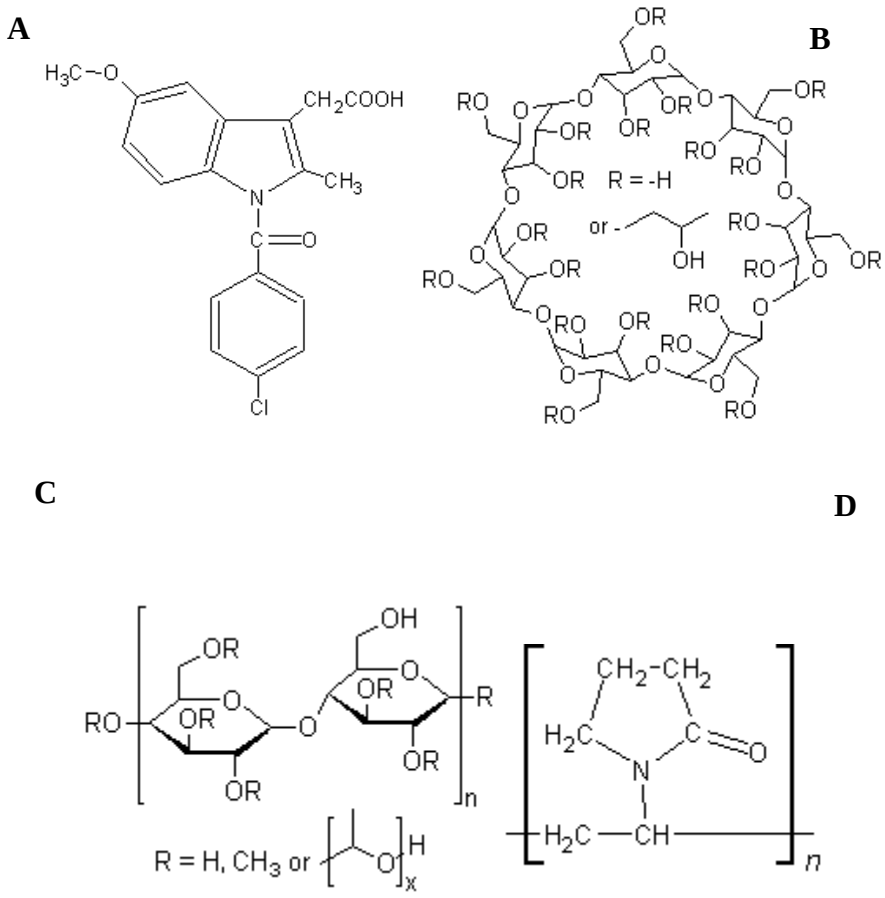

Figure 5.1. Chemical structures of indomethacin (A) and model pharmaceutical PPIs: (B) hydroxypropyl β-cyclodextrin (HP-β-CD), (C) hydroxypropyl methylcellulose (HPMC), and (D) polyvinylpyrrolidone (PVP).

THEORY

Reactive Diffusion Layer Theory

The effect of HP-β-CD on indomethacin crystal growth kinetics was modeled using the classical reactive diffusion layer theory. The theory assumes complexation between indomethacin (*HA*) and HP-β-CD (*CD*) in the diffusion layer during crystal growth, as described below.[165]

The following equilibrium will exist when *HA* and *HA-CD*, the complex of *HA* and *CD*, are diffusing through the diffusion layer from the supersaturated bulk to the crystal solid surface during crystal growth.

$$HA + CD \xleftrightarrow{K_{1:1}} HA - CD \tag{5.1}$$

$$K_{1:1} = \frac{[HA - CD]}{[HA][CD]} \tag{5.2}$$

where $K_{1:1}$ is the equilibrium or stability constant for the 1:1 complex of *HA* and *CD*, *HA-CD*. The concentration gradients of various solution species across the diffusion layer during indomethacin crystal growth in a low pH supersaturated solution containing HP-β-CD are schematically described in Figure 5.2. Here, the subscripts "*b*" and "*s*" represent bulk and surface, respectively. *HB* and B^- represent the concentrations of unionized and ionized species of a buffer. The thickness of the diffusion layer is *h*. Since the mass transfer occurs from the bulk to the solid-solution interface, the value for *X* (space variable) is assumed to be equal to zero at the bulk end of the diffusion layer and equal to *h* at the solid-solution interface.

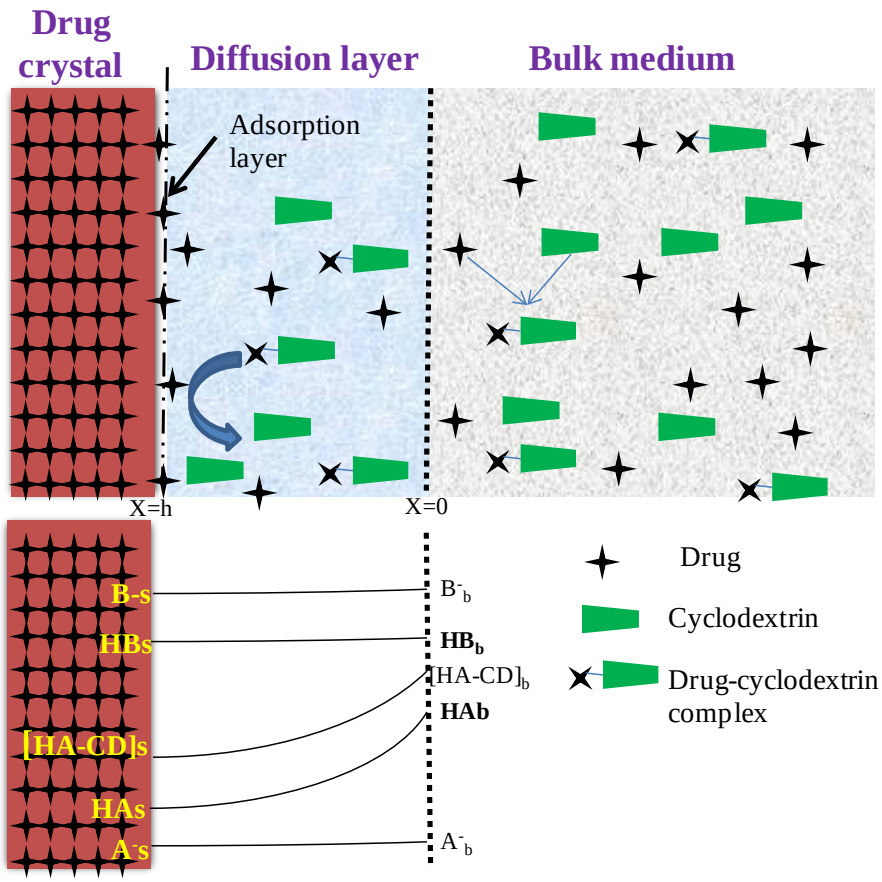

Figure 5.2. Schematic diagram describing concentration gradients of solution species across the diffusion layer during crystal growth of a model weak acid drug (HA) in supersaturated suspensions containing drug seed crystals, a complexing agent (CD or HP-β-CD) and a buffer (HB).

Mass balance of the species at any point *X* in the diffusion layer must take into account both diffusion and reaction. The reaction rate component is expressed as Φ. At steady state, the concentration change of each species with time can be expressed by the following equations:

$$\frac{\partial[HA]}{\partial t} = D_{HA}\frac{\partial^2[HA]}{\partial x^2} + \Phi_1 = 0 \tag{5.3}$$

$$\frac{\partial[CD]}{\partial t} = D_{CD}\frac{\partial^2[CD]}{\partial x^2} + \Phi_2 = 0 \tag{5.4}$$

$$\frac{\partial[HA-CD]}{\partial t} = D_{HA-CD}\frac{\partial^2[HA-CD]}{\partial x^2} + \Phi_3 = 0 \tag{5.5}$$

where, D_{HA}, $D_{HA\text{-}CD}$, and D_{CD} are the diffusion coefficients of *HA*, *HA-CD*, and *CD*, respectively. According to the mass balance relationships,

$$D_{HA}\frac{\partial^2[HA]}{\partial x^2} = -D_{HA-CD}\frac{\partial^2[HA-CD]}{\partial x^2} \tag{5.6}$$

$$D_{CD}\frac{\partial^2[CD]}{\partial x^2} = -D_{HA-CD}\frac{\partial^2[HA-CD]}{\partial x^2} \tag{5.7}$$

Integrating the above equations yields

$$D_{HA}\frac{\partial[HA]}{\partial x} + D_{HA-CD}\frac{\partial[HA-CD]}{\partial x} = C_1 \tag{5.8}$$

$$D_{CD}\frac{\partial[CD]}{\partial x} + D_{HA-CD}\frac{\partial[HA-CD]}{\partial x} = C_2 \tag{5.9}$$

where, C_1 and C_2 are the integration constants. Upon the second integration of the above equations one obtains

$$D_{HA}[HA] + D_{HA-CD}[HA-CD] = C_1 X + C_3 \tag{5.10}$$

$$D_{CD}[CD] + D_{HA-CD}[HA-CD] = C_2 X + C_4 \tag{5.11}$$

The following boundary conditions can be applied to determine the integration constants:

At X=0 (bulk):

$[HA]_b$=from total drug concentration

$[HA\text{-}CD]_b$= from total drug concentration

$[CD]_b$=known

At X=h (solid surface):

$[HA]_s$=indomethacin intrinsic solubility

$[HA\text{-}CD]_s$=unknown

$[CD]_s$=unknown

$\frac{\partial[CD]}{\partial x} = \frac{\partial[HA-CD]}{\partial x} = 0$; Since their fluxes at the solid boundary will be equal to zero.

From Eq. 5.9 and the boundary condition at X=h

$$D_{CD}\frac{\partial[CD]}{\partial x}+D_{HA-CD}\frac{\partial[HA-CD]}{\partial x}=C_2=0 \tag{5.12}$$

From Eq. 5.11 and the boundary conditions at X=0 and h

$$D_{CD}[CD]_b+D_{HA-CD}[HA-CD]_b=C_4 \tag{5.13}$$

$$D_{CD}[CD]_s+D_{HA-CD}[HA-CD]_s=C_2h+C_4 \tag{5.14}$$

Combining Eqs. 5.12, 5.13 and 5.14 one obtains

$$D_{CD}[CD]_b+D_{HA-CD}[HA-CD]_b=D_{CD}[CD]_s+D_{HA-CD}[HA-CD]_s \tag{5.15}$$

By substituting from Eq. 5.4,

$$[CD]_s=\frac{D_{CD}[CD]_b+D_{HA-CD}[HA-CD]_b}{D_{CD}+D_{HA-CD}K_{1:1}[HA]_s} \tag{5.16}$$

$[CD]_s$ can be calculated from Eq. 5.16. Furthermore, $[HA\text{-}CD]_s$ can be estimated using $[CD]_s$ and Eq. 5.2. The indomethacin bulk diffusion controlled crystal growth rate or mass deposition rate, J (moles cm^{-2} $time^{-1}$), in the presence of a complexing agent such as HP-β-CD can be defined as

$$\frac{1}{A}\frac{dm}{dt}=J=\frac{1}{h}\left[D_{HA}\left([HA]_b-[HA]_s\right)+D_{HA-CD}\left([HA-CD]_b-[HA-CD]_s\right)\right] \tag{5.17}$$

where A is the surface area of seed crystals in cm^2, m is the mass of indomethacin in moles, and t is time. The bulk diffusion controlled crystal growth rate of indomethacin without any complexing agent, J_0, can be defined as

$$J_0 = \frac{1}{h}\left[D_{HA}\left([HA]_b^{total} - [HA]_s^{total}\right)\right] \tag{5.18}$$

where $[HA]_b^{total}$ and $[HA]_s^{total}$ are total concentrations of ionized and unionized indomethacin in the bulk and at the solid-liquid interface, respectively. The indomethacin crystal growth inhibition factor (R) was defined as

$$R = J / J_0 \tag{5.19}$$

where J and J_0 are indomethacin crystal growth rates with and without a model PPI such as HP-β-CD.

MATERIALS AND METHODS

Materials

Indomethacin (1-(*p*-chlorobenzoyl)-5-methoxy-2-methylindole-3-acetic acid, 99+%, γ-polymorph, molecular weight =357.8 g/mole, pK_a=4.17[148]) and PVP (PVP K29-32, molecular weight: ~40,000 g/mole) were obtained from Sigma-Aldrich, Inc. (St. Louis, MO, USA). HP-β-CD (Cavitron 32005, molecular weight =1297 g/mole, degree of substitution: 0.4) was received from Cargill Food and Pharma Specialties (Cedar Rapids, IA). HPMC (Methocel E5, molecular weight =10,000 g/mole) was obtained from Dow Chemical Company (Midland, MI). Nylon net filters (30 μ) and polycarbonate membrane filters (3 μ) were purchased from Millipore Inc., (Milford, MA,

USA). Nylon membrane filters (0.2 µ) and 13 mm PTFE syringe filters (0.45 µ) were purchased from Whatman Int. Ltd. (Maidstone, England). Deionized water was obtained from a MilliQ water purification apparatus (Milli-Q Synthesis, Millipore Inc., Milford, MA, USA) and pre-filtered through a 0.22 µ filter (Millipak Express 20, Millipore Inc., Milford, MA, USA). All other reagents and materials were of an analytical grade.

Preparation of Indomethacin Seed Crystal Suspension

The indomethacin seed crystal suspension preparation method has been previously described in detail.[104] Briefly, the suspension was prepared by dispersing ~0.1% w/w indomethacin in 50 mM phosphate buffer at 25ºC for about 3 days using a shaker water bath. The pH and ionic strength were maintained at 2.15 and 0.1 M (using NaCl), respectively. The desired size distribution of the seed crystals was obtained by first passing the equilibrated suspension through a 30 µ filter followed by another pass through a 3 µ filter. The seed crystals retained on the 3 µ filter were re-suspended in saturated indomethacin solution. The saturated indomethacin suspension was stored at 25ºC prior use.

Indomethacin Equilibrium & Apparent Solubility with Model PPIs

The equilibrium solubility of indomethacin in the presence of model PPIs was measured using the same method that was used previously to determine its intrinsic solubility.[104] Briefly, a specific amount of indomethacin in excess of its saturation solubility was shaken end-to-end in the model PPI solution (pH 2.15) using a rotary shaker. Samples were withdrawn at 1, 2, 3 and 5-day time intervals and filtered through a 0.45 µ PTFE syringe filter while ensuring its saturation. The filtrates were assayed for

indomethacin using UV spectrophotometry (Lambda 40P, Perkin-Elmer Inc., USA) and 1-cm matched quartz cells (Starna Cells Inc., Atascadero, CA, USA) at 321 nm.

The indomethacin solubility after crystal growth in the presence of model PPIs, henceforth referred to as the indomethacin apparent solubility, was measured using the previously described method.[104,166] Briefly, the indomethacin apparent solubility was determined from the equilibrated suspensions of indomethacin after crystal growth from supersaturated concentrations in the presence of model PPIs. Indomethacin concentrations were measured directly in the suspensions using second-derivative UV spectroscopy as well as in clear solutions obtained by filtering the suspensions through a 0.45 μ syringe filter.

Viscosity Determination of Model PPI Solutions

The viscosity of model PPI solutions was measured using a programmable cone/plate rheometer (Brookfield DV-III LV; Brookfield Engineering, Stoughton, MA). The measurements were taken at 25°C using a CPE-40 spindle. The sample volume and RPM were 0.5 mL and 100, respectively.

Indomethacin Crystal Growth Rate Measurement in the Presence of Model PPIs

The method to measure indomethacin crystal growth rates in the absence of model PPIs has been described in detail in our previous publication.[104] Using the same method, indomethacin crystal growth rates in the presence of model PPIs were determined from the decline in indomethacin concentration versus time from a supersaturated concentration to a lower equilibrium concentration at 25ºC using an online second-derivative UV spectroscopic method. A more detailed description of the development

and validation of the second-derivative UV method is provided elsewhere.[104] The second-derivative UV absorbance of indomethacin was measured at 295 nm after taking the second-derivative of the original indomethacin UV spectrum (210 to 400 nm). Suspensions containing defined quantities of seed crystals at pH 2.15 were supersaturated by adding a highly concentrated indomethacin solution (pH 6.8) containing specific amounts of model PPIs using a micro-syringe pump. Both, the crystal growth suspensions and the highly concentrated indomethacin-model PPI solutions were in 50 mM phosphate buffer having an ionic strength of 0.1 M using NaCl. The suspensions were stirred using a pivoted magnetic stirrer at 400 RPM to ensure homogeneity.

Indomethacin Seed Crystal Characterization

Indomethacin seed crystals, before and after crystal growth, were characterized for their size, shape and physical form. The mean size, number concentration and the size distribution were obtained using a Coulter counter (Multisizer Z2, Beckman Coulter Inc., Miami, FL, USA). A 50 µ glass aperture tube was used, which provided size distribution data between 2 and 25 µ. The Coulter counter was calibrated using 3 and 10 µ particle size standards (Beckman Coulter Inc., Miami, FL, USA). The seed crystals were characterized for any morphological changes before and after growth using polarized light microscopy (PLM). The physical form of the indomethacin seed crystals was verified before and after growth using powder X-ray diffraction (PXRD). Indomethacin seed crystals were separated from suspension by filtration. The seed crystals were air dried for about 24 hours before being analyzed using an X-ray diffractometer (Bruker D8 Advance, Bruker AXS, Inc., Madison, WI, USA). The X-ray

copper anode (1.54A) was operated at 40 kV and 40 mA. The scans were performed from 3 to 35º 2θ with 0.05° step size and 4 or 0.6 seconds step time.

Data Analyses

Linear and non-linear least-squares analyses were performed using a software program (Scientist, Micromath Inc., St. Louis, MO, USA). The other statistical tests including the Student's t-test and ANOVA were performed using Microsoft Excel.

RESULTS

Model PPI Effects on Indomethacin Equilibrium & Apparent Solubility

The intrinsic solubility of indomethacin was determined previously to be $3.4 \pm 0.1 \times 10^{-6}$ M (95% CI).[104] The effects of model PPIs including HP-β-CD, PVP and HPMC on the equilibrium solubility were determined at 0 to 1% w/w PPI concentrations. As shown in Figure 5.3, HP-β-CD significantly increased the equilibrium solubility of indomethacin. For example, at 1% w/w HP-β-CD, indomethacin solubility increased by more than 100-fold from $3.4 \pm 0.1 \times 10^{-6}$ M to $3.9 \pm 0.2 \times 10^{-5}$ M (25 ºC, pH 2.15 at 0.1 M ionic strength using NaCl). The effects of PVP and HPMC on the equilibrium solubility of indomethacin were markedly less. The equilibrium solubilities of indomethacin were $7.7 \pm 0.7 \times 10^{-6}$ M and $6.9 \pm 0.2 \times 10^{-6}$ M in 1% w/w PVP and HPMC, respectively. These solubilities were approximately 50-fold lower than that observed with 1% w/w HP-β-CD.

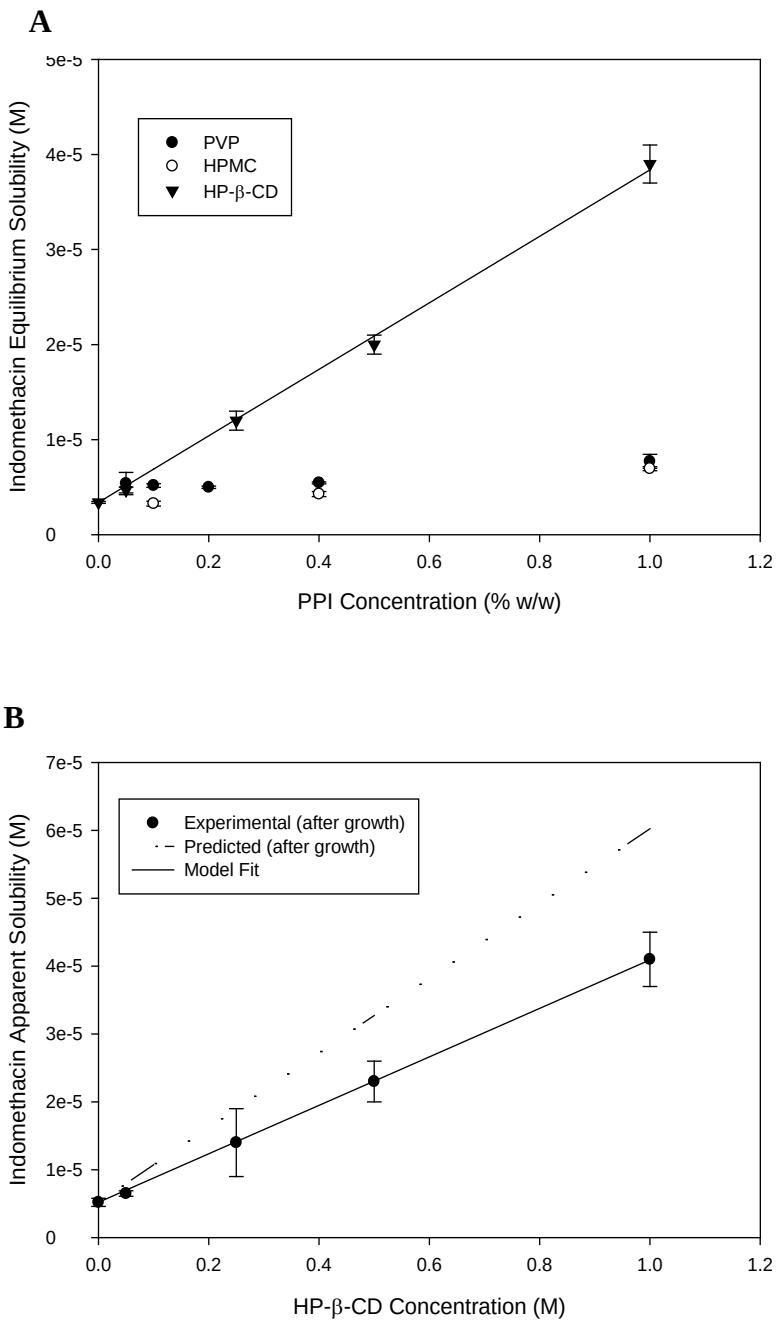

Figure 5.3. (A) Model PPI Effects on indomethacin equilibrium solubility. (B) Effect of HP-β-CD on indomethacin apparent solubility after crystal growth. The solid lines represent the model fit using Eq. 5.20. The broken line represents the predicted indomethacin apparent solubility after crystal growth using the indomethacin- HP-β-CD complexation constant before growth (1340 M^{-1}) and Eq. 5.20.

A linear relationship was observed for the effect of HP-β-CD concentration on the equilibrium solubility of indomethacin (Figure 5.3). The equilibrium constant ($K_{1:1}$) for 1:1 indomethacin:HP-β-CD complexation was estimated by fitting the indomethacin solubility profile as a function of HP-β-CD concentration to Eq. 5.20.

$$S_T = [HA] + \frac{K_{1:1}[HA][CD_T]}{1 + K_{1:1}[HA]} \tag{5.20}$$

where S_T is the equilibrium solubility of indomethacin in the presence of HP-β-CD, [*HA*] is the intrinsic solubility of indomethacin, and CD_T is the total concentration of HP-β-CD. The model fit the solubility profile very well (Figure 5.3, solid line). The estimated indomethacin:HP-β-CD complexation constant ($K_{1:1}$) was 1340 ± 40 (95% CI) M^{-1}.

In a previous study,[104] a significant difference between the solubilities of indomethacin before and after crystal growth (with no PPI present) was observed. The indomethacin solubility after crystal growth (i.e., indomethacin apparent solubility) was about 55% higher ($5.2 \pm 0.6 \times 10^{-6}$ M versus $3.4 \pm 0.1 \times 10^{-6}$ M) than the equilibrium solubility before crystal growth. The higher apparent solubility of indomethacin after crystal growth was attributed to the formation of a higher energy surface layer on the existing indomethacin seed crystals. As shown in Table 5.1 and Figure 5.3B, the apparent solubilities of indomethacin after crystal growth in the presence of HP-β-CD (up to 1% w/w) determined in the present study were higher than the equilibrium solubilities before growth. Moreover, it was observed that the higher indomethacin apparent solubility was a function of HP-β-CD concentration. The apparent/equilibrium solubility

ratios decreased as HP-β-CD concentration increased (Table 5.1). At higher concentrations, HP-β-CD may significantly influence the growth of the higher energy surface layer on indomethacin seed crystals from supersaturated solutions or HP-β-CD could enhance the rate of transformation of the higher energy form of indomethacin deposited on the crystal surface to a lower energy form. This in turn could provide a relatively lower indomethacin apparent solubility after crystal growth in the presence of HP-β-CD than that predicted using the indomethacin-HP-β-CD complexation constant and the higher apparent solubility obtained after crystal growth in the absence of HP-β-CD (Figure 5.3B). This hypothesis was further verified by determining the apparent solubility of indomethacin in the presence of 1% w/w HP-β-CD starting with seed crystals containing the higher energy surface obtained after crystal growth. According to the hypothesis, the experimental indomethacin apparent solubility should have been lower than the theoretically predicted apparent solubility. The experimental indomethacin apparent solubility ($4.5 \pm 0.4 \times 10^{-5}$ M) was lower than the theoretically predicted solubility ($5.9 \pm 0.6 \times 10^{-5}$ M), in accordance with the hypothesis. For PVP and HPMC, the indomethacin apparent solubilities after crystal growth were similar to the indomethacin equilibrium solubility indicating the absence of a higher energy surface film after crystal growth in the presence of PVP and HPMC (data not shown).

The apparent solubility profile for indomethacin after crystal growth in the presence of HP-β-CD (Table 5.1 and Figure 5.3B) was well described by Eq. 5.20 when a higher value for the solubility [*HA*] than that used in Figure 5.3A was employed (i.e., 5.2×10^{-6} M vs. 3.4×10^{-6} M) along with an indomethacin:HP-β-CD complexation constant ($K'_{1:1}$) of 895 ± 16 (95% CI) M^{-1}. These apparent parameter values were then utilized in

modeling the inhibitory effect of HP-β-CD on the bulk diffusion controlled indomethacin crystal growth at high S (Table 5.2).

Indomethacin Crystal Growth Rate Measurement in the Presence of Model PPIs

Representative indomethacin desupersaturation profiles (concentration versus time) determined from supersaturated indomethacin seed crystal suspensions in the presence and absence of model PPIs (HP-β-CD, PVP and HPMC) at high degrees of supersaturation (S>3) are shown in Figure 5.4. The degree of supersaturation *(S)* is defined by Eq. 5.21.

$$S = \frac{C}{C_s} \tag{5.21}$$

where c is indomethacin concentration immediately after supersaturation and c_s is the equilibrium solubility of indomethacin. The desupersaturation profiles were fit to a first order empirical crystal growth model[104] using Eq. 5.22.

$$-\frac{dc_b}{dt} = \frac{k_G A}{V_b}\left(C_b - C_s\right) \tag{5.22}$$

where C_b is the solute concentration in the bulk medium, k_G is an apparent crystal growth rate coefficient, A/V_b is the crystalline surface area per unit volume of the bulk medium, and C_s is the solution concentration of solute at equilibrium (i.e., the saturation solubility).

Table 5.1. Effect of HP-β-CD on Indomethacin Equilibrium & Apparent Solubility.

HP-β-CD concentration (% w/w)	Indomethacin Solubility (M)		Solubility Ratio (Apparent/Equilibrium)
	Equilibrium (Before Growth)	Apparent (After Growth)	
0	$3.4 \pm 0.1 \times 10^{-6}$	$5.2 \pm 0.6 \times 10^{-6}$	1.5
0.05	$4.7 \pm 0.3 \times 10^{-6}$	$6.5 \pm 0.4 \times 10^{-6}$	1.4
0.25	$1.2 \pm 0.1 \times 10^{-5}$	$1.4 \pm 0.5 \times 10^{-5}$	1.2
0.5	$2.0 \pm 0.1 \times 10^{-5}$	$2.3 \pm 0.3 \times 10^{-5}$	1.2
1	$3.9 \pm 0.2 \times 10^{-5}$	$4.1 \pm 0.4 \times 10^{-5}$	1.1

Table 5.2. Model Parameters Employed in Predicting Effects of HP-β-CD on Indomethacin Crystal Growth Kinetics at High Degrees of Supersaturation.

Parameters	Values	
Diffusion coefficient of indomethacin (D_{HA})	5.6×10^{-6}	cm^2/sec
Diffusion coefficient of indomethacin:HP-β-CD complex ($D_{HA\text{-}CD}$)	3.0×10^{-6}	cm^2/sec
Diffusion layer thickness (h)	1.2×10^{-3}	cm
Indomethacin apparent solubility	5.2×10^{-6}	M
Stability constant of indomethacin:HP-β-CD complex ($K'_{1:1}$)	9.0×10^{2}	M^{-1}

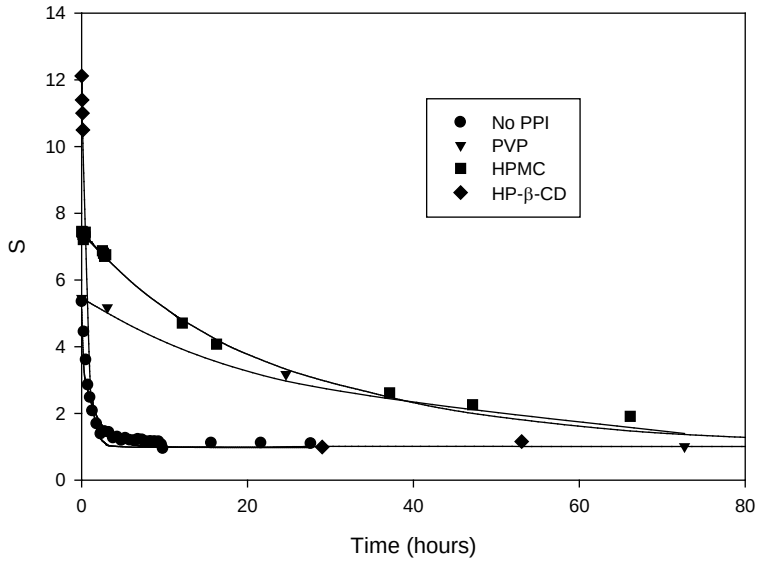

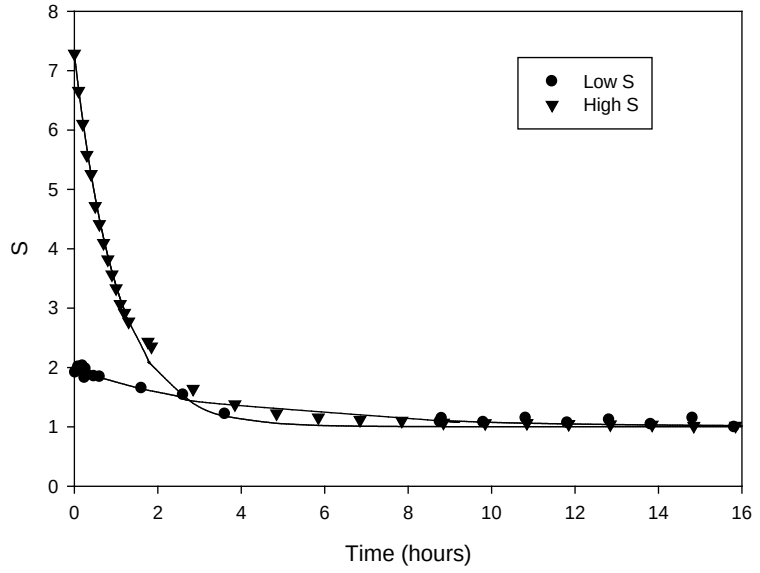

Figure 5.4. Representative indomethacin crystal growth kinetic profiles (A) in the presence and absence of model PPIs at high S and (B) in the presence of HP-β-CD at high and low S (0.05% w/w). The solid lines represent fits to the first-order empirical crystal growth model (Eq. 5.22).

The driving force for crystal growth was calculated using the previously determined indomethacin apparent solubilities either in the presence or absence of model PPIs. As shown in Figure 5.4A (solid lines), the first-order empirical crystal growth model (Eq. 5.22) fit the indomethacin desupersaturation (or crystal growth kinetic) profiles in the presence or absence of model PPIs at high S very well. Indomethacin crystal growth rates measured from model fitting were further utilized to estimate an indomethacin crystal growth inhibition factor (R) for each model PPI at high S using Eq. 5.19 and the previously determined indomethacin crystal growth rate coefficient in the absence of any PPI at high S ($4.7 \pm 0.7 \times 10^{-3}$ cm/sec). The values of the indomethacin crystal growth rate coefficient (k_G) decreased from $4.0 \pm 0.3 \times 10^{-3}$ to $2.3 \pm 0.4 \times 10^{-3}$ cm/sec and R decreased from 0.84 to 0.49 when the concentration of HP-β-CD was increased from 0.05 to 1% w/w (Table 5.3). The values of R at high S for 0.05, 0.2, 0.5 and 1% w/w HP-β-CD were 0.84, 0.75, 0.65 and 0.49, respectively. The relationship between the concentration of HP-β-CD and R was modeled using the reactive diffusion layer theory (Eq. 5.16 & 5.17). As shown in Figure 5.5, the predicted values of R using the reactive diffusion layer model were in good agreement with the experimental values of R.

The inhibitory effects of model PPIs on the crystal growth of indomethacin at high S were further evaluated by comparing the values of k_G and R for indomethacin crystal growth in the presence of each model PPI (Table 5.3 & Figure 5.6). The k_G values for indomethacin crystal growth at high S in the presence of 0.05% w/w HP-β-CD, HPMC, and PVP were $4.0 \pm 0.3 \times 10^{-3}$, $1.4 \pm 0.6 \times 10^{-4}$, $3.0 \pm 1.9 \times 10^{-5}$cm/sec, respectively (Table 5.3). The values of R at high S for HP-β-CD, HPMC and PVP (0.05% w/w) were 0.84, 0.03, and 0.006, respectively. Significantly smaller values of k_G and R for PVP and HPMC indicated that the indomethacin crystal growth inhibitory effects of PVP and HPMC were significantly greater than those of HP-β-CD at high S. Moreover, PVP was a better inhibitor of the crystal growth of indomethacin as compared to HP-β-CD and HPMC. While the indomethacin crystal growth inhibitory effect of HP-β-CD increased as function of its concentration, no significant relationship was observed between the crystal growth inhibitory effects of PVP and HPMC and their concentrations at high S. This indicates that the mechanisms of action for the complexing agent HP-β-CD and polymers such as PVP and HPMC were different at high S.

The model PPI effects on indomethacin crystal growth inhibition at low S (<3) were also determined using the same method of measurement. The indomethacin crystal growth kinetic profiles at low S in the presence of model PPIs were also modeled using Eq.5.22. The model fit the profiles well (Figure 5.4B) and the indomethacin crystal growth rate coefficients (k_G) at low S in the presence of the model PPIs were estimated. The k_G values determined at high and low S in the presence of HP-β-CD, HPMC, and PVP are compared in Table 5.3 and Figure 5.6. The k_G for indomethacin crystal growth at low S in the presence of 0.05% w/w HP-β-CD, HPMC, and PVP were $2.2 \pm 0.3 \times 10^{-4}$,

$1.6 \pm 0.3 \times 10^{-4}$, $1.6 \pm 0.1 \times 10^{-5}$cm/sec, respectively (Table 5.3). The rank order for the effectiveness of the PPIs as inhibitors of indomethacin crystal growth changed from PVP > HPMC > HP-β-CD at high S to PVP > HPMC ≈ HP-β-CD at low S.

Although the kG values at high and low S for PVP and HPMC were similar, their inhibitory effects at high S were dramatic (Figure. 5.6). This is due to the fact that the mechanism of crystal growth in the absence of these PPIs was diffusion controlled at high S but was shifted to surface integration-controlled in the presence of PVP or HPMC. At low S, indomethacin crystal growth became surface integration-controlled even in the absence of PPIs and therefore the inhibition factors at low S (calculated relative to the crystal growth rate of indomethacin at low S) were modest. This further indicated that the mechanisms of crystal growth in the presence of PVP and HPMC were similar at high and low S. In contrast to the effects of PVP and HPMC, there was a significant difference between the indomethacin kG at high and low S in the presence of HP-β-CD. The value of R at low S was estimated using Eq. 5.19 and the previously determined indomethacin kG at low S (5.5 ± 1.3 × 10-4 cm/sec) in the absence of any PPI. The R for HP-β-CD at high and low S were 0.84 and 0.40 indicating that HP-β-CD showed a 2-fold greater inhibitory effect on the crystal growth of indomethacin at low S as compared to high S, which may suggest a possible change in the mechanism of action of HP-β-CD between high and low S.

Table 5.3. Comparison of Model PPI Effects on Indomethacin Crystal Growth Inhibition at High and Low Degrees of Supersaturation (S).

PPI	PPI Conc. (% w/w)	High S (>3)		Low S (<3)	
		k_G[b] (cm/sec)	R[c]	k_G[b] (cm/sec)	R[c]
No PPI[104,166]	--	$4.7 \pm 0.7 \times 10^{-3}$	1.0 ± 0.1	$5.5 \pm 1.3 \times 10^{-4}$	1.0 ± 0.2
HP-β-CD	0.05	$4.0 \pm 0.3 \times 10^{-3}$	$8.4 \pm 0.3 \times 10^{-1}$	$2.2 \pm 0.3 \times 10^{-4}$	$4.0 \pm 0.6 \times 10^{-1}$
	0.2	$3.5 \pm 0.3 \times 10^{-3}$	$7.5 \pm 0.7 \times 10^{-1}$	--	--
	0.5	$3.0 \pm 0.2 \times 10^{-3}$	$6.4 \pm 0.5 \times 10^{-1}$	--	--
	1	$2.3 \pm 0.4 \times 10^{-3}$	$5.0 \pm 0.9 \times 10^{-1}$	--	--
PVP	0.05	$3.0 \pm 1.9 \times 10^{-5}$	$6.0 \pm 4.0 \times 10^{-3}$	$1.6 \pm 0.1 \times 10^{-5}$	$2.9 \pm 0.2 \times 10^{-2}$
	0.2	$3.2 \pm 2.1 \times 10^{-5}$	$7.0 \pm 4.0 \times 10^{-3}$	--	--
HPMC	0.05	$1.4 \pm 0.6 \times 10^{-4}$	$3.1 \pm 1.0 \times 10^{-2}$	$1.6 \pm 0.3 \times 10^{-4}$	$2.9 \pm 0.6 \times 10^{-1}$
	0.2	$9.0 \pm 0.7 \times 10^{-5}$	$2.0 \pm 1.0 \times 10^{-2}$	--	--

[a] Preliminary data(single runs) at selected PPI concentrations are reported in a conference proceedings[25]; [b] k_G: Indomethacin crystal growth rate coefficient (cm/sec); [c]R: Indomethacin crystal growth inhibition factor

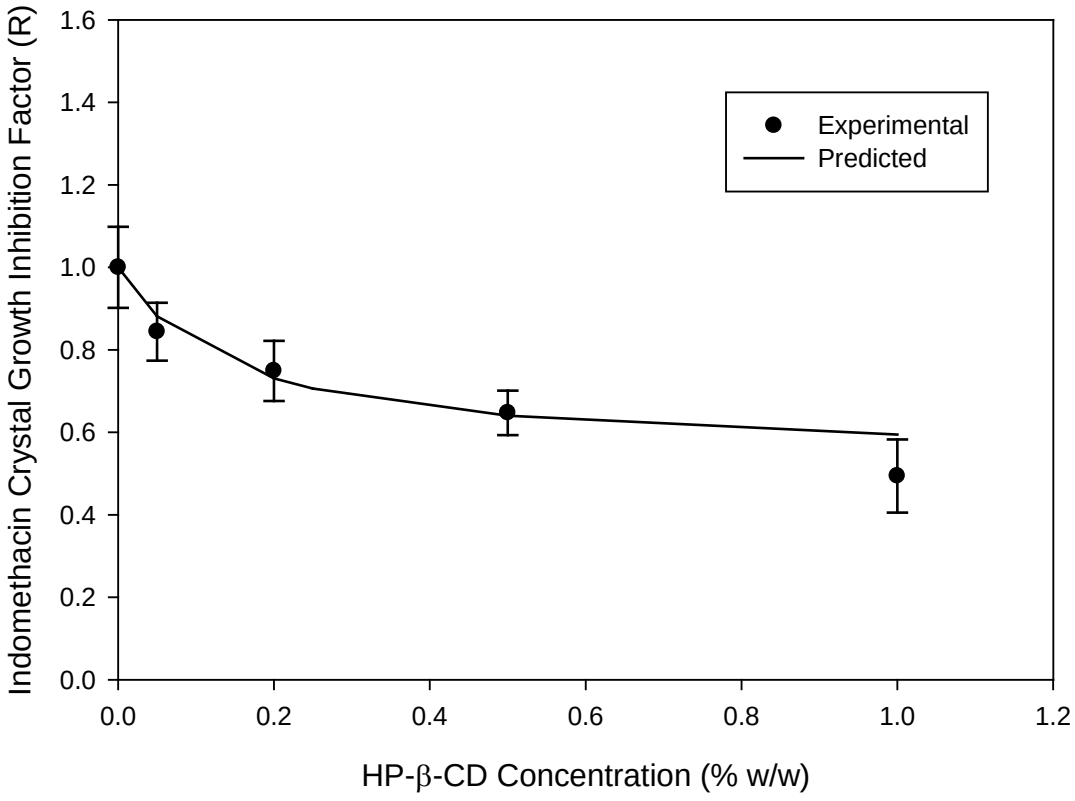

Figure 5.5. Inhibitory effects of HP-β-CD on the bulk diffusion controlled crystal growth of indomethacin at high degrees of supersaturation. Error bars represent 95% confidence intervals.

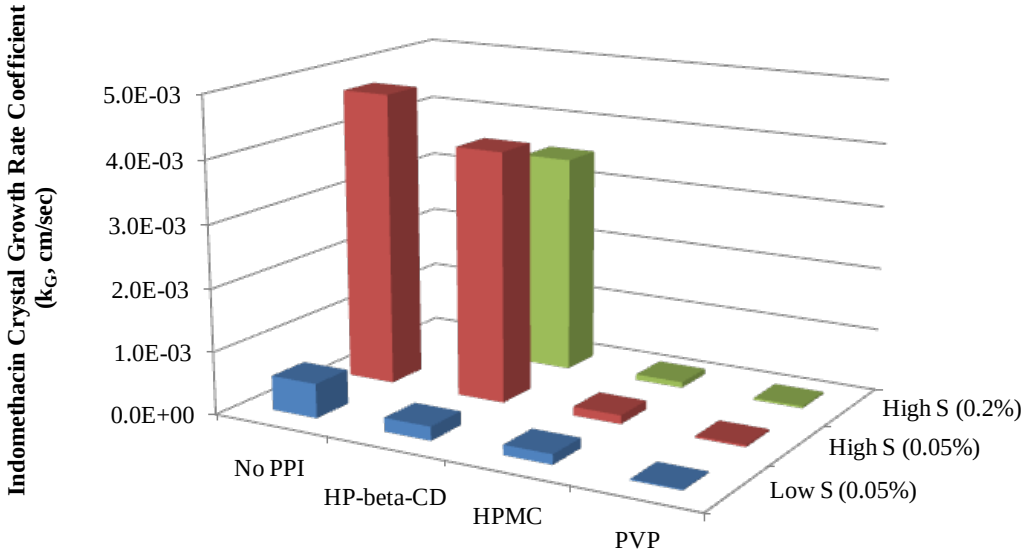

Figure 5.6. Inhibitory effects of model PPIs on indomethacin crystal growth at high and low degrees of supersaturation.

Viscosity of Model PPI Solutions at Different Concentrations

Since the bulk viscosity of supersaturated indomethacin samples could change the bulk-diffusion controlled rate of indomethacin crystal growth by affecting the diffusion of indomethacin molecules from the bulk to the solid-liquid interface, viscosities of model PPI solutions at different concentrations (0 to 3 % w/w) were measured. As shown in Figure 5.7, the viscosity of HPMC solutions was significantly higher than that of PVP and HP-β-CD solutions. The observed rank order for the viscosity of PPI solutions at concentrations between 0 to 1% w/w was HPMC >PVP >HP-β-CD. The viscosity of HPMC solutions increased significantly at higher HPMC concentrations (up to 1% w/w), from 1 to 1.7 cP when the concentration was increased from 0.1 to 1% w/w, respectively. An almost linear relationship was observed for the effect of HPMC concentration on solution viscosity. While the viscosity of PVP solutions increased moderately as a function of PVP concentration (up to 1% w/w), no significant change in the viscosity of HP-β-CD solutions was observed up to 3% w/w concentration. Between 0 to 3% w/w concentrations, the viscosity of HP-β-CD solutions remained at approximately 0.9 cP at 25°C, which was similar to the viscosity of the blank buffer vehicle that was used to prepare the model PPI solutions. The viscosity of PVP solutions increased from 0.9 to 1.2 cP when the concentration was increased from 0.25 to 1% w/w, respectively. Below a 0.5% w/w PVP concentration, the viscosity remained constant at ~0.9 cP.

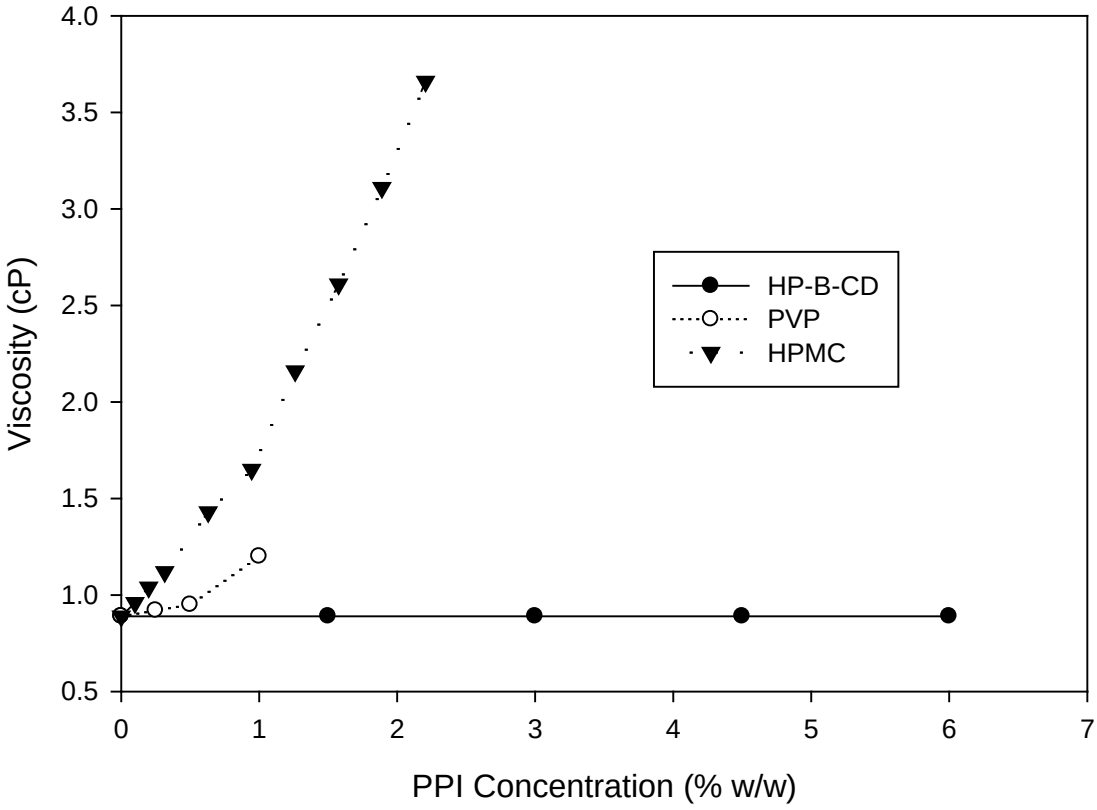

Figure 5.7. Viscosity of model PPI solutions at different concentrations.

Indomethacin Seed Crystal Suspension Characterization after Crystal Growth with Model PPIs

Indomethacin seed crystals were characterized for their mean size, size distribution and number concentration before and after crystal growth using a Coulter counter. The seed crystals had a typical mass median diameter of ~11 micron and surface area of ~0.04 cm^2 per mL of suspension. The indomethacin seed crystal concentration (# of seed crystals per mL) was approximately 41,000/mL, which amounted to approximately 150 μg of indomethacin per 3 mL in a typical crystal growth experiment. Additional details on the size distribution analysis of these seed crystals as well as a typical indomethacin seed crystal size distribution profile can be found in an earlier publication.[104] The seed crystals after growth in the presence of model PPIs were also characterized using PXRD. A comparison of the PXRD spectra of indomethacin crystals ("as received") and indomethacin seed crystals after growth in the presence of model PPIs is shown in Figure 5.8. The PXRD analysis indicated that there was no significant change in indomethacin crystalline form (γ-polymorph) upon crystal growth with model PPIs, although this technique would not provide information on the nature of the thin film deposited on the crystal surface during growth.

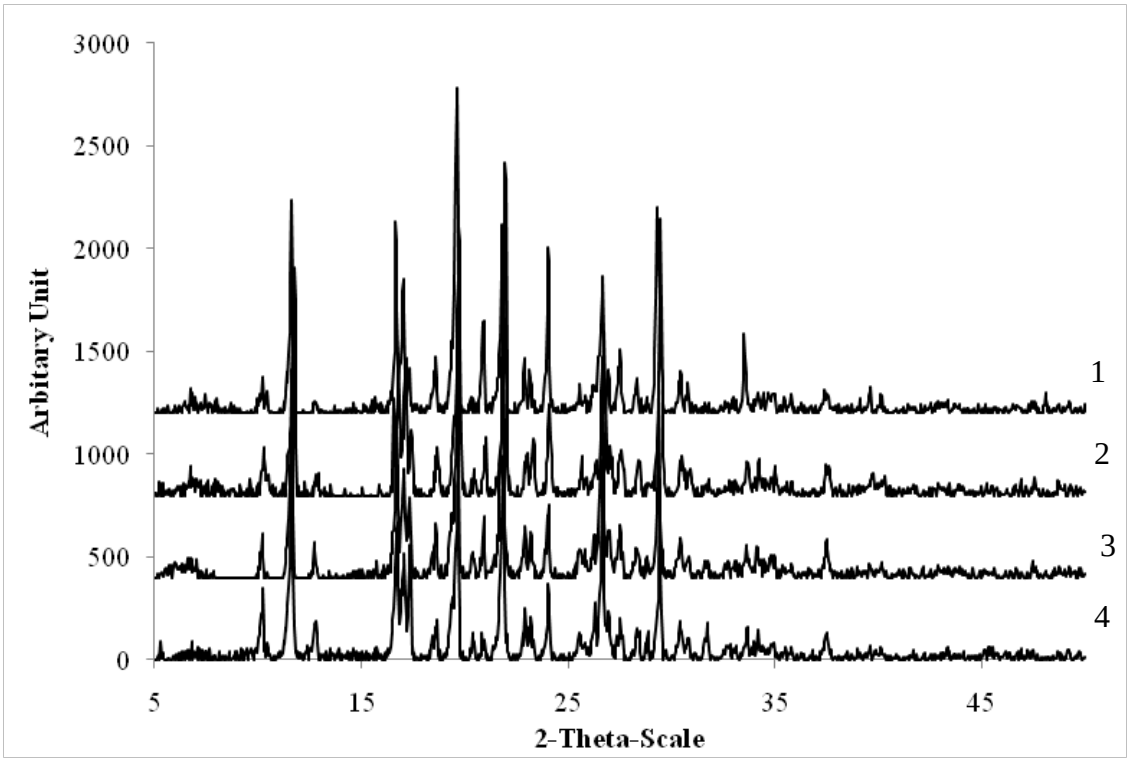

Figure 5.8. PXRD patterns of indomethacin seed crystals after growth with (1) no PPI (indomethacin "as received"), (2) hydroxypropyl β-cyclodextrin, (3) polyvinylpyrrolidone, and (4) hydroxypropyl methylcellulose.

DISCUSSION

Comparison of Model PPI Effects on Indomethacin Crystal Growth Kinetics

With the growth in popularity of high energy dispersion formulations for drug development, interest in factors that prolong supersaturation in both solids and solutions has also grown in recent years.[1,53] The physical instability of supersaturated drug products still remains a major challenge for pharmaceutical scientists. Quantitative, mechanistic modeling to assess the degree of stabilization of supersaturated systems provided by PPIs would be beneficial in addressing this major challenge.

Cyclodextrins[74] and polymers such as PVP[108,164] and HPMC[108,164] have been used in drug product development to improve the stability of solid and solution based supersaturated states. In the case of solution-state supersaturation, the beneficial effects of these PPIs could be classified into three hypothetical case scenarios. Case (1): Higher molecular weight PPIs could enhance viscosity, which would lower the diffusivity of drugs. The lower diffusivity could inhibit drug nucleation and crystal growth (the two major processes that affect the stability of the supersaturated state) and, in turn, maintain supersaturation. Case (2): PPIs could form complexes with the drug, which would not only enhance the equilibrium solubility of the drug but also reduce the driving force for drug nucleation and crystal growth and, in turn, drug precipitation. Finally, Case (3): PPIs act at the solid-solution interface to inhibit incorporation of molecules from solution into the growing crystal lattice. The main objective of this study was to quantitatively explore the inhibitory effects of some of the pharmaceutically relevant PPIs (HP-β-CD, PVP & HPMC) on the crystal growth of indomethacin, a model poorly water soluble drug and to classify these effects based on the scenarios described above. For this effort,

we have utilized our recent understanding of the crystal growth kinetics of indomethacin from a previous study where we employed a newly developed second-derivative UV technique to determine the kinetic order and the rate limiting steps of indomethacin crystal growth kinetics in the absence of PPIs.

All three model PPIs including HP-β-CD, PVP & HPMC inhibited indomethacin crystal growth at high S (Table 5.3 & Figures 5.4, 5.5 & 5.6). While the inhibitory effects of PVP and HPMC at high S were significantly higher than that of HP-β-CD, a good correlation between the crystal growth inhibitory effects of HP-β-CD and its concentration was observed (Table 5.3 & Figure 5.5). As described in Case 1, the higher molecular weight model PPIs could increase the viscosity of indomethacin suspensions, which in turn could inhibit the rate of bulk diffusion controlled crystal growth of indomethacin at high S by increasing the diffusive barrier for indomethacin. To test this hypothesis, the change in indomethacin diffusivity due to higher bulk viscosity was theoretically calculated using the Stokes-Einstein equation as shown below.

$$D = \frac{kT}{6\pi\eta r} \tag{5.23}$$

where D is the diffusion coefficient or diffusivity of the solute, k is Boltzmann's constant, T is the absolute temperature, η is the viscosity of the bulk medium and r is the radius of the solute. Using the estimated indomethacin diffusivity, indomethacin crystal growth rates at high S were calculated using Eq. 5.22 for each model PPI. The bulk viscosity-adjusted indomethacin crystal growth inhibitory factor (R) for each model PPI was determined from the theoretically estimated bulk diffusion controlled indomethacin crystal growth rates in the presence and absence of a model PPI at high S (Eq. 5.19). The

bulk viscosity-adjusted R was compared with previously described ("Results" section) experimental R for HP-β-CD, PVP, and HPMC at a 0.2% w/w model PPI concentration. The values of the bulk viscosity-adjusted R for 0.2% w/w HP-β-CD, PVP, and HPMC were 1, 0.97, and 0.85, respectively. The values of the experimental R for 0.2% w/w HP-β-CD, PVP, and HPMC were 0.75, 0.007, and 0.02, respectively. Since there was no change in the bulk viscosity of indomethacin seed crystal suspensions in the presence of 0.2% w/w HP-β-CD, no significant effect of HP-β-CD on indomethacin crystal growth inhibition due to viscosity effects was predicted as indicated by the theoretical R value of 1. However, at 0.2% w/w HP-β-CD, the theoretical R (i.e., 1) for indomethacin was higher than the experimental R (i.e., 0.75). Similarly, the theoretical R values for PVP and HPMC were significantly different from the experimental R values at high S. The theoretical R values for PVP and HPMC at 0.2% were 0.97 and 0.85, respectively, whereas the experimental R values were 0.007 and 0.02. These results clearly indicate that Case 1, which invokes effects of model PPIs on bulk viscosity to account for their crystal growth inhibitory effects, could not account for the PPI effects on indomethacin crystal growth.

Modeling the Effects of HP-β-CD on Bulk Diffusion Controlled Crystal Growth Kinetics of Indomethacin

Unlike PVP and HPMC, HP-β-CD has a significant effect on the equilibrium solubility of indomethacin due to 1:1 complex formation between indomethacin and HP-β-CD (Figure 5.3). The Case 2 scenario, as mentioned earlier, was applied to explain the inhibitory effects of HP-β-CD on indomethacin crystal growth at high S. In supersaturated systems, a complexing agent such as HP-β-CD changes the equilibrium

solubility of the drug and reduces the driving force for crystal growth. The prediction of the inhibitory effect of a complexing agent such as HP-β-CD on crystal growth would depend on the way in which the degree of supersaturation (S) is calculated. If S is calculated using the concentration of free drug species then the calculated R (Eq. 5.19) would be equal to 1 indicating the absence of any expected inhibitory effect of the complexing agent on drug crystal growth. However, if the R is calculated using the total solution concentration then the predicted R would be less than 1 indicating significant inhibitory effects of the complexing agent on drug crystal growth.

The reactive diffusion layer theory has been successfully used to predict the exact nature of the driving force for drug dissolution under the influence of various bulk medium variables including pH and buffer concentration.[148,158,167,168] This theory simultaneously accounts for the mass transfer and the reaction processes accompanying diffusion and thereby precisely calculates the concentration gradients of various species of interest in the sample under investigation. In the present study, concentration gradients of free and complexed indomethacin species were required to predict the inhibitory effects of HP-β-CD on the bulk diffusion controlled crystal growth of indomethacin at high S. Therefore, the HP-β-CD concentration at the solid-liquid interface ($[CD]_s$) was estimated using Eq. 5.16 and other parameters listed in Table 5.2 for different HP-β-CD concentrations in the bulk ($[CD]_b$). The estimated $[CD]_s$ was about 3% higher than $[CD]_b$ at all HP-β-CD concentrations. This was attributed to the fact that only the free indomethacin was being incorporated into the existing indomethacin crystal lattice and therefore the free HP-β-CD was being recycled at the solid:liquid interface. The other parameters used in the predictions (Table 5.2) including

the apparent solubility of indomethacin and the thickness of the diffusion layer for indomethacin seed crystals were experimentally determined earlier.[104] The R for HP-β-CD was predicted using Eq. 5.16, 5.17, 5.22 and the parameters listed in Table 5.2. The predicted R values at a high S (>3) for 0.05, 0.2, 0.5 and 1% w/w HP-β-CD were 0.89, 0.71, 0.64 and 0.59. These were in good agreement with the experimental R values of 0.91, 0.78, 0.63 and 0.50 for 0.05, 0.2, 0.5 and 1% w/w HP-β-CD. The plot of predicted R vs. HP-β-CD concentration is shown in Figure 5.5 which shows that the reactive diffusion layer theory (i.e., complexation in the diffusion layer) predictions for the indomethacin crystal growth inhibitory effects of HP-β-CD were in reasonable agreement with the experimental values. The values of R for HP-β-CD decreased with increasing HP-β-CD concentrations, which is indicative of greater inhibition of indomethacin crystal growth at higher HP-β-CD concentration. A good agreement between the predicted and experimental values of R for HP-β-CD indicated that the inhibitory effect of HP-β-CD on the bulk diffusion controlled indomethacin crystal growth can be accounted for by reversible complexation in the diffusion layer.

Effect of Model PPIs on Indomethacin Surface Integration at Higher Degrees of Supersaturation

Since PVP and HPMC did not exhibit significant complexation with indomethacin, the Case 2 scenario was not applicable. Moreover, the significantly greater inhibitory effects of PVP and HPMC at high S (Figure 5.6 and Table 5.3) could not be explained by adjusting the indomethacin mass transfer rates to reflect changes in bulk viscosity in the presence of PVP and HPMC. Hence, the Case 3 scenario was considered to understand the crystal growth inhibitory effects PVP and HPMC.

It was hypothesized that the significantly higher indomethacin crystal growth inhibition factors of PVP and HPMC at high S could be attributed to their adsorption on to the growing indomethacin crystal surface. These polymers could adsorb to indomethacin surfaces due to hydrophobic and hydrogen bonding type interactions[12] thus providing an interfacial barrier for crystal growth, which in turn could retard the surface integration rate significantly.[164] For example, adsorbed polymers could block the active indomethacin growth sites. Since it is known from the literature[92,99,101,103] and a previous study from this laboratory[166] that crystal growth kinetics at low S are generally surface integration controlled, the above-mentioned hypothesis was tested by comparing the indomethacin crystal growth rate coefficients (k_G) at high S in the presence of PVP and HPMC with k_G at low S without any PPI (previously[166] determined as $5.5 \pm 1.3 \times 10^{-4}$ cm/sec). As shown in Table 5.3, the k_G values at high S in the presence of PVP and HPMC were at least similar or even lower than $5.5 \pm 1.3 \times 10^{-4}$ cm/sec. This supports our hypothesis that both polymers, HPMC and PVP, significantly inhibited indomethacin crystal growth at high S by changing the rate limiting step from bulk diffusion to surface integration. For both HPMC and PVP, the values of k_G at high and low S were very similar and indicative of their impact on the rate of surface integration of indomethacin. The impact of PVP on the indomethacin surface integration rate was significantly greater (20-30 fold) than that of HPMC (~4 fold) at 0.05%. This also indicated that the adsorbed PVP polymer not only changed the rate limiting step at high S but also significantly retarded indomethacin surface integration at both high and low S. In the case of HP-β-CD (0.05% w/w), the indomethacin crystal growth inhibitory effect was ~2-fold greater at low S as compared to high S. Similar to PVP and HPMC, the indomethacin crystal

growth inhibition factor of HP-β-CD at low S is also attributed to its impact on the surface integration rate, as that was established to be the mechanism for indomethacin crystal growth at low S in the absence of PPIs. Finally, the significantly higher indomethacin crystal growth inhibition factors of the model PPIs PVP and HPMC at high S could be attributed to their adsorption on to the growing indomethacin crystal surface, resulting in a change in the indomethacin crystal growth rate limiting step from bulk diffusion to surface integration.

CONCLUSIONS

HP-β-CD significantly increased indomethacin equilibrium solubility due to 1:1 complex formation between indomethacin and HP-β-CD. PVP and HPMC did not substantially alter the solubility of indomethacin. Viscosity of HPMC solutions increased significantly as a function of HPMC concentration. The rank order of solution viscosity at similar PPI concentrations was HPMC > PVP > HP-β-CD. PVP and HPMC were better indomethacin crystal growth inhibitors than HP-β-CD at high degrees of supersaturation (S), which was attributed their ability to change the indomethacin crystal growth rate limiting step from bulk diffusion to surface integration. HP-β-CD's crystal growth inhibitory effects at high S increased with an increase in its concentration up to 1% w/w concentration. The inhibitory effect of HP-β-CD on bulk diffusion controlled indomethacin crystal growth at high S could be rationalized by reversible complexation between HP-β-CD and indomethacin in the diffusion layer. The crystal growth inhibition factors of PVP and HPMC were dramatically greater at high S than that for HP-β-CD, which indicated that both PPIs changed the rate limiting step of indomethacin crystal growth at high S from bulk diffusion to surface integration.

At low S, the crystal growth rate of indomethacin becomes surface integration controlled even in the absence of PPIs. Under these conditions all PPIs exhibited only modest inhibitory effects. For example, a twofold greater indomethacin crystal growth inhibition factor was observed for HP-β-CD at low S than that at high S, reflecting its effect on the rate of indomethacin surface integration at low S. The relative effects of the model PPIs at low S may be attributable to their adsorption on to the growing crystal surface and the effect of this adsorption on the rate of surface integration.

Chapter Six

Adsorption of Polyvinylpyrrolidone and Its Impact on Maintenance of Aqueous Supersaturation of Indomethacin via Crystal Growth Inhibition

INTRODUCTION

Polymeric precipitation inhibitors (PPIs) have been used to maintain aqueous supersaturation of poorly water soluble drugs.[9] PPIs including polyvinylpyrrolidone (PVP), hydroxypropyl methylcellulose (HPMC), polyethylene glycol (PEG) as well as their derivatives such as polyvinylpyrrolidone-co-polyvinyl acetate (PVP-VA), hydroxypropyl methylcellulose acetate succinate (HPMC-AS), d-α-tocopheryl polyethylene glycol 1000 succinate (TPGS), and polysorbate 80 are frequently incorporated into various supersaturating drug delivery systems (SDDS) including amorphous solid dispersions and lipid-based drug delivery systems.[1,8] Upon oral administration of the SDDS, the PPIs maintain supersaturation by significantly inhibiting the precipitation of drugs in the gastrointestinal (GI) tract.[91]

While some PPIs including surfactants such as TPGS and polysorbate 80 could increase the thermodynamic equilibrium solubility of drugs, the precipitation inhibitory effects of PPIs are generally kinetic in nature. The PPIs maintain supersaturation through the inhibition of nucleation, crystal growth, or both.[20,23,27,104,108,169] The inhibitory effects of PPIs on nucleation, crystal growth, or both vary significantly with the specific drug and PPI combination. For example, HPMC and PVP significantly inhibited the nucleation and crystal growth of two model drugs, griseofulvin and danazol, while Eudragit® did not. Moreover, the selectivity of HPMC for the inhibition of nucleation or crystal growth of the two model drugs varied. HPMC was a more effective inhibitor of the nucleation of griseofulvin, but equally effective in inhibiting both the nucleation and

crystal growth of danazol.[108] PVP was a better inhibitor of the crystal growth as compared to the nucleation of bicalutamide.[20] These observations clearly indicate that the inhibition of nucleation and crystal growth of drugs by PPIs is complex, involving multiple mechanisms that could vary depending on the drug-PPI combination.

Drug nucleation and crystal growth may be influenced by the intermolecular interactions between PPI and drug molecules in the bulk solution.[13-16] For example, the effectiveness of PPIs in inhibiting the formation of carbamazepine dihydrate was related to the intermolecular hydrogen bonding and hydrophobic interactions between PPIs and carbamazepine but their relative impact on the effectiveness of a given PPI could not be determined due to experimental limitations.[14] In another study, the superiority of HPMC-AS HF over HPMC-AS LF, two different grades of HPMC-AS containing different ratios of acetate and succinate substituents, in inhibiting the precipitation of carbamazepine from an aqueous solution was attributed to stronger hydrophobic interactions between HPMC-AS HF and carbamazepine in the bulk solution.[13] Similarly, the inhibitory effect of cellulosic PPIs on the nucleation of three model drugs, celecoxib, efavirenz, and ritonavir, from their supersaturated aqueous solutions correlated well with the hydrophobicity of the PPI relative to that of the drugs.[15]

Adsorption of PPIs on the surface of growing crystals could also influence the crystal growth of drugs.[4,12,17-24] The inhibition of crystal growth by the PPI is generally attributed to its effect on either bulk diffusion or surface integration of drug molecules.[9,10,18,27] The inhibition of the crystal growth of sulfathiazole by PVP was attributed to the formation of a possible net like structure on the crystal surface by the adsorbed PVP. It was proposed that the pore size of the net like structure would be

smaller when the relative transport rate of PVP to sulfathiazole is higher, which in turn would provide greater inhibition of the crystal growth.[18] Stronger inhibitory effects of HPMC as compared to PVP and PEG 400 on the crystal growth of hydrocortisone acetate (HA) were attributed to: (i) a greater diffusive barrier provided by HPMC in the hydrodynamic boundary layer; and (ii) stronger adsorption of HPMC on the crystalline surface of HA. The extent of HPMC adsorption correlated with the hydrogen bonding capacity of different faces of the HA crystal.[12] Cellulosic polymers with moderate levels of hydrophobicity, semi-rigid structure, and amphiphilic nature were more effective in inhibiting the crystal growth of ritonavir. It was proposed that these properties of PPIs could likely promote adsorption on to the crystal surface of ritonavir.[10] Despite the above-mentioned studies, the adsorption of PPIs is seldom directly correlated with their crystal growth inhibitory effect on poorly water soluble drugs. Consequently, the nature of the adsorbed PPI layer as well as the key physicochemical properties of PPIs and drugs such as molecular weight, hydrogen bonding capability and hydrophobicity that could influence the adsorbed PPI layer and, in turn, the effectiveness of PPIs are not well understood. A thorough understanding of the correlation between the adsorption of a given PPI and its crystal growth inhibitory effect is still required. Knowledge of the adsorption behavior of PPIs on to drug surfaces would help in exploring the mechanisms of crystal growth inhibition by PPIs such as the creation of a barrier for surface diffusion of the adsorbed drug molecules or the blocking of active growth sites for the incorporation of drug molecules into crystal lattices and thereby aid in the rational selection of PPIs for the development of SDDS.

The main objectives of this study were: (i) to determine the factors that govern the adsorption of the model PPI PVP on to the crystalline surface of indomethacin, a model poorly water soluble drug; and (ii) to relate the adsorption behavior of PVP to its effectiveness as a crystal growth inhibitor of indomethacin. This chapter discusses: (a) the characterization of the adsorption of PVP polymers of different molecular weights and their monomer, N-vinylpyrrolidone, on to indomethacin crystals dispersed in an aqueous medium; and (b) the correlation of PVP adsorption with indomethacin crystal growth inhibition as a function of PVP concentration and molecular weight.

MATERIALS AND METHODS

Materials

Polyvinylpyrrolidone (PVP) polymers with different weight average molecular weights including PVP K12 (3500 g/mole), PVP K16-18 (8000 g/mole), and PVP K29-32 (58000 g/mole) as well as their monomer (N-vinylpyrrolidone, 111 g/mole) were purchased from Fisher Scientific Inc. Indomethacin (1-(*p*-chlorobenzoyl)-5-methoxy-2-methylindole-3-acetic acid, 99+%, γ-polymorph, molecular weight =357.8 g/mole, pK_a=4.17[148]) was purchased from Sigma-Aldrich, Inc. (St. Louis, MO, USA). Nylon net filters (30 µ) and polycarbonate membrane filters (3 µ) were purchased from Millipore Inc., (Milford, MA, USA). Nylon membrane filters (0.2 µ) and 13 mm PTFE syringe filters (0.45 µ) were purchased from Whatman Int. Ltd. (Maidstone, England). Deionized water was obtained from a MilliQ water purification apparatus (Milli-Q Synthesis, Millipore Inc., Milford, MA, USA) and pre-filtered through a 0.22 µ filter (Millipak Express 20, Millipore Inc., Milford, MA, USA). All other reagents and materials were of an analytical grade.

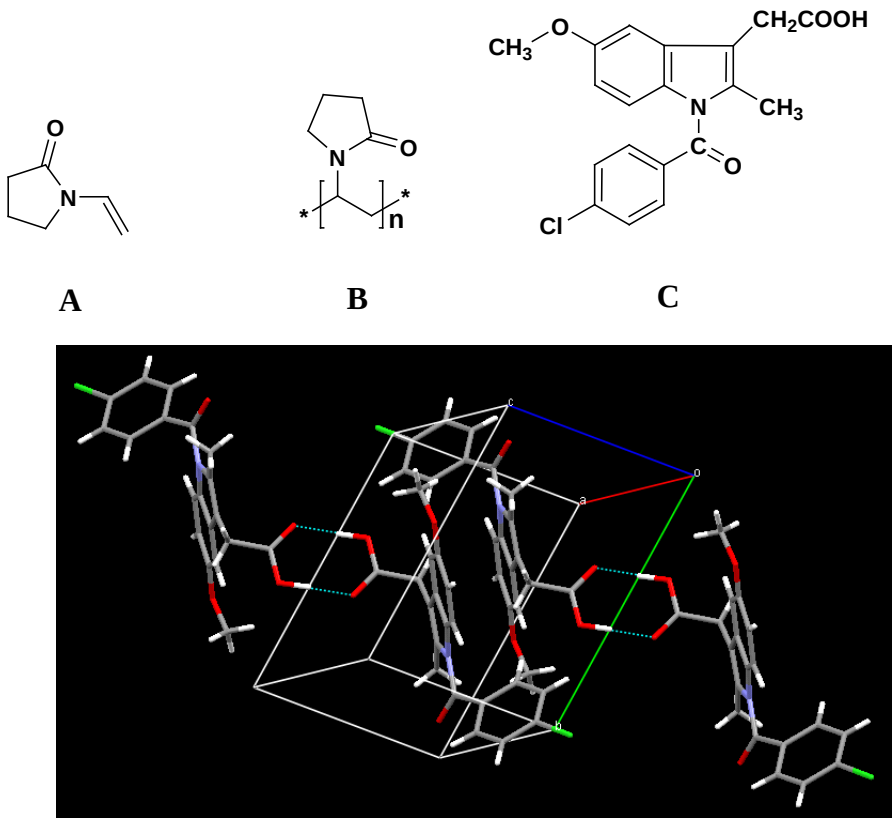

Figure 6.1. Chemical structures of N-vinylpyrrolidone (A), polyvinylpyrrolidone (B), chemical structure (C) and molecular packing (D) of indomethacin (Cambridge Structural Database reference code INDMET).

PVP Assay using Size Exclusion Chromatography

PVP (PVP K12, K16-18 and K29-32) and N-vinylpyrrolidone samples were analyzed using size-exclusion chromatography (SEC). The SEC system consisted of a Waters Alliance 2690 HPLC system with a photo-diode array absorbance detector. A size exclusion chromatography column (Ultrahydrogel 500, 7.8 × 300 mm, Waters Inc.) was used to resolve the chromatographic peaks of three PVP polymers and their monomer (N-vinylpyrrolidone). The pore size of the Ultrahydrogel 500 was 500 Å. The molecular weight cut off was 4×10^5. An isocratic HPLC method with a mobile phase containing deionized water (0.01% TFA) and acetonitrile in a ratio of 80:20 was used to resolve chromatographic peaks. The flow rate was maintained at 1 mL/min providing the column pressure of approximately 333 psi. The injection volume was 50 µl and the UV detection wavelength was set at 210 nm. Sample compartment temperature was maintained at 25°C whereas the column was kept at ambient room temperature. The column was equilibrated for about 1-2 hours before analyzing PVP samples. The standard solutions for PVP polymers and their monomer were prepared in 50 mM phosphate buffer (pH 2.15).

Measurement of PVP Adsorption on to Indomethacin Seed Crystals

Adsorption of PVP polymers and their monomer on indomethacin seed crystals was measured using the solution depletion method. A specific quantity of indomethacin powder was mixed with the solutions of either PVP polymers or their monomer in scintillation glass vials. The PVP (or its monomer) solutions containing different amounts of PVP (or its monomer) were prepared using 50 mM phosphate buffer (pH 2.15 at 0.1M ionic strength using NaCl). The final mixture or dispersion was equilibrated at

25°C for about 12 hrs using a shaker water bath. Samples were withdrawn at regular time intervals and were filtered through a 0.45 µ PTFE syringe filter. The filtrate was assayed for PVP (or its monomer) concentration using the SEC method.

Preparation and Characterization of Indomethacin Seed Crystal Suspension for Crystal Growth

A previously reported method was used to prepare indomethacin seed crystal suspensions. Briefly, approximately 0.1% w/w indomethacin was dispersed in 50 mM phosphate buffer (pH 2.15). The dispersion was equilibrated for 72 hours at 25ºC in a shaker water bath. The ionic strength was maintained at 0.1M using NaCl. A narrow and unimodal size distribution was obtained by filtering the saturated suspension through a 30 µ nylon net filter. The filtered suspension was further passed through a 3 µ polycarbonate filter to collect the seed crystals retained on the top of the 3 µ filter. The final indomethacin seed crystal suspension was prepared by redispersing the retained seed crystals in a saturated solution of indomethacin.

The surface area of indomethacin crystals was measured using the BET adsorption isotherm equation. The samples were degassed at 120 °C for about 4 hours under nitrogen purge prior to analysis. The adsorption of nitrogen on to indomethacin crystals was measured using Tristar 3000 automated adsorption apparatus (Micromeritics, USA).

Indomethacin seed crystals, before and after growth, were characterized for physical form, size, number, and morphology using Powder X-ray diffraction (PXRD) technique, a Coulter counter and polarized light microscopy. A more detailed description of these characterization methods can be found elsewhere.[104] Briefly, the PXRD patterns

of indomethacin crystals before and after crystal growth were obtained using an X-ray diffractometer (Bruker D8 Advance, Bruker AXS, Inc., Madison, WI, USA) to determine, any possible, change in the form of indomethacin from the most stable γ-form to either an amorphous form or any other metastable form such as α-form. Additionally, the polarized light microscope (Olympus, Tokyo, Japan) was used to characterize any shape and size related changes. The number concentration and size distribution including volume based diameter of indomethacin crystals in the seed crystal suspension were measured using a Coulter counter (Multisizer Z2, Beckman Coulter Inc., Miami, FL, USA) containing a 50 μ glass aperture tube that was filled with clear indomethacin saturated solution.

Indomethacin Crystal Growth Rate Measurement in the Presence of PVP

The crystal growth rates of indomethacin in the presence of PVP polymers and their monomer were measured using a previously published method.[27,104] Briefly, indomethacin desupersaturation profiles (i.e., the plots of concentration vs. time) were determined from supersaturated suspensions containing PVP or N-vinylpyrrolidone at 25ºC. Supersaturation was attained by the addition of 100-250 μl of concentrated indomethacin solution (50 mM phosphate buffer, pH 6.8, ionic strength of 0.1M using NaCl) containing a specific amount of PVP or N-vinylpyrrolidone to 3 mL of indomethacin saturated suspension (50 mM phosphate buffer, pH 2.15, ionic strength of 0.1M using NaCl) using a micro-syringe pump (final pH < 2.2). The supersaturated suspensions were magnetically stirred at about 400 RPM using a pivoted rod-shaped magnetic stir bar. The concentration of indomethacin from its supersaturated suspensions was measured using a second derivative online UV spectroscopy method. The second

derivative UV absorbance at 295 nm, obtained from an indomethacin UV absorbance spectrum from 210 to 400 nm wavelength, was used to determine indomethacin concentration. Additional details on the second derivative UV method development and validation are provided in a previous publication.[104]

Crystal Packing

The molecular packing of the γ-form shown in Figure 6.1D was obtained using Mercury 3.5.1 (Cambridge Crystallographic Data Centre, Cambridge, UK) as well as the single crystal structure parameters from the Cambridge Structural Database reference code INDMET.[170]

Data Analyses

The Student t-test and ANOVA tests were carried out using Microsoft Excel software program. Scientist software program (Micromath Inc., St. Louis, MO, USA) was used to perform non-linear least-squares analyses and to obtain 95% S-plane confidence intervals.

RESULTS

Indomethacin Seed Crystal Suspension Characterization Before and After Crystal Growth

The surface area of indomethacin crystals determined using the BET method was 0.23 ± 0.05 (95% CI) m^2/g. The seed crystal mass median diameter in suspension was ~11 µ. No significant change in suspension concentration and particle morphology was observed by Coulter counting and optical microscopy before and after crystal growth indicating the absence of significant primary nucleation during crystal growth (e.g., the

seed crystal concentration/mL was $2.8 \pm 0.8 \times 10^4$ before crystal growth and $3.0 \pm 0.2 \times 10^4$ crystals/mL after crystal growth in the presence of PVP K29-32). PXRD patterns also showed no significant change upon crystal growth. Additional discussions on the seed crystal characterization before and after crystal growth in the absence of PPIs are provided in an earlier publication.[104]

Size Exclusion Chromatography Method for Polyvinylpyrrolidone

The size exclusion chromatography (SEC) assay successfully resolved the peaks of N-vinylpyrrolidone, PVP K12, PVP K16-18, and PVP K29-32. A representative chromatogram of PVP K12 with a major peak at the retention time of around ~10 minutes is shown in Figure 6.2. Similar chromatograms were obtained for N-vinylpyrrolidone, PVP K16-18, and PVP K29-32. The SEC retention times of PVP polymers decreased with an increase in their molecular weight. The retention times of N-vinylpyrrolidone, PVP K12, K16-18, and K29-32 were 11.1, 10.2, 9.9, and 8.9 minutes, respectively (Table 6.1). Plots of the SEC standard peak areas versus concentration were linear for all three PVP polymers and N-vinylpyrrolidone over the concentration range of interest (Figure 6.3), from which response factors (ratios of peak area to concentration) were generated (Table 6.1) and utilized in determining unknown PVP polymer and N-vinylpyrrolidone concentrations in adsorption samples.

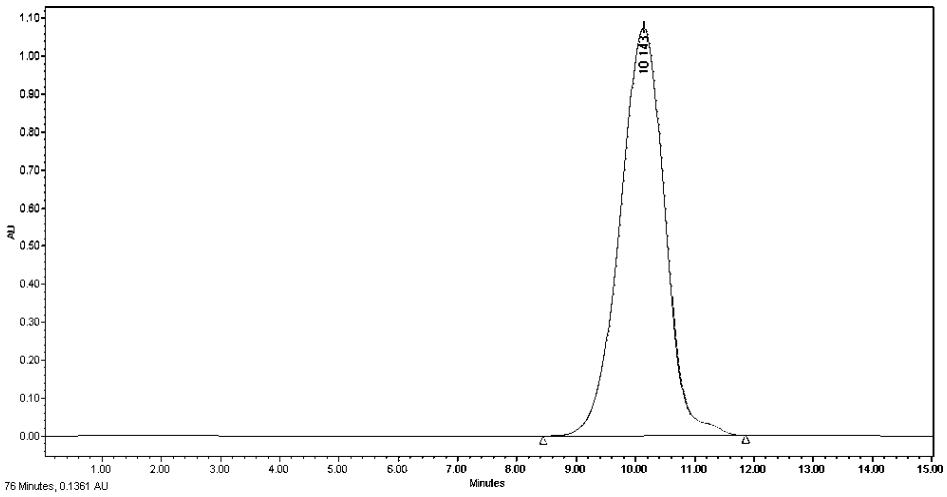

Figure 6.2. Representative size exclusion chromatogram of a model polyvinylpyrrolidone polymer (PVP K12).

Table 6.1. Size-Exclusion Chromatography Parameters for Polyvinylpyrrolidone (PVP) Polymers and Their Monomer (N-vinylpyrrolidone)

	Retention Time (min)	Average Response Factor ± 95% CI (area.mg.mL^{-1})
PVP K29-32	8.9	$5.6 \pm 0.1 \times 10^7$
PVP K16-18	9.9	$6.3 \pm 0.3 \times 10^7$
PVP K12	10.2	$6.0 \pm 0.2 \times 10^7$
N-vinylpyrrolidone	11.1	$4.3 \pm 0.2 \times 10^7$

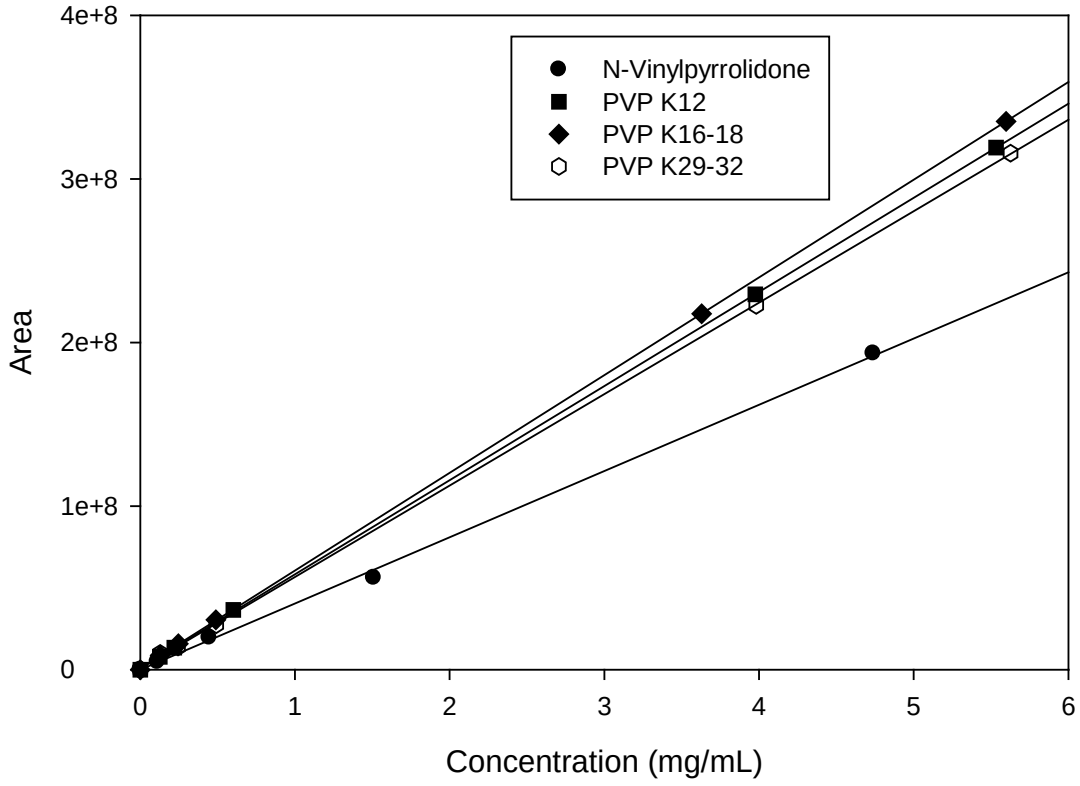

Figure 6.3. Standard curves of polyvinylpyrrolidones (PVP K12, K16-18 & K29-32) and N-vinylpyrrolidone using size exclusion chromatography.

Characteristics of PVP Adsorption on to Indomethacin Seed Crystals

The kinetics of PVP adsorption on to indomethacin crystals was studied by determining the amount of PVP adsorbed per unit surface area of indomethacin crystals over time. Representative adsorption kinetic profiles for PVP K12 and PVP K29-32 are shown in Figure 6.4. Similar profiles were obtained for N-vinylpyrrolidone and PVP K16-18. The kinetic profiles clearly indicate that equilibrium was achieved within 2 hours. Adsorption isotherms were constructed by plotting the plateau values from the adsorption kinetic profiles against the respective bulk concentrations of PVP or N-vinylpyrrolidone (Figure 6.5). The adsorption isotherms of PVP polymers and N-vinylpyrrolidone exhibit different plateau values above a critical polymer (or monomer) concentration depending on molecular weight (Figure 6.5). The plateau values, representing the maximum extent of PVP (or N-vinylpyrrolidone) adsorption on to indomethacin crystals (A_{max}) were expressed using different units: 1) weight-basis (A_{max}^{W}, mg/m^2), 2) monomer mole-basis (A_{max}^{mM}, moles of monomer/m^2), and 3) mole-basis (A_{max}^{M}, moles/m^2). The extent of PVP adsorption on to indomethacin crystals on a monomer mole-basis (A_{max}^{mM}, moles of monomer/m^2) was calculated by dividing the extent of PVP adsorption on a weight basis (A_{max}^{W}, mg/m^2) by the molecular weight of the PVP monomer (i.e., 111 g/mole).

The adsorption isotherms of PVP were modeled using the Langmuir adsorption isotherm model (Eq. 6.1).[171,172]

$$A = A_{\max} \frac{Kc}{1 + Kc} \tag{6.1}$$

where *A* is the amount of adsorbate (e.g., PVP) per unit surface area of the adsorbent (e.g., indomethacin crystals) (mg/m^2, moles of monomer/m^{2,} or mole/m^2) at a specific adsorbate concentration, *c* (mg/mL, moles of monomer/mL, or moles/mL). *K* is the Langmuir affinity constant (mL/mg, mL/mole of monomer or mL/mole). The extent of adsorption (A_{max}) reflects the adsorption capacity of an adsorbent whereas the values of K provide an insight into the affinity of an adsorbate for an adsorbent. The Langmuir adsorption model fit the adsorption isotherms of PVP and N-vinylpyrrolidone well (Figure 6.5). Values of the Langmuir constant (K ± 95% CI) determined from the adsorption isotherms are listed in Table 6.2 using two different units: 1) weight-basis (K^w, mg/m^2), and 2) mole-basis (K^M, mg/m^2). The affinity constant of PVP polymers for indomethacin crystals is significantly higher (e.g., 23-fold higher for PVP 29-32) than that of N-vinylpyrrolidone. The higher molecular weight PVP K29-32 polymer exhibits a greater affinity for indomethacin crystals than the lower molecular weight PVP K12 and PVP K16-18 polymers. The values of K^w for PVP K12 and PVP K16-18 are similar, whereas the values of K^M for the same polymers suggest that the affinity of PVP K16-18 is slightly higher than that of PVP K12.

As shown in Table 6.2, the polymeric PVPs have significantly higher A^w_{max} and A^{mM}_{max} for indomethacin crystals as compared to N-vinylpyrrolidone, however the trend reverses when the same comparison is made using A^m_{max}. These results clearly indicate that the adsorption capacities of indomethacin crystals for polymeric PVPs and N-vinylpyrrolidone differ significantly. Moreover, the adsorption capacity of indomethacin crystals is a function of PVP molecular weight (Table 6.2 and Figure 6.6). The values of A^w_{max} and A^{mM}_{max} increase whereas the values of A^m_{max} decrease with an increase in the

molecular weight of PVP. The A^{w}_{max} for PVP K29-32 is ~9-fold, ~3-fold and ~2-fold greater than those for N-vinylpyrrolidone, PVP K12 and PVP K16-18, respectively (Table 6.2). The relationship between the molecular weight of PVP and the extent of PVP adsorption on to indomethacin crystals ($A^{w}_{\max}$) was further characterized by Eq. 6.2.[173]

$$A^{w}_{\max} = bM^{\alpha} \tag{6.2}$$

where M is the molecular weight of PVP (g/mol) and b as well as α are constants. The value of α is generally used to get an insight into the conformation of adsorbed polymer at the solid-liquid interface.[173] A linear relationship (R^2 = 0.99) was observed when the extent of PVP adsorption ($A^{w}_{\max}$) was plotted against the molecular weight of PVP on a logarithmic scale (Figure 6.6). The value of α of 0.36, derived from the slope of this curve, suggests a random coil conformation for PVP adsorbed at the indomethacin solid-liquid interface.[173]

Inhibitory Effects of PVP on the Crystal Growth of Indomethacin

To quantitatively explore the inhibitory effects of PVP on the crystal growth of indomethacin, the crystal growth rates of indomethacin were measured at a high degree of supersaturation (S~5) in the presence and absence of PVP or N-vinylpyrrolidone using a previously established method.[27,104,166] Briefly, desupersaturation profiles for the crystal growth of indomethacin were generated by plotting the supersaturated concentration of indomethacin against time.

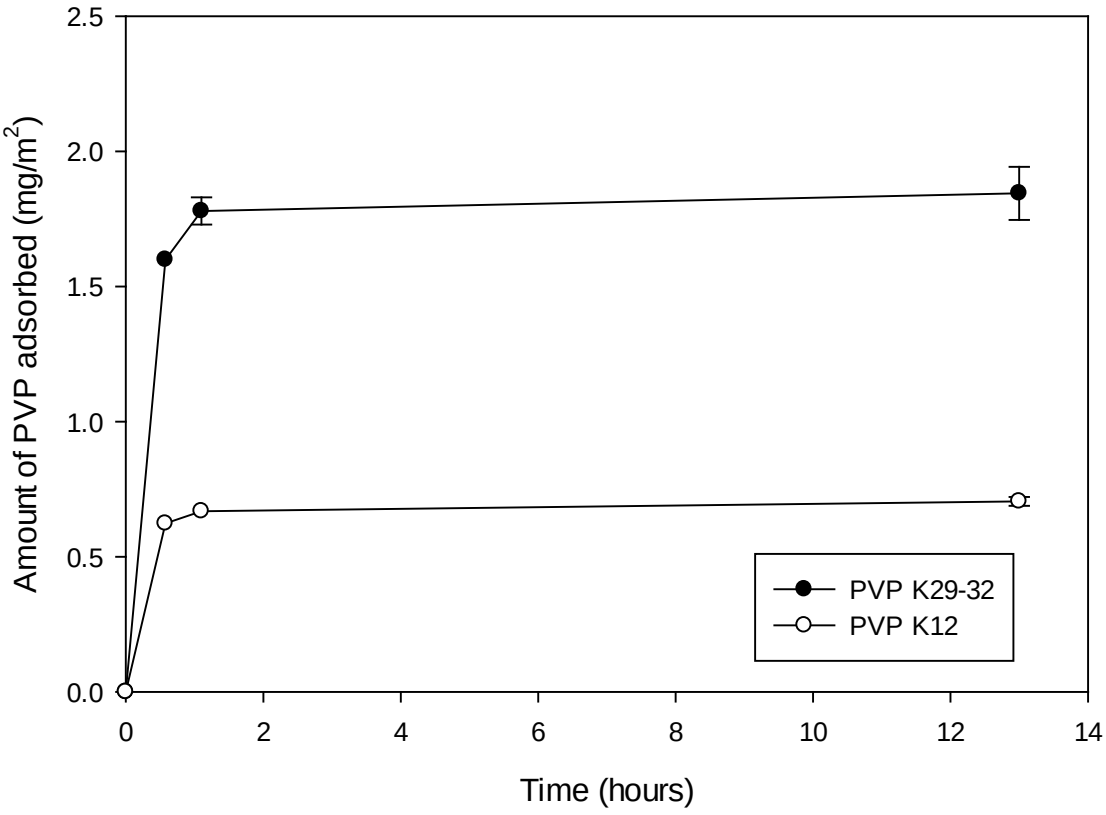

Figure 6.4. Representative kinetic profiles for the adsorption of polyvinylpyrrolidone (PVP K12 and PVP K29-32) on to indomethacin crystals.

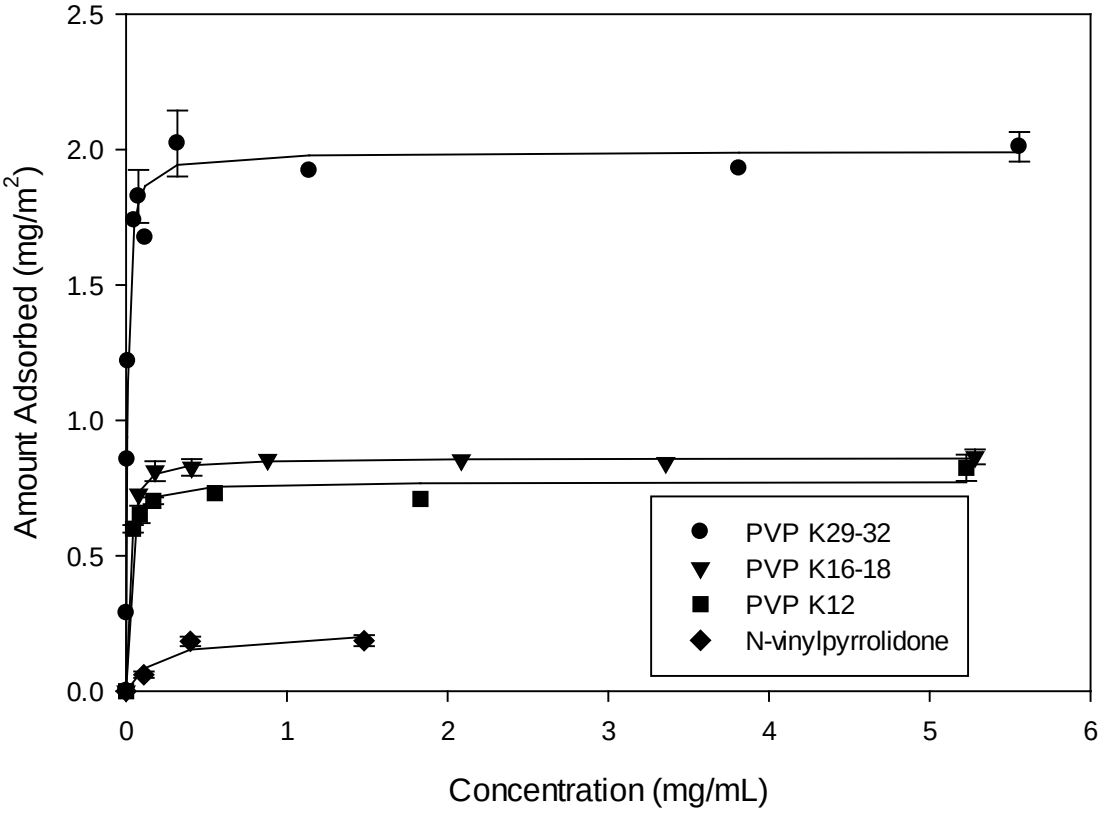

Figure 6.5. Adsorption isotherms of polyvinylpyrrolidone (PVP K12, K16-18 and K29-32) and their monomer (N-vinylpyrrolidone) for indomethacin crystals. The solid lines represent model fits using the Langmuir adsorption isotherm model (Eq. 6.2).

Table 6.2. Langmuir Adsorption Isotherm Model Parameters (±95%CI) for Polyvinylpyrrolidone (PVP) Polymers and N-vinylpyrrolidone

	Maximum Amount Adsorbed (A^{w}_{max}, mg.m^{-2})	**Maximum Amount Adsorbed (A^{mM}_{max}, monomoles.m^{-2})**	**Maximum Amount Adsorbed (A^{M}_{max}, moles.m^{-2})**	**Langmuir Constant (K^{w}, mg^{-1}.mL)**	**Langmuir Constant (K^{M}, moles^{-1}.mL)**
N-vinylpyrrolidone	0.2 ± 0.1	21 ± 5.4 × 10^{-7}	21 ± 5.4 × 10^{-7}	5.3 ± 4.7	5.9 ± 5.2 × 10^{5}
PVP K12	0.8 ± 0.0	69 ± 0.3 × 10^{-7}	1.9 ± 0.08 × 10^{-7}	73 ± 24	2900 ± 970 × 10^{5}
PVP K16-18	0.9 ± 0.0	77 ± 0.9 × 10^{-7}	1.1 ± 0.01 × 10^{-7}	74 ± 21	5900 ± 1700 × 10^{5}
PVP K29-32	2.0 ± 0.1	179 ± 5.4 × 10^{-7}	0.34 ± 0.01 × 10^{-7}	124 ± 28	72100 ± 16500 × 10^{5}

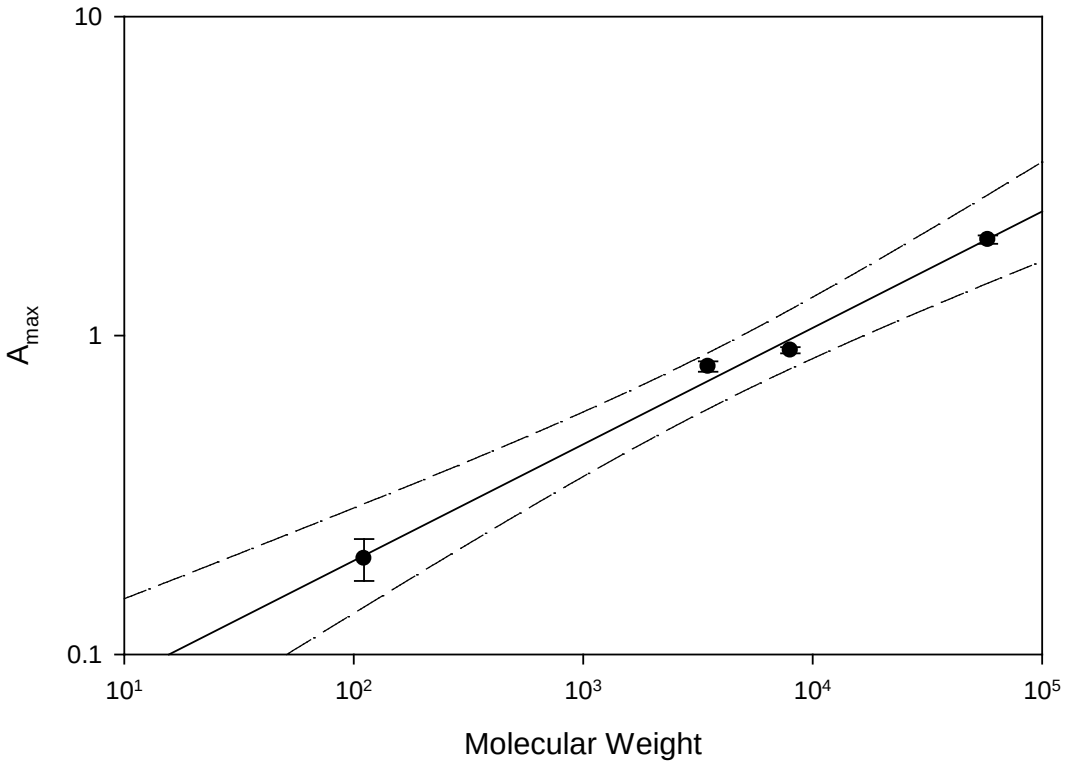

Figure 6.6. Relationship between the maximum amounts of PVP adsorbed on to indomethacin crystals (A_{max}) and the molecular weight of PVP.

The degree of supersaturation (S), also known as the supersaturation ratio, is defined as

$$S = \frac{C_b}{C_s} \tag{6.3}$$

where C_b is the supersaturated concentration of indomethacin and C_s is the equilibrium solubility of indomethacin.

The desupersaturation profiles of indomethacin were modeled using a first order empirical crystal growth model[104] as shown in Eq. 6.4.

$$-\frac{dc_b}{dt} = \frac{k_G A}{V_b}\left(C_b - C_s\right) \tag{6.4}$$

where k_G is an apparent crystal growth rate coefficient, and A/V_b is the crystalline surface area per unit volume of the bulk medium. The rates of indomethacin crystal growth in the presence and absence of PVP were used to compare the inhibitory effects of PVP on the crystal growth of indomethacin. The inhibitory effects of PVP on the crystal growth of indomethacin were quantitatively expressed as an indomethacin crystal growth inhibition factor (R). R is defined as the ratio of indomethacin crystal growth rates with and without PVP.

$$R = \frac{J}{J_0} \tag{6.5}$$

where J is the crystal growth rate (moles cm^{-2} $time^{-1}$) of indomethacin in the presence of inhibitor and J_0 is the crystal growth rate of indomethacin in the absence of inhibitor. As determined previously[104], the indomethacin crystal growth rate coefficient (k_G) in the absence of any PPI at a high S (>3) is $4.7 \pm 0.7 \times 10^{-3}$ cm/sec. In the present study, the indomethacin k_G values determined at a high S (~5) in the presence of 0.05% w/w N-vinylpyrrolidone, PVP K12, K16-18, and K29-32 are $4.9 \pm 0.4 \times 10^{-3}$, $1.0 \pm 0.2 \times 10^{-4}$, $1.1 \pm 0.6 \times 10^{-4}$, and $3.0 \pm 1.9 \times 10^{-5}$ cm/sec, respectively (Figure 6.7). The R values at a high S (~5) for 0.05% w/w N-vinylpyrrolidone, PVP K12, K16-18, and K29-32 are 1, 0.02, 0.02, and 0.006, respectively (Figure 6.7). PVP K29-32 is ~160-fold more effective at inhibiting the crystal growth of indomethacin than N-vinylpyrrolidone and ~3-fold more effective than PVP K12 and PVP K16-18 at 0.05% w/w concentrations. These results indicate that the polymeric PVPs are better crystal growth inhibitors of indomethacin than N-vinylpyrrolidone. The higher molecular weight PVP K29-32 showed greater inhibition of the crystal growth of indomethacin as compared to the lower molecular weight PVP K16-18 and PVP K12.

In addition to the molecular weight of PVP, the effect of PVP concentration on the rate of indomethacin crystal growth was evaluated at different concentrations of PVP K29-32 (0 to 0.2% w/w). The indomethacin k_G decreases significantly as the concentration of PVP K29-32 increases indicating significantly greater crystal growth inhibition at higher PVP K29-32 concentrations (Figure 6.8A). The indomethacin k_G reaches a plateau above ~0.05% w/w PVP K29-32 concentration. A comparison of the three parameters including PVP K29-32 concentration, indomethacin k_G, and the extent of PVP adsorption (A_{max}^{w}, mg/m^2) indicates that PVP K29-32 is more effective at

inhibiting the crystal growth of indomethacin at higher extents of PVP adsorption (Figure 6.8A). The relationship between the extent of PVP K29-32 adsorption and the inhibition of indomethacin crystal growth was further characterized by comparing the degree of inhibition (1/R) to the fractional surface coverage (S_f) of indomethacin crystals by the adsorbed PVP K29-32 (Figure 6.8B). The S_f of indomethacin crystals by PVP K29-32 was calculated using Eq. 6.6:

$$S_f = \frac{A^w}{A^w_{surface}} \tag{6.6}$$

where A^w(mg/m^2) is the amount of PVP K29-32 adsorbed on to indomethacin crystal per unit surface area at a specific concentration of PVP K29-32 and $A^w_{surface}$(mg/m^2) is the calculated maximum amount of PVP K29-32 adsorbed on to indomethacin crystal per unit surface area (i.e., ~1 mg/m^2) based on the condensed monolayer adsorption of the monomeric units of PVP having the estimated area of 0.2 nm^2.[174,175] The degree of inhibition (1/R) of indomethacin crystal growth by PVP K29-32 increases as the fractional surface coverage of indomethacin crystals by PVP K29-32 increases (Figure 6.8B). The degree of inhibition increases steadily at $S_f \leq 1$ then more dramatically at $S_f > 1$. These results suggest that the inhibition of the crystal growth of indomethacin becomes significant as the surface coverage by PVP K29-32 approaches 1. Moreover, a higher extent of PVP adsorption beyond complete surface coverage ($S_f > 1$) further enhances the crystal growth inhibitory effect of PVP K29-32.

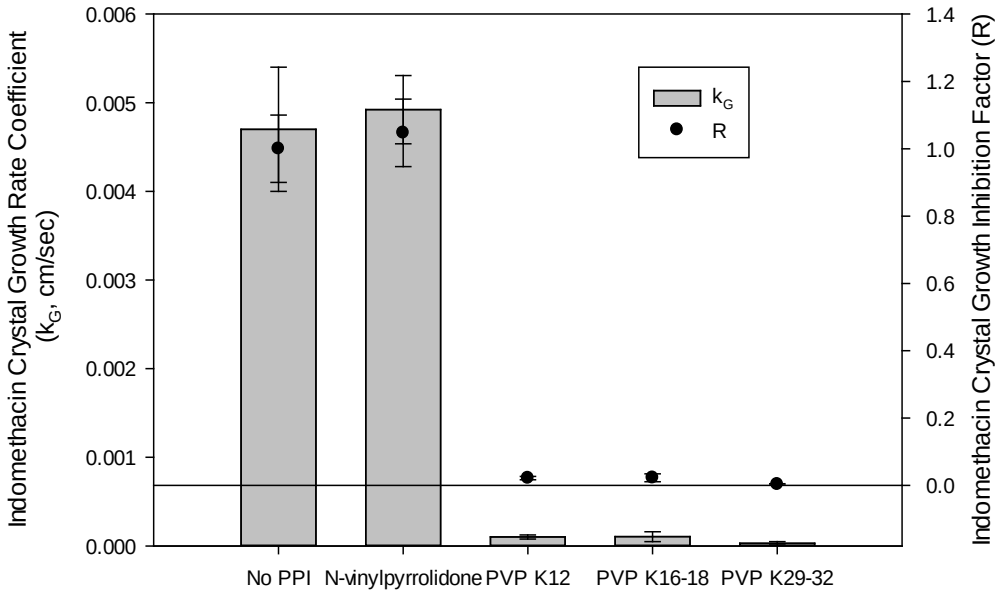

Figure 6.7. Comparison of the effects of PVP polymers (0.05% w/w) and their monomer (N-vinylpyrrolidone) on indomethacin crystal growth at a high degree of supersaturation (S~5).

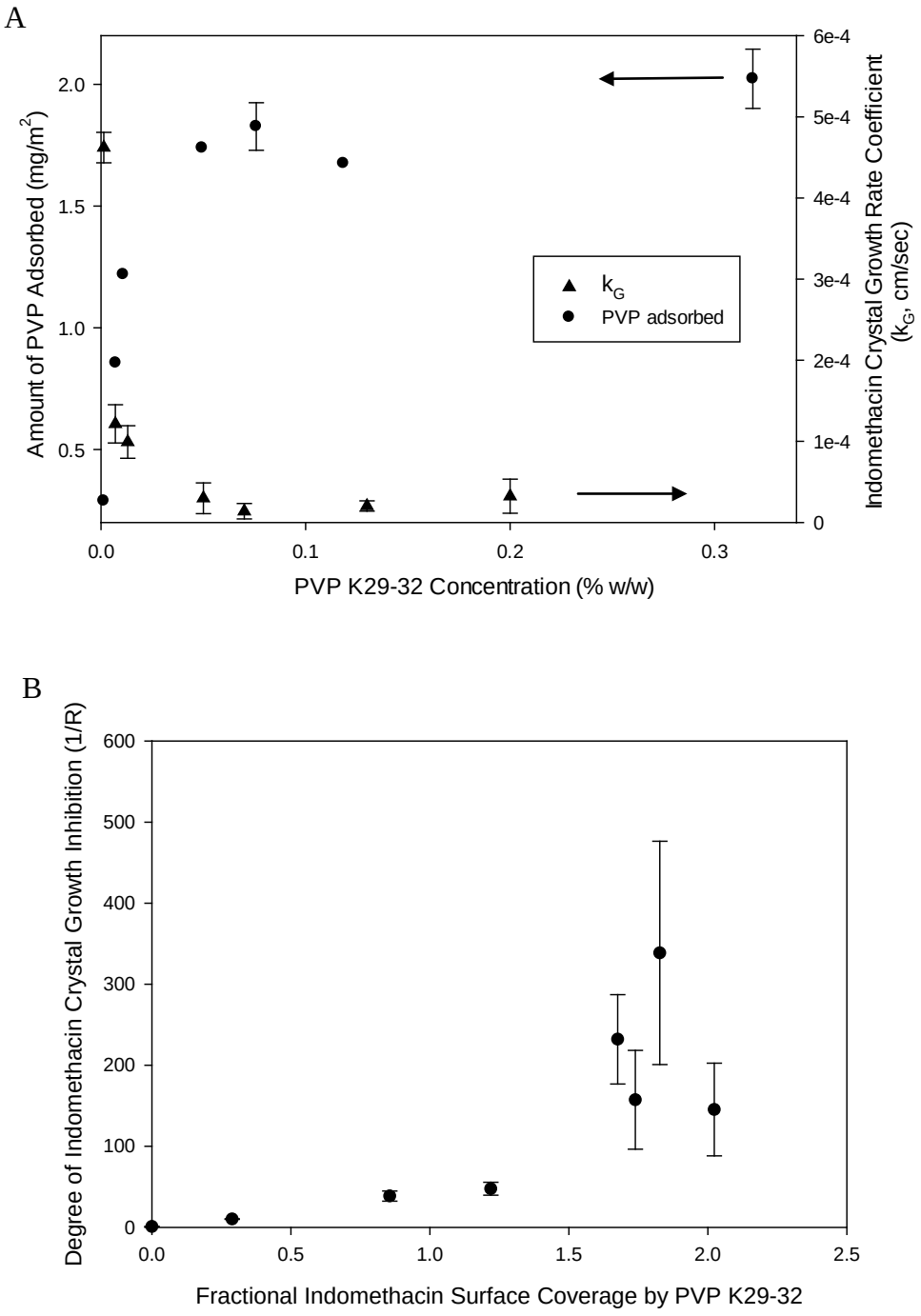

Figure 6.8. (A) Relationship between the adsorption of PVP K29-32 and the crystal growth inhibition of indomethacin at different concentrations of PVP K29-32 (S~5), and (B) Effect of the fractional surface coverage of indomethacin crystals by PVP K29-32 on its crystal growth inhibitory effect for indomethacin (S~5).

DISCUSSION

To understand the inhibitory effect of PVP on the crystal growth of indomethacin and, in turn, on the maintenance of supersaturation, we focused on two main aspects of the interaction of PVP with indomethacin crystals: 1) the adsorption behavior and nature of the adsorbed layer of PVP on to indomethacin crystals; and 2) the correlation between PVP adsorption and crystal growth inhibitory effects for indomethacin.

Several adsorption isotherm models including Langmuir,[172,176] Freundlich,[172,177] Redlich-Peterson,[178] and Hinz,[178] have commonly been used to understand the characteristics of adsorption equilibria. The Langmuir adsorption isotherm model was utilized in the present study, which assumes an interaction between an adsorbate and free adsorbent sites subject to the following assumptions: (1) the adsorbent has a limited adsorption capacity and all adsorption sites are identical; and (2) each site retains one adsorbate molecule (monolayer assumption). The parameters of the Langmuir adsorption isotherm model including the Langmuir constant (K) and the maximum amount adsorbed (A_{max}) describe the affinity of the adsorbate for a specific adsorbent and the adsorption capacity of the adsorbent, respectively.

The polymer adsorption process depends on several factors including the nature of the polymer, solvent, and the surface of the adsorbent.[179-181] The adsorption behavior of a polymer could be influenced by the adsorption energy and related intermolecular polymer-solvent, solvent-surface, and polymer-surface interactions such as van der Waals, electrostatic, hydrogen bonding, and hydrophobic interactions.[9,182,183] The free energy changes related to the interactions of a surface with both the polymer and solvent are expressed by the adsorption energy parameter (χ_s). Adsorption only occurs when χ_s

exceeds a critical value (χ_{sc}), which accounts for the loss of configurational entropy of the polymer chain upon surface adsorption. The polymer-solvent interactions are sometimes described using the Flory interaction parameter (χ), which also describes the solvent quality. Decreasing solvent quality (i.e., higher χ) generally increases the adsorbed amount.[174] The adsorption of most pharmaceutical PPIs involves hydrophobic drug surfaces such as indomethacin crystals dispersed in aqueous media where hydrophobic interactions, driven mainly by the gain in water entropy, could also play an important role along with the hydrogen bonding interactions.[12,183-186]

The adsorption of polymers also depends on the properties of polymers such as molecular weight, chain length, chain conformation, and chain flexibility.[182] The longer chains of higher molecular weight polymers can interact at multiple sites of the surface thus providing a greater number of interactions as well as higher stability of the adsorbed polymer as compared to the shorter chains of lower molecular weight polymers and monomers.[19] Although the adsorption energy of an individual polymer subunit could be as low as that of its monomer, it is higher for a polymer chain due to multiple synergistic or cooperative interactions with the surface. The polymer subunits involved in the interaction with the adsorbent surface are locally constrained by neighboring sub-units that are also bonded with the surface.[19] This limits the distance by which a subunit may be displaced from its original site of interaction during dynamic bond breakage and reformation events and, in turn, enhances the binding affinity.[19,187]

Besides cooperative interactions, the effects of molecular weight and chain length on the adsorption of polymers have also been associated with the conformation of the adsorbed polymer chain characterized as trains, loops, and tails.[188] The polymer chains

are in direct contact with the surface in the train conformation, protruding out into the solution in the loop conformation, and unattached at one end in the tail conformation. While the different configurations attained by the loops and tails define the entropy of the adsorbed chain, the enthalpy of adsorption is determined by the interaction energy between trains and the surface. The train conformation is more prevalent at high adsorption energy, whereas loops and tails are common at low adsorption energies. In most cases, higher chain length provides longer loops and tails and, in turn, a thicker adsorbed layer. The adsorbed amount and surface coverage also increase with the chain length up to a critical length beyond which the effect saturates due to lower diffusivity of very long chains.[174] However, a molecular weight effect on the fraction bound to the surface (i.e., trains) could be absent at a very high adsorption energy. For example, Kramarenko[182] demonstrated using molecular dynamics simulations that the fraction of adsorbed polymer in train conformations decreased as the chain length increased only at a low adsorption energy. At higher adsorption energy, the chain length did not influence the fraction of adsorbed polymer in a train conformation.

The polymer concentration significantly affects the structure of the adsorbed layer mainly due to the competition for the limited number of adsorption sites at high polymer concentrations. The adsorbed polymer is generally in a train conformation at low surface coverage whereas it forms loops and tails at higher extents of adsorption.[189,190] The concentration range can be divided into three regions and related three secondary polymer conformations including pancake, mushroom, and brush.[181] The first concentration region is the low polymer concentration region where no entanglement occurs between the adsorbed polymer chains that are present in the pancake conformation

containing loops, tails, and trains structures. The second region is the moderate concentration region where chain entanglement and overlapping occurs resulting in the mushroom conformation. The third high concentration region is where chains are only attached to the surface with either one end segment or a few segments while forming a brush-like structure.

PVP: A Model PPI for Indomethacin Crystals

PVP was selected as a model PPI in this study due to several factors including the amphiphilic nature of PVP owing to its structural features: (1) the pyrrolidone ring containing a highly polar amide group, and (2) the ring and backbone containing non-polar methylene and methine groups (Figure 6.1A). The adsorption of PVP on to indomethacin, a model pharmaceutically active adsorbent, could be driven by polar and non-polar interactions (e.g., hydrogen bonding, Van der Waals, and hydrophobic interactions) provided by the amide and methylene-methine groups, respectively.[183] Recently, Wen et al.[183] observed that Van der Waals interactions played a more significant role than hydrogen bonding for the interactions between PVP and the model drug acetaminophen.

Accurate and precise measurements of PVP concentrations are required to construct the adsorption isotherms of PVP. Several analytical methods including differential refractometry, UV spectroscopy, and fluorescence spectroscopy have been used to determine the concentrations of PVP in aqueous and non-aqueous solutions.[174,176,188] In the present study, we used SEC-HPLC to measure the concentration of PVP due to its superior sensitivity at very low PVP concentrations across different molecular weights. The PVP concentrations measured by the SEC-

HPLC method were further utilized in constructing the isotherms for PVP adsorption on to indomethacin crystals.

The adsorption of PVP on to pharmaceutically inactive adsorbents including polystyrene,[176,188] graphite,[191] silica,[174,191] alumina,[191] clay minerals,[175,192] and titanium dioxide[193] has been studied previously, however very few studies[183,194] have been carried out to determine the absorption behavior of PVP onto pharmaceutically active adsorbents.[38,49] Additionally, a majority of the above-mentioned PVP adsorption studies have used adsorbents that are either non-polar such as polystyrene and graphite or polar with only hydrogen bond accepting capability such as silica and titanium dioxide. Since PVP has no hydrogen bond donors, no significant hydrogen bonding interactions could occur between PVP and these adsorbents. While PVP lacks hydrogen bond donors and cannot form an extensive hydrogen bond network by itself, indomethacin has four hydrogen bond acceptors and one hydrogen bond donor that could facilitate the formation of hydrogen bonds between PVP and indomethacin.[129] The selection of indomethacin as an adsorbent in this study could provide additional understanding of the adsorption behavior of PVP onto a pharmaceutically active adsorbent with hydrogen bond donating capability.

The crystallographic analyses of indomethacin reveals that strongly hydrogen bonded carboxylic dimers are present in the γ-form of indomethacin rendering higher thermodynamic stability. The carboxylic groups as well as the hydrophobic phenyl and indole rings are present on the faces of indomethacin. The density of these groups on different faces of indomethacin varies. Chen et al[195] suggested that the hydrogen bonded carboxylic acid dimers are surrounded by more hydrophobic groups. Due to the shielding

of carboxyl groups from all sides by hydrophobic groups, hydrogen bonding would not be likely between the surface of the γ-form of indomethacin and PVP. It should also be noted that unlike the dissolution process, the surface of indomethacin crystals during the crystal growth process could change significantly in terms of the physical form of indomethacin in the newly grown layer.[104] Depending on the experimental conditions such as pH, temperature and degree of supersaturation, a wide variety of indomethacin forms ranging from an amorphous form to the meta-stable forms could grow in the newly grown layer, which could provide different densities of certain functional groups on the surface. This could significantly change the interactions of PPIs and the surface and, in turn, the PPI adsorption profiles. A previous study showed that the surface of the γ-form of indomethacin did not change during crystal growth in the presence of PVP and the crystal growth was surface integration controlled at a high degree of supersaturation.[27] However, in the absence of PVP and at high supersaturation, the crystal growth of indomethacin was found to be bulk diffusion controlled due to the formation of a higher energy surface layer on the growing crystal.[104]

Polymer Adsorption and Crystal Growth Inhibition

The crystal growth process is generally divided into two major steps: (1) diffusion of molecules from bulk to the surface, and (2) integration of molecules into the surface. The surface integration process can be further divided into two sub-steps: (1) surface diffusion of the molecules in the adsorbed layer, and (2) incorporation of the adsorbed molecules into the active growth sites such as kinks.[104] PPIs could change the kinetics of drug crystal growth by influencing several factors including viscosity, solubility, bulk diffusion, surface diffusion, and incorporation of drug molecules into active growth

sites.[9,27] The adsorption of polymers[9] or impurities[124] on the growing crystal surface has been linked to their crystal growth inhibitory effects. While the adsorption of PPI has been linked with its crystal growth inhibitory effects, the detailed understanding of this mechanism is still lacking. For example, it is not well understood if the blocking of the active growth sites by the adsorbed PPI is the only primary mechanism of inhibition or the barrier for surface diffusion provided by the adsorbed PPI is also equally important in achieving higher inhibitory effects. The goal of this study was to provide better insight into the nature of PVP adsorption onto indomethacin crystals and, in turn, enhance understanding of the mechanisms of crystal growth inhibitory effects of PVP.

Adsorption and Crystal Growth Inhibition of Indomethacin by N-vinylpyrrolidone

The affinity of N-vinylpyrrolidone for indomethacin crystals, as expected, was significantly lower than that of polymeric PVP, which was attributed to cooperative or synergistic interactions between PVP and the indomethacin surface (Table 6.2). The extent of adsorption, A^{w}_{max}, for N-vinylpyrrolidone was ~9-fold smaller than that for PVP K29-32 (Table 6.2). Moreover, N-vinylpyrrolidone did not inhibit the crystal growth of indomethacin whereas PVP K29-32 showed ~160-fold greater crystal growth inhibitory effect as compared to N-vinylpyrrolidone (Figure 6.7). This clearly indicated that although N-vinylpyrrolidone and PVP K29-32 could have similar intermolecular interactions with indomethacin in solution as well as at the surface, the surface interactions of N-vinylpyrrolidone are dynamic and ineffective at providing higher extent of adsorption as well as inhibiting the crystal growth of indomethacin. Due to the dynamic nature of interactions, when the bond between the monomer, N-vinylpyrrolidone, and the crystal surface of indomethacin is broken, the monomer could

displace to form a new bond at a new site leaving the original site open for further crystal growth. Additionally, the comparison between the experimentally observed and theoretically predicted values of A_{max}^{w} for N-vinylpyrrolidone (0.2 vs. 1.0 mg/m^2) indicated that a complete surface coverage of the indomethacin surface was not achieved by N-vinylpyrrolidone. This also indicated that some of the active growth sites for the crystal growth of indomethacin were not blocked by N-vinylpyrrolidone resulting in the complete absence of the inhibition of indomethacin crystal growth. The equilibrium solubility of indomethacin after crystal growth at high degree of supersaturation in the presence of N-vinylpyrrolidone was higher than the equilibrium solubility measured without any induced crystal growth, which indicated that a higher energy surface layer was formed on the growing crystal.[104] The lack of significant surface adsorption by the monomer found in this study could also explain previously observed ineffectiveness of non-polymeric molecules at inhibiting crystal growth.[14,19,107,196] For example, 2-pyrrolidinone did not shown any effect on the etching pattern, nucleation and crystal growth of acetaminophen as compared to PVP K30.[19] Unlike polymeric hydrogen bond donors such as PVP and PVA, the small molecule hydrogen bond donors such as glycerol, glucose, adipic acid, and methanol could not inhibit the crystal growth of caffeine hydrate.[107]

Effect of Molecular Weight & Concentration of PVP on the Adsorption and Crystal Growth Inhibition of Indomethacin

Adsorption isotherms of PVP for indomethacin show a high-affinity character (Figure 6.5). Similar high-affinity isotherms have been observed for the adsorption of PVP onto other surfaces including kaolinite,[175] Na-montmorillonite,[192] polystyrene,[176,188]

graphite,[191] silica,[174,189,191] and titanium dioxide.[193] However, the adsorption isotherm of PVP for alumina showed a low-affinity character, which was attributed to the weak interactions between PVP and alumina.[191]

The extent of adsorption (A_{max}^{W}) of PVP K29-32 for indomethacin crystals dispersed in an aqueous medium is 1.99 mg/m^2 (Table 6.2 and Figure 6.5), which was similar to previously determined values of the A_{max}^{W} of PVP K29-32 or PVP K30 halofantrine (1.8 mg/m^2)[194] and polystyrene (2 mg/m^2)[188] dispersed in aqueous media. However, the A_{max}^{W} of PVP K30 for kaolinite was slightly lower (i.e., 1.2 mg/m^2) than that for indomethacin crystals indicating a difference between the interaction of PVP with the two surfaces.[175] Additional previous studies[176,189,191,192] have also reported the A_{max}^{W} of PVP on various surfaces, however the values of A_{max}^{W} are described in very specific units such as the weight of adsorbed polymer per unit weight of adsorbent (e.g., mg/g or g/g) instead of a more universal unit such as the weight of adsorbed polymer per unit surface area (e.g., mg/m^2), which makes the direct comparison of A_{max}^{W} values of PVP across various studies very difficult.

The affinity and the extent of adsorption onto indomethacin crystals (A_{max}^{W}, mg/m^2) were greater for higher molecular weight PVP K29-32 as compared to those for lower molecular weight PVP K12 and PVP K16-18 (Table 6.2 and Figure 6.6). The higher affinity, as discussed earlier, could be attributed to cooperative interactions. It was hypothesized that the greater A_{max}^{W} for higher molecular weight PVP could be attributed to a change in conformation of the adsorbed PVP from trains to loops and tails at higher molecular weight. To characterize the change in conformation of the adsorbed PVP with

molecular weight, the extent of PVP adsorption onto indomethacin crystals was analyzed in multiple ways: (1) by comparing the A_{max} of PVP using different units, (2) by plotting the A_{max} against the molecular weight of PVP, and (3) by comparing the experimental and theoretical A_{max} of PVP.

The values of A_{max} of PVP were compared using different units: 1) weight-basis (A_{max}^{W}, mg/m^2), 2) monomer mole-basis (A_{max}^{mM}, monomoles/m^2), and 3) mole-basis (A_{max}^{M}, moles/m^2). A_{max}^{W} and A_{max}^{mM} increased while A_{max}^{M} decreased with the molecular weight of PVP (Table 6.2 and Figure 6.6). Thus, for a given number of interaction sites, fewer molecules of higher molecular weight PVP were adsorbed onto indomethacin crystals. This could be attributed to the fact that the long chains of higher molecular weight polymers would have cooperative or synergistic interactions at multiple sites on the surface. However, this observation also poses a new question as to whether all sub-units of a higher molecular weight polymer chain are interacting with the surface at same time or, in other words, whether the fraction of monomers or sub-units attached to the surface (i.e., in train conformation) is 1. If this were to occur then A_{max}^{W} and A_{max}^{mM} would be similar for different molecular weights of PVP as the number of sub-units bonded with the surface would be similar across the molecular weight range. However, the experimental A_{max}^{W} and A_{max}^{mM} data clearly show that this is not the case for the adsorption of PVP onto indomethacin crystals indicating that not all monomeric units are bonded to the surface of indomethacin. Since all PVP monomeric units are not attached to the indomethacin surface, loops and tails of the polymer must extend from the indomethacin surface.

When the A_{max}^{W} of PVP is plotted against its molecular weight, a linear relationship with a slope (α) of 0.36 is obtained (Eq. 6.2), indicative of both loops and tails in a random coil conformation extending from the indomethacin crystal surface (Figure 6.6).[173] The values of α for PVP adsorbed onto polystyrene latex and kaolinite suspended in aqueous media were reported to be α=0.2 and 0.44.[175,176] Alternatively, PVP could be adsorbed in a train conformation (α=0) or a tail conformation (α=1).[175,176,193] For example, PVP adsorbed in a train conformation onto titanium dioxide dispersed in methanol resulting in the extent of adsorption being independent of the molecular weight.[193]

The experimental A_{max}^{W} of PVP K12 (0.8 mg/m^2) and PVP K16-18 (0.9 mg/m^2) were similar to the theoretical A_{max}^{W} of PVP (i.e., ~1 mg/m^2) calculated based on the condensed monolayer adsorption of the monomeric units of PVP having the estimated area of 0.2 nm^2.[174,175] This indicated that a majority fraction of the adsorbed of PVP K12 and K16-18 could be in a train conformation with fewer loops and tails. It should be noted that instead of being either equal to or slightly higher than the theoretical A_{max}^{W} of PVP (i.e., ~1 mg/m^2), the experimental A_{max}^{W} values for PVP K12 and K16-18 were slightly lower. This may be attributable to an overestimation of the effective surface area available for the adsorption of larger molecules such as PVP polymers onto indomethacin crystals using smaller adsorbate molecules such as nitrogen. Unlike PVP K12 and PVP K16-18, the experimental A_{max}^{W} of PVP K29-32 was almost 2-fold higher than the theoretical A_{max}^{W}, indicating that a significant fraction of the adsorbed PVP K29-32 could reside in loops and tails extending away from the surface. Moreover, assuming that all three PVPs were occupying similar number of sites on the surface, the additional extent

of adsorption of PVP K29-32 above the theoretical A_{max}^{W} (i.e., ~1 mg/m^2) could be attributed to longer loops and tails and a thicker adsorption layer. The difference in the thickness of the adsorption layer between the higher molecular weight PVP K29-32 and lower molecular weight PVP K16-18 was estimated from their respective A_{max}^{W} values (0.9 vs. 1.99 mg/m^2) and previously determined thickness of the adsorption layer of PVP K16-18 of ~4 nm. From the adsorption layer thickness of 4 nm and the A_{max}^{W} of 0.9 mg/m^2 for PVP K16-18, the density of the adsorption layer could be calculated as 2.3×10^8 mg/m^3. If it is assumed that the density of the adsorbed layer would be similar between the two polymers, then the thickness of the adsorption layer for PVP K29-32 could be estimated as ~9 nm using the A_{max}^{W} of PVP K29-32 of 1.99 mg/m^2. Thus, at saturation, the thickness of PVP K29-32 adsorption layer for indomethacin could be more than two-fold greater than that of PVP K16-18.

Overall, the above analysis of A_{max}^{W} of PVP for indomethacin crystals indicated that, at saturation, the lower molecular weight PVP K12 and K16-18 could be adsorbed in mostly train conformations with a fewer loops and tails than exhibited by the higher molecular weight PVP K29-32. Similar correlations between the molecular weight of PVP, the extent of PVP adsorption, and the thickness of PVP adsorption layer have been made in previous studies.[174,175,190,192,197] For example, the adsorption of PVP on kaolinite increased with the molecular weight of PVP up to ≤ 44000 g/mol beyond which the extent of PVP adsorption leveled off.[175] The higher extent of adsorption with higher molecular weight PVP was attributed to the change in the adsorbed PVP conformation from trains at a lower molecular weight to loops and tails at a higher molecular weight. In cases such as the adsorption of PVP onto halofantrine where the conformation of PVP

remained unchanged while increasing the molecular weight of PVP over the average weight range of 3−46 kg/mol, no significant effect of the molecular weight of PVP on the extent of adsorption was seen.[194] Smith et al.[188] observed that there was no effect of PVP molecular weight on the adsorption capacity of polystyrene lattices when they were suspended in water. However, the adsorption capacity of polystyrene lattices for PVP increased with an increase in the molecular weight of PVP when the lattices were suspended in water containing 0.5 M NaCl. This was attributed to the significant weakening of the polar interactions between PVP and polystyrene due to shielding of PVP dipoles by NaCl. PVP adopted a more extended conformation of loops and tails in the presence of NaCl as compared to a flatter conformation of trains in water.[188] Cohen Stuart et. al.[190] measured the fraction of bound PVP segments onto silica using NMR and EPS at different molecular weights of PVP. A greater number of loops and tails was observed for higher molecular weight PVP, whereas the lower molecular weight PVP was mostly adsorbed in a train conformation at the silica-liquid interface. Sequaris et al.[192] showed that, unlike PVP K12, the fraction of higher molecular weight PVP K30 segments bound in train conformations to montmorillonite measured using a microcalorimetric technique decreased from 1 to 0.3 when the adsorbed PVP K30 amount increased from 0 to ~4.5 mM/g, which was attributed to longer tail and loop segments in the adsorbed layer at higher surface coverage. Kellaway et. al.[176] attributed the linear increase in the thickness of the PVP layer adsorbed onto polystyrene latex measured by U-tube viscometry with an increase in the molecular weight of PVP to a significant contribution of loops to the thickness of the adsorbed layer. Hild et. al.[175] also attributed the higher extent of adsorption by higher molecular weight PVP to loops and

tails yielding a large increase in the thickness of the hydrodynamic layer measured using microelectrophoresis. At low surface coverage, PVP chains lie flat in train conformations onto kaolinite. However, at high surface coverage the polymer chains would be in loops or random coil tail conformations yielding a large increase in the thickness of the hydrodynamic layer in relative to the amount adsorbed for higher molecular weight PVP. The thickness of the adsorbed PVP onto kaolinite particles was ~6-fold greater at higher amounts of PVP adsorbed ($\geq$0.6 mg/m^2) as compared to lower amounts of PVP adsorbed (<0.6 mg/m^2).[175]

The inhibitory effect of PVP on the crystal growth of indomethacin is ~3-fold greater for higher molecular weight PVP K29-32 as compared to those for the lower molecular weight PVP K12 and PVP K16-18 (Table 6.2 and Figure 6.7). This could be attributed to the greater affinity and greater extent of adsorption of higher molecular weight PVP for indomethacin crystals as compared to lower molecular weight PVP. The values of k_G of indomethacin at a high degree of supersaturation (S~5) in the presence of PVP K12, K16-18, and K29-32 (i.e., $1.0 \pm 0.2 \times 10^{-4}$, $1.1 \pm 0.6 \times 10^{-4}$, and $3.0 \pm 1.9 \times 10^{-5}$ cm/sec, respectively) were similar to the k_G of the surface integration controlled crystal growth of indomethacin as determined in a previous study (i.e., $5.5 \pm 1.3 \times 10^{-4}$ cm/sec).[166] The k_G of the bulk diffusion controlled crystal growth of indomethacin in the absence of PVP is $4.7 \pm 0.7 \times 10^{-3}$ cm/sec.[104] This suggested that the adsorbed PVP changed the mechanism of indomethacin crystal growth at high S such that the rate limiting step changed from bulk diffusion to surface integration.[27,104,166] The change in crystal growth mechanism could be attributed to the inhibition of the formation a high energy surface layer on indomethacin crystals by the adsorbed PVP as indicated by the

similarity between the apparent solubility of indomethacin after crystal growth in the presence of PVP and the equilibrium solubility in the presence of PVP without any crystal growth.[27] To further understand the crystal inhibitory effect of PVP, we determined the crystal growth inhibition of indomethacin at different extents of PVP K29-32 adsorption (Figure 6.8A). The extent of PVP adsorption was also represented as the fractional surface coverage of indomethacin while assuming a complete surface coverage of indomethacin by PVP at an A_{max}^{W} of 1 mg/m^2. The fractional surface coverage was correlated with the degree of crystal growth inhibition (1/R) (Figure 6.8B). The degree of indomethacin crystal growth inhibition increased as the fractional surface coverage of the surface of indomethacin increased from 0 to 1 indicating the significant impact of surface coverage on the inhibition of crystal growth. Moreover, the degree of crystal growth inhibition was even greater at fractional surface coverages of higher than 1. As discussed earlier, at lower extents of adsorption, a majority of the adsorbed PVP K29-32 molecules could be in a much flatter "train" conformation providing a thinner layer of the adsorbed polymer. As the extent of adsorption increases, the fraction of PVP K29-32 molecules with a "trains and loops" conformation could grow significantly resulting in a thicker layer of the adsorbed polymer.[175] These results indicate that while more surface coverage provides higher inhibition of the crystal growth, the greater resistance for surface diffusion of indomethacin molecules provided by the thicker adsorption layer of PVP enhances the crystal growth inhibitory effect further. A comparison between a low molecular weight PVP polymer (PVP K16-18) and a high molecular weight PVP polymer (PVP K29-32) showed that the inhibition of indomethacin crystal growth was ~3-fold greater when the thickness of the PVP

adsorption layer increased ~2-fold. The stronger inhibitory effects of PVP K29-32 on the crystal growth of indomethacin at higher fractional surface coverage may be attributed to the thicker adsorbed layer and larger barrier for indomethacin crystal growth provided by the adsorbed PVP K29-32.

CONCLUSIONS

The relationship between the adsorption and crystal growth inhibitory effect of PVP on indomethacin seed crystals was explored at different molecular weights and bulk concentrations of PVP. The adsorption of PVP was successfully modeled using the Langmuir equation. PVP exhibited significantly higher affinity and extent of maximum adsorption for indomethacin crystals as compared to its monomer (N-vinylpyrrolidone), indicating stronger interactions of PVP with the surface of indomethacin. The extent of maximum adsorption for PVP onto indomethacin crystals increased with the molecular weight of PVP. The higher extent of adsorption with longer chain, higher molecular weight PVP was attributed not only to stronger interactions between PVP and the indomethacin crystal surface but also to a greater thickness of the adsorbed layer due to the formation of loops and tails. Unlike N-vinylpyrrolidone, PVP significantly inhibited the crystal growth of indomethacin at high degree of supersaturation, which was attributed to the change in the indomethacin crystal growth mechanism that also resulted in a change in the rate limiting step from bulk diffusion to surface integration at a high S. The adsorption and crystal growth inhibitory effect of PVP for indomethacin correlated well across different molecular weights and concentrations of PVP. The crystal growth inhibitory effect of PVP for indomethacin was greater at higher extents of PVP adsorption. The effectiveness of PVP K29-32 as a crystal growth inhibitor was about 3-

fold greater than that of PVP K16-18 and PVP K12 (0.05% w/w), which was attributed to a greater thickness of the adsorbed PVP layer. Finally, the greater effectiveness of PVP as a crystal growth inhibitor of indomethacin was not only attributed to higher surface coverage of indomethacin crystals but also to a greater barrier for the surface diffusion of indomethacin molecules provided by a thicker PVP adsorption layer.

Chapter Seven

Conclusions and Future Studies

A non-invasive, online, simple and reliable method to determine crystal growth rates using a batch crystallization technique and second derivative UV spectroscopy was been developed. The second derivative UV spectroscopy successfully removed the spectral interference due to the presence of seed crystals in the crystal growth samples during indomethacin concentration measurements. The presence of seed crystals obviated primary nucleation of indomethacin at higher degrees of supersaturation during crystal growth. The apparent equilibrium solubility of indomethacin after crystal growth was about 55% higher than its equilibrium solubility, which could be attributed to the growth of a higher energy indomethacin form on seed crystals of the thermodynamically most stable form. The first order desupersaturation kinetic profiles and the similarity between the mass transfer coefficients determined from indomethacin powder dissolution and crystal growth clearly indicated that the indomethacin crystal growth at a high degree of supersaturation of S=6 is bulk diffusion rate limited. Indomethacin crystal growth kinetics from supersaturated aqueous suspensions was compared at varying degrees of supersaturation ($2 \leq S \leq 9$). The higher indomethacin apparent solubility after crystal growth at S between 2 and 9 indicated that a higher energy surface was formed on the seed crystals initially having a lower energy surface. The indomethacin crystal growth rate coefficient (k_G) increased with S between an S of 2-6. At high S ($6 \leq S \leq 9$), the k_G reached a plateau value that was similar to the theoretically predicted k_G assuming bulk diffusion controlled crystal growth. The indomethacin k_G at a low S of 2 was ~10 times smaller than the theoretically predicted k_G assuming bulk diffusion controlled crystal growth. The smaller indomethacin k_G at S=2 could be due to a change in the rate limiting

step from bulk diffusion to surface integration. The change in rate-limiting step from bulk diffusion to surface integration for the indomethacin crystal growth at a low S of 2 was attributed to a longer lag time for the conversion of initial lower energy indomethacin seed crystal surface to a high energy surface due to reduced thermodynamic driving force for crystal growth at the low S of 2. The k_G determined at a low S of 2 using higher energy seed crystals was similar to that predicted assuming bulk diffusion controlled crystal growth. This result further verified the hypothesis that the higher energy surface provided faster bulk diffusion controlled crystal growth. Using an infusion-based method, the indomethacin k_G at very low S (<1.6) was determined without transforming the initial lower energy surface to the higher energy surface. The indomethacin apparent solubility after crystal growth at S<1.6 was lower and similar to the equilibrium solubility indicating that crystal growth at S below the higher indomethacin apparent solubility (i.e., S < 1.6) did not form the higher energy surface. The k_G at S < 1.6 was similar to that determined at an S of 2 supporting the hypothesis that the smaller k_G at low S could be attributed to the lower energy indomethacin seed crystal surface. Finally, the higher energy surface provided faster, bulk diffusion controlled indomethacin crystal growth at high and low S, whereas the lower energy surface was associated with significantly slower surface integration controlled crystal growth rate at low S. The quantitative mechanistic understanding derived from the indomethacin crystal growth kinetics at high and low S was useful in exploring the inhibitory effects of model pharmaceutical excipients on indomethacin crystal growth and, in turn, on its supersaturation maintenance. HP-β-CD significantly increased indomethacin equilibrium solubility due to 1:1 complex formation between indomethacin

and HP-β-CD. PVP and HPMC did not substantially alter the solubility of indomethacin. Viscosity of HPMC solutions increased significantly as a function of HPMC concentration. The rank order of solution viscosity at similar PPI concentrations was HPMC > PVP > HP-β-CD. PVP and HPMC were better indomethacin crystal growth inhibitors than HP-β-CD at high degrees of supersaturation (S), which was attributed their ability to change the indomethacin crystal growth rate limiting step from bulk diffusion to surface integration. HP-β-CD's crystal growth inhibitory effects at high S increased with an increase in its concentration up to 1% w/w concentration. The inhibitory effect of HP-β-CD on bulk diffusion controlled indomethacin crystal growth at high S could be rationalized by reversible complexation between HP-β-CD and indomethacin in the diffusion layer. The crystal growth inhibition factors of PVP and HPMC were dramatically greater at high S than that for HP-β-CD, which indicated that both PPIs changed the rate limiting step of indomethacin crystal growth at high S from bulk diffusion to surface integration. At low S, the crystal growth rate of indomethacin becomes surface integration controlled even in the absence of PPIs. Under these conditions all PPIs exhibited only modest inhibitory effects. For example, a twofold greater indomethacin crystal growth inhibition factor was observed for HP-β-CD at low S than that at high S, reflecting its effect on the rate of indomethacin surface integration at low S. The relative effects of the model PPIs at low S may be attributable to their adsorption onto the growing crystal surface and the effect of this adsorption on the rate of surface integration. The relationship between the adsorption and crystal growth inhibitory effect of PVP for indomethacin was explored at different molecular weights and bulk concentrations of PVP. The adsorption isotherms of PVP were successfully

modeled using the Langmuir adsorption isotherm model. The adsorption isotherms of PVP showed a high affinity character. PVP showed significantly higher affinity and the extent of adsorption for indomethacin crystals as compared to its monomer (N-vinylpyrrolidone), which were attributed to stronger interactions of PVP with the surface of indomethacin. The extent of adsorption for PVP onto indomethacin crystals was a function of the molecular weight of PVP. The extent of adsorption for PVP K29-32 was 2-fold and 3-fold greater than those for PVP K 16-18 and PVP K12, respectively. The higher extent of adsorption with longer chain higher molecular weight PVP was attributed not only to stronger interactions between PVP and the surface of indomethacin but also to a greater thickness of the adsorbed layer due to the formation of loops and tails structures by the adsorbed longer chain higher molecular weight PVP. Unlike N-vinylpyrrolidone, PVP significantly inhibited the crystal growth of indomethacin at high degree of supersaturation, which was attributed to the change in indomethacin crystal growth mechanism resulting in a change in the rate limiting step from bulk diffusion to surface integration at a high S. The adsorption and crystal growth inhibitory effect of PVP for indomethacin correlated well across different molecular weights and concentrations of PVP. The crystal growth inhibitory effect of PVP for indomethacin was greater at higher extents of PVP adsorption onto indomethacin crystals. The effectiveness of PVP K29-32 as a crystal growth inhibitor was about 3-fold greater than that of PVP K16-18 and PVP K12 (0.05% w/w), which was attributed to higher thickness of the PVP adsorption layer. The greater effectiveness of PVP as a crystal growth inhibitor of indomethacin was not only attributed to higher surface coverage of indomethacin crystals but also to greater barrier for the surface diffusion of indomethacin molecules provided

by a thicker PVP adsorption layer. Overall, the PPI effect on the change in growth mechanism, from bulk diffusion to surface integration, provided about 10-fold inhibition of the crystal growth of indomethacin. Additionally, the suppression of surface integration by PPIs resulted in another 30-fold inhibition of indomethacin crystal growth.

The future studies could develop a similar quantitative and mechanistic understanding of the effects of PIs on the inhibition of nucleation of poorly water soluble drugs. Since the effects of PIs are highly drug molecule specific and vary with different drugs, the next step could be to determine the molecular descriptors (e.g., hydrogen bond donor-acceptor capacity, polymer chain length, and presence of rigid-planar structure and its size) of drugs that significantly influence the effectiveness of PPIs. Quantitative models that could predict the effect of PIs on the precipitation (i.e., nucleation and crystal growth) of drugs could be created, and in turn facilitate the development of drug candidates for the life-threatening diseases. The quantitative models explaining nucleation and crystal growth phenomena may be integrated into a master equation predicting drug precipitation kinetics. A more extensive database of the effects of PIs on the precipitation of poorly water soluble drugs could be created. A framework for rational and efficient decision making leading to the rapid selection of excipient(s) or excipient combinations specific to the drug candidate under evaluation could be created that could provide high oral bioavailability for compounds that otherwise might exhibit solubility-limited absorption or undergo extensive precipitation/recrystallization after dissolution. Moreover, the understanding and predictive approaches emerging from the future studies are likely to save significant amounts of time and resources, which will in

turn enable pharmaceutical scientists to support greater numbers of drug product development programs for new therapeutic entities.

Appendix 1: List of Abbreviations

SDDS: Supersaturating Drug Delivery Systems

S: Degrees of supersaturation

PIs: Precipitation inhibitors

PPIs: Polymeric precipitation inhibitors

PVP: Polyvinylpyrrolidone ()

PVP-VA: Polyvinylpyrrolidone-co-polyvinyl acetate

HPMC: Hydroxypropyl methylcellulose

HPMC-AS: Hydroxypropyl methylcellulose-acetate succinate

PEG: Polyethylene glycol

PVA: Polyvinyl alcohol

TPGS: d-α-tocopheryl polyethylene glycol 1000 succinate

HP-β-CD: Hydroxypropyl β-cyclodextrin

SBE-CD: β-cyclodextrin sulfobutyl ether

ASD: Amorphous solid dispersions

SEDDS: Self-emulsifying drug delivery systems

SMEDDS: Self-microemulsifying drug delivery systems

SNEDDS: Self-nanoemulsifying drug delivery systems

S-SEDDS: Supersaturable SEDDS

ADME: Absorption, distribution, metabolism, and excretion

BCS: Biopharmaceutical classification system

MAD: Maximum absorbable dose (MAD)

SIWV: Small intestinal water volume

SITT: Small intestinal transit time

BCF: Burton, Cabrera and Frank

PXRD: Powder X-ray diffraction

SEM: Scanning electron microscopy

PLM: Polarized light microscopic analysis

UV: Ultraviolet

SEC: Size-exclusion chromatography

References

1. Brouwers J, Brewster ME, Augustijns P 2009. Supersaturating Drug Delivery Systems: The Answer to Solubility-Limited Oral Bioavailability? Journal of Pharmaceutical Sciences 98(8):2549-2572.

2. Dai WG, Dong LC, Shi XF, Nguyen J, Evans J, Xu YD, Creasey AA 2007. Evaluation of Drug Precipitation of Solubility-Enhancing Liquid Formulations Using Milligram Quantities of a New Molecular Entity (NME). Journal of Pharmaceutical Sciences 96(11):2957-2969.

3. DiNunzio JC, Miller DA, Yang W, McGinity JW, Williams RO 2008. Amorphous Compositions Using Concentration Enhancing Polymers for Improved Bioavailability of Itraconazole. Molecular Pharmaceutics 5(6):968-980.

4. Gao P, Akrami A, Alvarez F, Hu J, Li L, Ma C, Surapaneni S 2009. Characterization and Optimization of Amg 517 Supersaturatable Self-Emulsifying Drug Delivery System (S-SEDDS) for Improved Oral Absorption. Journal of Pharmaceutical Sciences 98(2):516-528.

5. Gao P, Rush BD, Pfund WP, Huang TH, Bauer JM, Morozowich W, Kuo MS, Hageman MJ 2003. Development of a Supersaturable Sedds (S-SEDDS) Formulation of Paclitaxel with Improved Oral Bioavailability. Journal of Pharmaceutical Sciences 92(12):2386-2398.

6. Overhoff K, McConville J, Yang W, Johnston K, Peters J, Williams R 2008. Effect of Stabilizer on the Maximum Degree and Extent of Supersaturation and Oral Absorption of Tacrolimus Made by Ultra-Rapid Freezing. Pharmaceutical Research 25(1):167-175.

7. Xiang T-X, Anderson BD 2002. Stable Supersaturated Aqueous Solutions of Silatecan 7-T-Butyldimethylsilyl-10-Hydroxycamptothecin Via Chemical Conversion in the Presence of a Chemically Modified B-Cyclodextrin. Pharmaceutical Research 19(8):1215-1222.

8. Gao P, Shi Y 2012. Characterization of Supersaturatable Formulations for Improved Absorption of Poorly Soluble Drugs. The AAPS Journal 14(4):703-713.

9. Warren DB, Benameur H, Porter CJH, Pouton CW 2010. Using Polymeric Precipitation Inhibitors to Improve the Absorption of Poorly Water-Soluble Drugs: A Mechanistic Basis for Utility. Journal of Drug Targeting 18(10):704-731.

10. Ilevbare GA, Liu H, Edgar KJ, Taylor LS 2012. Understanding Polymer Properties Important for Crystal Growth Inhibition—Impact of Chemically Diverse Polymers on Solution Crystal Growth of Ritonavir. Crystal Growth & Design 12(6):3133-3143.

11. Tian F, Baldursdottir S, Rantanen J 2009. Effects of Polymer Additives on the Crystallization of Hydrates: A Molecular-Level Modulation. Molecular Pharmaceutics 6(1):202-210.

12. Raghavan SL, Trividic A, Davis AF, Hadgraft J 2001. Crystallization of Hydrocortisone Acetate: Influence of Polymers. International Journal of Pharmaceutics 212(2):213-221.

13. Ueda K, Higashi K, Yamamoto K, Moribe K 2013. Inhibitory Effect of Hydroxypropyl Methylcellulose Acetate Succinate on Drug Recrystallization from a Supersaturated Solution Assessed Using Nuclear Magnetic Resonance Measurements. Molecular Pharmaceutics 10(10):3801-3811.

14. Tian F, Saville DJ, Gordon KC, Strachan CJ, Zeitler JA, Sandler N, Rades T 2007. The Influence of Various Excipients on the Conversion Kinetics of Carbamazepine Polymorphs in Aqueous Suspension. Journal of Pharmacy and Pharmacology 59(2):193-201.

15. Ilevbare GA, Liu H, Edgar KJ, Taylor LS 2012. Maintaining Supersaturation in Aqueous Drug Solutions: Impact of Different Polymers on Induction Times. Crystal Growth & Design 13(2):740-751.

16. Dalsin MC, Tale S, Reineke TM 2013. Solution-State Polymer Assemblies Influence Bcs Class Ii Drug Dissolution and Supersaturation Maintenance. Biomacromolecules 15(2):500-511.

17. Gift AD, Luner PE, Luedeman L, Taylor LS 2008. Influence of Polymeric Excipients on Crystal Hydrate Formation Kinetics in Aqueous Slurries. Journal of Pharmaceutical Sciences 97(12):5198-5211.

18. Simonelli AP, Mehta SC, Higuchi WI 1970. Inhibition of Sulfathiazole Crystal Growth by Polyvinylpyrrolidone. Journal of Pharmaceutical Sciences 59(5):633-638.

19. Wen H, Morris K, Park K 2008. Synergic Effects of Polymeric Additives on Dissolution and Crystallization of Acetaminophen. Pharmaceutical Research 25(2):349-358.

20. Lindfors L, Forssén S, Westergren J, Olsson U 2008. Nucleation and Crystal Growth in Supersaturated Solutions of a Model Drug. Journal of Colloid and Interface Science 325(2):404-413.

21. Ziller KH, Rupprecht H 1988. Control of Crystal Growth in Drug Suspensions: 1) Design of a Control Unit and Application to Acetaminophen Suspensions. Drug Development and Industrial Pharmacy 14(15):2341 - 2370.

22. Ilevbare GA, Liu H, Edgar KJ, Taylor LS 2012. Inhibition of Solution Crystal Growth of Ritonavir by Cellulose Polymers - Factors Influencing Polymer Effectiveness. CrystEngComm 14(20):6503-6514.

23. Ilevbare GA, Liu H, Edgar KJ, Taylor LS 2013. Impact of Polymers on Crystal Growth Rate of Structurally Diverse Compounds from Aqueous Solution. Molecular Pharmaceutics 10(6):2381-2393.

24. Mullin JW. 2001. Crystallization. Fourth ed., Oxford; Boston: Butterworth-Heinemann.

25. Boistelle R, Astier JP 1988. Crystallization Mechanisms in Solution. Journal of Crystal Growth 90(1-3):14-30.

26. Ohara M, Reid RC. 1973. Modeling Crystal Growth Rates from Solution. First ed., Englewood Cliffs, NJ: Prentice-Hall.

27. Patel DD, Anderson BD 2014. Effect of Precipitation Inhibitors on Indomethacin Supersaturation Maintenance: Mechanisms and Modeling. Molecular Pharmaceutics 11(5):1489-1499.

28. Greco K, Bogner R 2012. Solution-Mediated Phase Transformation: Significance During Dissolution and Implications for Bioavailability. Journal of Pharmaceutical Sciences 101(9):2996-3018.

29. Murphy D, Rodríguez-Cintrón F, Langevin B, Kelly RC, Rodríguez-Hornedo N 2002. Solution-Mediated Phase Transformation of Anhydrous to Dihydrate

Carbamazepine and the Effect of Lattice Disorder. International Journal of Pharmaceutics 246(1–2):121-134.

30. Mosharraf M, Sebhatu T, Nyström C 1999. The Effects of Disordered Structure on the Solubility and Dissolution Rates of Some Hydrophilic, Sparingly Soluble Drugs. International Journal of Pharmaceutics 177(1):29-51.

31. Østergaard J, Wu JX, Naelapää K, Boetker JP, Jensen H, Rantanen J 2014. Simultaneous Uv Imaging and Raman Spectroscopy for the Measurement of Solvent-Mediated Phase Transformations During Dissolution Testing. Journal of Pharmaceutical Sciences 103(4):1149-1156.

32. Elamin AA, Ahlneck C, Alderborn G, Nyström C 1994. Increased Metastable Solubility of Milled Griseofulvin, Depending on the Formation of a Disordered Surface Structure. International Journal of Pharmaceutics 111(2):159-170.

33. Pikal MJ, Lukes AL, Lang JE, Gaines K 1978. Quantitative Crystallinity Determinations for B-Lactam Antibiotics by Solution Calorimetry: Correlations with Stability. Journal of Pharmaceutical Sciences 67(6):767-773.

34. Duddu SP, Grant DJW 1995. The Use of Thermal Analysis in the Assessment of Crystal Disruption. Thermochimica Acta 248(0):131-145.

35. Bergfors T 2003. Seeds to Crystals. Journal of Structural Biology 142(1):66-76.

36. Niekawa N, Kitamura M 2013. Role of Epitaxy-Mediated Transformation in Ostwald's Step Rule: A Theoretical Study. CrystEngComm 15(35):6932-6941.

37. Rodríguez-hornedo N, Murphy D 1999. Significance of Controlling Crystallization Mechanisms and Kinetics in Pharmaceutical Systems. Journal of Pharmaceutical Sciences 88(7):651-660.

38. Buckton G, Darcy P 1999. Assessment of Disorder in Crystalline Powders-a Review of Analytical Techniques and Their Application. International Journal of Pharmaceutics 179(2):141-158.

39. Vippagunta RR, LoBrutto R, Pan C, Lakshman JP 2010. Investigation of Metformin Hcl Lot-to-Lot Variation on Flowability Differences Exhibited During Drug Product Processing. Journal of Pharmaceutical Sciences 99(12):5030-5039.

40. Burt HM, Mitchell AG 1981. Crystal Defects and Dissolution. International Journal of Pharmaceutics 9(2):137-152.

41. Greco K, Bogner R 2010. Crystallization of Amorphous Indomethacin During Dissolution: Effect of Processing and Annealing. Molecular Pharmaceutics 7(5):1406-1418.

42. Usui F, Maeda K, Kusai A, Nishimura K, Yamamoto K 1997. Inhibitory Effects of Water-Soluble Polymers on Precipitation of Rs-8359. International Journal of Pharmaceutics 154(1):59-66.

43. Vandecruys R, Peeters J, Verreck G, Brewster ME 2007. Use of a Screening Method to Determine Excipients Which Optimize the Extent and Stability of Supersaturated Drug Solutions and Application of This System to Solid Formulation Design. International Journal of Pharmaceutics 342(1-2):168-175.

44. Scholl J, Lindenberg C, Vicum L, Mazzotti M, Brozio J 2007. Antisolvent Precipitation of PDI 747: Kinetics of Particle Formation and Growth. Crystal Growth & Design 7(9):1653-1661.

45. Lipinski CA, Lombardo F, Dominy BW, Feeney PJ 1997. Experimental and Computational Approaches to Estimate Solubility and Permeability in Drug Discovery and Development Settings. Advanced Drug Delivery Reviews 23(1-3):3-25.

46. Brewster ME, Vandecruys R, Verreck G, Peeters J 2008. Supersaturating Drug Delivery Systems: Effect of Hydrophilic Cyclodextrins and Other Excipients on the Formation and Stabilization of Supersaturated Drug Solutions. Pharmazie 63(3):217-220.

47. Amidon G, Lennernäs H, Shah V, Crison J 1995. A Theoretical Basis for a Biopharmaceutic Drug Classification: The Correlation of in Vitro Drug Product Dissolution and in Vivo Bioavailability. Pharmaceutical Research 12(3):413-420.

48. Serajuddin ATM 2007. Salt Formation to Improve Drug Solubility. Advanced Drug Delivery Reviews 59(7):603-616.

49. Childs SL, Chyall LJ, Dunlap JT, Smolenskaya VN, Stahly BC, Stahly GP 2004. Crystal Engineering Approach to Forming Cocrystals of Amine Hydrochlorides with Organic Acids. Molecular Complexes of Fluoxetine Hydrochloride with Benzoic, Succinic, and Fumaric Acids. Journal of the American Chemical Society 126(41):13335-13342.

50. Constantinides PP 1995. Lipid Microemulsions for Improving Drug Dissolution and Oral Absorption: Physical and Biopharmaceutical Aspects. Pharmaceutical Research 12(11):1561-1572.

51. Jannin V, Musakhanian J, Marchaud D 2008. Approaches for the Development of Solid and Semi-Solid Lipid-Based Formulations. Advanced Drug Delivery Reviews 60(6):734-746.

52. Rane SS, Anderson BD 2008. What Determines Drug Solubility in Lipid Vehicles: Is It Predictable? Advanced Drug Delivery Reviews 60(6):638-656.

53. Serajuddin ATM 1999. Solid Dispersion of Poorly Water-Soluble Drugs: Early Promises, Subsequent Problems, and Recent Breakthroughs. Journal of Pharmaceutical Sciences 88(10):1058-1066.

54. Van Eerdenbrugh B, Van den Mooter G, Augustijns P 2008. Top-Down Production of Drug Nanocrystals: Nanosuspension Stabilization, Miniaturization and Transformation into Solid Products. International Journal of Pharmaceutics 364(1):64-75.

55. Mellaerts R, Mols R, Kayaert P, Annaert P, Van Humbeeck J, Van den Mooter G, Martens JA, Augustijns P 2008. Ordered Mesoporous Silica Induces Ph-Independent Supersaturation of the Basic Low Solubility Compound Itraconazole Resulting in Enhanced Transepithelial Transport. International Journal of Pharmaceutics 357(1–2):169-179.

56. Guzmán HR, Tawa M, Zhang Z, Ratanabanangkoon P, Shaw P, Gardner CR, Chen H, Moreau J-P, Almarsson Ö, Remenar JF 2007. Combined Use of Crystalline Salt Forms and Precipitation Inhibitors to Improve Oral Absorption of Celecoxib from Solid Oral Formulations. Journal of Pharmaceutical Sciences 96(10):2686-2702.

57. Fernandez S, Chevrier S, Ritter N, Mahler B, Demarne F, Carrière F, Jannin V 2009. In Vitro Gastrointestinal Lipolysis of Four Formulations of Piroxicam and Cinnarizine with the Self Emulsifying Excipients Labrasol® and Gelucire® 44/14. Pharmaceutical Research 26(8):1901-1910.

58. Tran TH, Guo Y, Song D, Bruno RS, Lu X 2014. Quercetin-Containing Self-Nanoemulsifying Drug Delivery System for Improving Oral Bioavailability. Journal of Pharmaceutical Sciences 103(3):840-852.

59. Chauhan H, Hui-Gu C, Atef E 2013. Correlating the Behavior of Polymers in Solution as Precipitation Inhibitor to Its Amorphous Stabilization Ability in Solid Dispersions. Journal of Pharmaceutical Sciences 102(6):1924-1935.

60. Verreck G, Six K, Van den Mooter G, Baert L, Peeters J, Brewster ME 2003. Characterization of Solid Dispersions of Itraconazole and Hydroxypropylmethylcellulose Prepared by Melt Extrusion—Part I. International Journal of Pharmaceutics 251(1–2):165-174.

61. Dhumal RS, Biradar SV, Yamamura S, Paradkar AR, York P 2008. Preparation of Amorphous Cefuroxime Axetil Nanoparticles by Sonoprecipitation for Enhancement of Bioavailability. European Journal of Pharmaceutics and Biopharmaceutics 70(1):109-115.

62. Bak A, Gore A, Yanez E, Stanton M, Tufekcic S, Syed R, Akrami A, Rose M, Surapaneni S, Bostick T, King A, Neervannan S, Ostovic D, Koparkar A 2008. The Co-Crystal Approach to Improve the Exposure of a Water-Insoluble Compound: AMG 517 Sorbic Acid Co-Crystal Characterization and Pharmacokinetics. Journal of Pharmaceutical Sciences 97(9):3942-3956.

63. Kim J-S, Kim M-S, Park HJ, Jin S-J, Lee S, Hwang S-J 2008. Physicochemical Properties and Oral Bioavailability of Amorphous Atorvastatin Hemi-Calcium Using Spray-Drying and SAS Process. International Journal of Pharmaceutics 359(1–2):211-219.

64. Stella VJ, Nti-Addae KW 2007. Prodrug Strategies to Overcome Poor Water Solubility. Advanced Drug Delivery Reviews 59(7):677-694.

65. Ghosh I, Snyder J, Vippagunta R, Alvine M, Vakil R, Tong W-Q, Vippagunta S 2011. Comparison of Hpmc Based Polymers Performance as Carriers for Manufacture of Solid Dispersions Using the Melt Extruder. International Journal of Pharmaceutics 419(1–2):12-19.

66. Abu-Diak OA, Jones DS, Andrews GP 2011. An Investigation into the Dissolution Properties of Celecoxib Melt Extrudates: Understanding the Role of Polymer Type and Concentration in Stabilizing Supersaturated Drug Concentrations. Molecular Pharmaceutics 8(4):1362-1371.

67. Chiou WL, Riegelman S 1971. Pharmaceutical Applications of Solid Dispersion Systems. Journal of Pharmaceutical Sciences 60(9):1281-1302.

68. Leuner C, Dressman J 2000. Improving Drug Solubility for Oral Delivery Using Solid Dispersions. European Journal of Pharmaceutics and Biopharmaceutics 50(1):47-60.

69. Friesen DT, Shanker R, Crew M, Smithey DT, Curatolo WJ, Nightingale JAS 2008. Hydroxypropyl Methylcellulose Acetate Succinate-Based Spray-Dried Dispersions: An Overview. Molecular Pharmaceutics 5(6):1003-1019.

70. Morgen M, Bloom C, Beyerinck R, Bello A, Song W, Wilkinson K, Steenwyk R, Shamblin S 2012. Polymeric Nanoparticles for Increased Oral Bioavailability and Rapid Absorption Using Celecoxib as a Model of a Low-Solubility, High-Permeability Drug. Pharmaceutical Research 29(2):427-440.

71. Pouton CW, Porter CJH 2008. Formulation of Lipid-Based Delivery Systems for Oral Administration: Materials, Methods and Strategies. Advanced Drug Delivery Reviews 60(6):625-637.

72. Anby MU, Williams HD, McIntosh M, Benameur H, Edwards GA, Pouton CW, Porter CJH 2012. Lipid Digestion as a Trigger for Supersaturation: Evaluation of the Impact of Supersaturation Stabilization on the in Vitro and in Vivo Performance of Self-Emulsifying Drug Delivery Systems. Molecular Pharmaceutics 9(7):2063-2079.

73. Williams H, Trevaskis N, Yeap Y, Anby M, Pouton C, Porter CH 2013. Lipid-Based Formulations and Drug Supersaturation: Harnessing the Unique Benefits of the Lipid Digestion/Absorption Pathway. Pharmaceutical Research 30(12):2976-2992.

74. Brewster ME, Loftsson T 2007. Cyclodextrins as Pharmaceutical Solubilizers. Advanced Drug Delivery Reviews 59(7):645-666.

75. Xu S, Dai W-G 2013. Drug Precipitation Inhibitors in Supersaturable Formulations. International Journal of Pharmaceutics 453(1):36-43.

76. Paulekuhn GS, Dressman JB, Saal C 2007. Trends in Active Pharmaceutical Ingredient Salt Selection Based on Analysis of the Orange Book Database. Journal of Medicinal Chemistry 50(26):6665-6672.

77. Serajuddin ATM, Jarowski CI 1985. Effect of Diffusion Layer pH and Solubility on the Dissolution Rate of Pharmaceutical Acids and Their Sodium Salts Ii: Salicylic Acid, Theophylline, and Benzoic Acid. Journal of Pharmaceutical Sciences 74(2):148-154.

78. Higuchi T, Ikeda M 1974. Rapidly Dissolving Forms of Digoxin: Hydroquinone Complex. Journal of Pharmaceutical Sciences 63(5):809-811.

79. Stanton MK, Bak A 2008. Physicochemical Properties of Pharmaceutical Co-Crystals: A Case Study of Ten Amg 517 Co-Crystals. Crystal Growth & Design 8(10):3856-3862.

80. Remenar JF, Morissette SL, Peterson ML, Moulton B, MacPhee JM, Guzmán HR, Almarsson Ö 2003. Crystal Engineering of Novel Cocrystals of a Triazole Drug with 1,4-Dicarboxylic Acids. Journal of the American Chemical Society 125(28):8456-8457.

81. Davis AF, Hadgraft J 1991. Effect of Supersaturation on Membrane Transport: 1. Hydrocortisone Acetate. International Journal of Pharmaceutics 76(1-2):1-8.

82. Pellett MA, Roberts MS, Hadgraft J 1997. Supersaturated Solutions Evaluated with an in Vitro Stratum Corneum Tape Stripping Technique. International Journal of Pharmaceutics 151(1):91-98.

83. Gao P, Guyton ME, Tiehua H, Bauer JM, Stefanski KJ, Qun L 2004. Enhanced Oral Bioavailability of a Poorly Water Soluble Drug Pnu-91325 by Supersaturatable Formulations. Drug Development & Industrial Pharmacy 30(2):221-229.

84. Miller DA, DiNunzio JC, Yang W, McGinity JW, Williams RO 2008. Targeted Intestinal Delivery of Supersaturated Itraconazole for Improved Oral Absorption. Pharmaceutical Research 25(6):1450-1459.

85. Williams HD, Trevaskis NL, Charman SA, Shanker RM, Charman WN, Pouton CW, Porter CJH 2013. Strategies to Address Low Drug Solubility in Discovery and Development. Pharmacological Reviews 65(1):315-499.

86. Johnson K, Swindell A 1996. Guidance in the Setting of Drug Particle Size Specifications to Minimize Variability in Absorption. Pharmaceutical Research 13(12):1795-1798.

87. Curatolo W 1998. Physical Chemical Properties of Oral Drug Candidates in the Discovery and Exploratory Development Settings. Pharmaceutical Science & Technology Today 1(9):387-393.

88. Six K, Daems T, de Hoon J, Van Hecken A, Depre M, Bouche M-P, Prinsen P, Verreck G, Peeters J, Brewster ME, Van den Mooter G 2005. Clinical Study of Solid Dispersions of Itraconazole Prepared by Hot-Stage Extrusion. European Journal of Pharmaceutical Sciences 24(2–3):179-186.

89. Kostewicz ES, Wunderlich M, Brauns U, Becker R, Bock T, Dressman JB 2004. Predicting the Precipitation of Poorly Soluble Weak Bases Upon Entry in the Small Intestine. Journal of Pharmacy and Pharmacology 56(1):43-51.

90. Variankaval N, Wenslow R, Murry J, Hartman R, Helmy R, Kwong E, Clas S-D, Dalton C, Santos I 2006. Preparation and Solid-State Characterization of Nonstoichiometric Cocrystals of a Phosphodiesterase-IV Inhibitor and L-Tartaric Acid. Crystal Growth & Design 6(3):690-700.

91. Ozaki S, Kushida I, Yamashita T, Hasebe T, Shirai O, Kano K 2012. Evaluation of Drug Supersaturation by Thermodynamic and Kinetic Approaches for the Prediction of Oral Absorbability in Amorphous Pharmaceuticals. Journal of Pharmaceutical Sciences 101(11):4220-4230.

92. Myerson AS, Ginde R, Allan SM. 2002. Crystals, Crystal Growth, and Nucleation. Handbook of Industrial Crystallization, Second ed., Woburn: Butterworth-Heinemann. p 33-65.

93. Garside J, Mersmann A, Nývlt J. 2002. Measurement of Crystal Growth and Nucleation Rates. Second ed., Rugby, UK: Institution of Chemical Engineers (IChemE).

94. McCoy AJ. 1999. Energy Diagram for Crystallization. University of Cambridge. [Online]. Available: www-structmed.cimr.cam.ac.uk. [Accessed June 2015].

95. Galkin O, Vekilov PG 1999. Are Nucleation Kinetics of Protein Crystals Similar to Those of Liquid Droplets? Journal of the American Chemical Society 122(1):156-163.

96. Roelands CPM, terHorst JH, Kramer HJM, Jansens PJ 2006. Analysis of Nucleation Rate Measurements in Precipitation Processes. Crystal Growth & Design 6(6):1380-1392.

97. Söhnel O, Garside J 1981. On Supersaturation Evaluation for Solution Growth. Journal of Crystal Growth 54(2):358-360.

98. Gilmer GH, Bennema P 1972. Simulation of Crystal Growth with Surface Diffusion. Journal of Applied Physics 43(4):1347-1360.

99. Burton WK, Cabrera N, Frank FC 1951. The Growth of Crystals and the Equilibrium Structure of Their Surfaces. Philosophical Transactions of the Royal Society of London Series A-Mathematical and Physical Sciences 243(866):299-358.

100. Bennema P, Vandereerden JP 1977. Crystal-Growth from Solution - Development in Computer-Simulation. Journal of Crystal Growth 42(12):201-213.

101. Bennema P 1969. The Importance of Surface Diffusion for Crystal Growth from Solution. Journal of Crystal Growth 5(1):29-43.

102. Cuppen HM, Meekes H, van Enckevort WJP, Vlieg E 2006. Birth-and-Spread Growth on the Kossel and a Non-Kossel Surface. Journal of Crystal Growth 286(1):188-196.

103. Li L, Rodríguez-Hornedo N 1992. Growth Kinetics and Mechanism of Glycine Crystals. Journal of Crystal Growth 121(1-2):33-38.

104. Patel DD, Joguparthi V, Wang Z, Anderson BD 2011. Maintenance of Supersaturation I: Indomethacin Crystal Growth Kinetic Modeling Using an Online Second-Derivative Ultraviolet Spectroscopic Method. Journal of Pharmaceutical Sciences 100(7):2623-2641.

105. Granberg RA, Rasmuson AC 2005. Crystal Growth Rates of Paracetamol in Mixtures of Water Plus Acetone Plus Toluene. AIChE Journal 51(9):2441-2456.

106. Thomas N, Holm R, Garmer M, Karlsson JJ, Mullertz A, Rades T 2013. Supersaturated Self-Nanoemulsifying Drug Delivery Systems (Super-SNEDDS) Enhance the Bioavailability of the Poorly Water-Soluble Drug Simvastatin in Dogs. The AAPS Journal 15(1):219-227.

107. Gift AD, Southard LA, Riesberg AL 2012. Influence of Polymeric Excipient Properties on Crystal Hydrate Formation Kinetics of Caffeine in Aqueous Slurries. Journal of Pharmaceutical Sciences 101(5):1755-1762.

108. Ozaki S, Kushida I, Yamashita T, Hasebe T, Shirai O, Kano K 2013. Inhibition of Crystal Nucleation and Growth by Water-Soluble Polymers and Its Impact on the Supersaturation Profiles of Amorphous Drugs. Journal of Pharmaceutical Sciences 102(7):2273-2281.

109. Amjad Z 1988. Kinetics of Crystal Growth of Calcium Sulfate Dehydrate: The Influence of Polymer Composition, Molecular Weight, and Solution pH. Canadian Journal of Chemistry-Revue Canadienne De Chimie 66(6):1529-1536.

110. Kuntze RA 1966. Retardation of Crystallization of Calcium Sulphate Dihydrate. Nature 211(5047):406-407.

111. Nancollas G, Reddy MM, Tsai F 1973. Calcium Sulfate Dihydrate Cyrstal-Growth in Aqueous-Solution at Elevated-Temperatures. Journal of Crystal Growth 20(2):125-134.

112. Amjad Z 1987. Kinetic-Study of the Seeded Growth of Calcium-Carbonate in the Presence of Benzenepolycarboxylic Acids. Langmuir 3(2):224-228.

113. Dalpi M, Karayianni E, Koutsoukos PG 1993. Inhibition of Hydroxyapatite Formation in Aqueous-Solutions by Zinc and 1,2-Dihydroxy-1,2-Bis(Dihydroxyphosphonyl)Ethane. Journal of the Chemical Society-Faraday Transactions 89(6):965-969.

114. Chen BD, Garside J. 1996. Crystallization of Tetracosane from Dodecane Solutions with Homologous Additives. Journal of Crystal Growth 166 (1-4):1094-1098.

115. Davey R, Mullin J 1974. Growth of the {101} Faces of Ammonium Dihydrogen Phosphate Crystals in the Presence of Ionic Species. Journal of Crystal Growth 23:89-94.

116. Nancollas G 1979. The Growth of Crystals in Solution. Advances in Colloid and Interface Science 10(1):215-252.

117. Berkovitch-Yellin Z, Van Mil J, Addadi L, Idelson M, Lahav M, Leiserowitz L 1985. Crystal Morphology Engineering by" Tailor-Made" Inhibitors; a New Probe to Fine Intermolecular Interactions. Journal of the American Chemical Society 107(11):3111-3122.

118. Li T, Wen H, Park K, Morris K 2002. How Specific Interactions between Acetaminophen and Its Additive 4-Methylacetanilide Affect Growth Morphology: Elucidation Using Etching Patterns. Crystal Growth & Design 2(3):185-189.

119. Van Rosmalen GM, Bennema P 1990. Characterization of Additive Performance on Crystallization: Habit Modification. Journal of Crystal Growth 99(1-4, Part 2):1053-1060.

120. Chow AHL, Chow PKK, Zhongshan W, Grant DJW 1985. Modification of Acetaminophen Crystals: Influence of Growth in Aqueous Solutions Containing P-Acetoxyacetanilide on Crystal Properties. International Journal of Pharmaceutics 24(2-3):239-258.

121. Chow KY, Go J, Zhongshan W, Mehdizadeh M, Grant DJW 1985. Modification of Adipic Acid Crystals. Ii. Influence of Growth in the Presence of Oleic Acid on Crystal Properties. International Journal of Pharmaceutics 25(1):41-55.

122. Dai WG, Dong LC, Li S, Deng ZY 2008. Combination of Pluronic/Vitamin E TPGS as a Potential Inhibitor of Drug Precipitation. International Journal of Pharmaceutics 355(1-2):31-37.

123. Chow AHL, Grant DJW 1988. Modification of Acetaminophen Crystals. II. Influence of Stirring Rate During Solution-Phase Growth on Crystal Properties in the Presence and Absence of P-Acetoxyacetanilide. International Journal of Pharmaceutics 41(1-2):29-39.

124. Kubota N, Yokota M, Mullin JW 2000. The Combined Influence of Supersaturation and Impurity Concentration on Crystal Growth. Journal of Crystal Growth 212(3–4):480-488.

125. Yani Y, Chow PS, Tan RBH 2011. Molecular Simulation Study of the Effect of Various Additives on Salbutamol Sulfate Crystal Habit. Molecular Pharmaceutics 8(5):1910-1918.

126. Aceves-Hernandez JM, Nicolás-Vázquez I, Aceves FJ, Hinojosa-Torres J, Paz M, Castaño VM 2009. Indomethacin Polymorphs: Experimental and Conformational Analysis. Journal of Pharmaceutical Sciences 98(7):2448-2463.

127. Legendre B, Feutelais Y 2004. Polymorphic and Thermodynamic Study of Indomethacin. Journal of Thermal Analysis & Calorimetry 76(1):255-264.

128. Slavin PA, Sheen DB, Shepherd EEA, Sherwood JN, Feeder N, Docherty R, Milojevic S 2002. Morphological Evaluation of the γ-Polymorph of Indomethacin. Journal of Crystal Growth 237-239(Part 1):300-305.

129. Xiang T-X, Anderson BD 2013. Molecular Dynamics Simulation of Amorphous Indomethacin–Poly(Vinylpyrrolidone) Glasses: Solubility and Hydrogen Bonding Interactions. Journal of Pharmaceutical Sciences 102(3):876-891.

130. Hajratwala B, Dawson J 2006. Kinetics of Indomethacin Degradation I: Presence of Alkali. Journal of Pharmaceutical Sciences 66(1):27-29.

131. Krasowska H 1974. Kinetics of Indomethacin Hydrolysis. Acta Pharm Jugosl 24:193-201.

132. Hancock BC, Parks M 2000. What Is the True Solubility Advantage for Amorphous Pharmaceuticals? Pharmaceutical Research 17(4):397-404.

133. Wassvik CM, Holmén AG, Bergström CAS, Zamora I, Artursson P 2006. Contribution of Solid-State Properties to the Aqueous Solubility of Drugs. European Journal of Pharmaceutical Sciences 29(3-4):294-305.

134. Yoshioka M, Hancock BC, Zografi G 1995. Inhibition of Indomethacin Crystallization in Poly(Vinylpyrrolidone) Coprecipitates. Journal of Pharmaceutical Sciences 84(8):983-986.

135. Andronis V, Zografi G 2000. Crystal Nucleation and Growth of Indomethacin Polymorphs from the Amorphous State. Journal of Non-Crystalline Solids 271(3):236-248.

136. Chen S, Dudhedia MS, Wang Z, Darrington RT, Tamblyn T, Smoliga JA, Jones P-J, Krill SL 2009. Drug-Excipient Complexation in Lipid Based Delivery Systems: An Investigation of the Tipranavir-1,3-Dioctanoylglycerol Complex. Journal of Pharmaceutical Sciences 98(5):1732-1743.

137. Mellaerts R, Aerts A, Caremans TP, Vermant J, Van dMG, Martens JA, Augustijns P 2010. Growth of Itraconazole Nanofibers in Supersaturated Simulated Intestinal Fluid. Molecular Pharmaceutics 7(3):905-913.

138. Femi-Oyewo MN, Spring MS 1994. Studies on Paracetamol Crystals Produced by Growth in Aqueous Solutions. International Journal of Pharmaceutics 112(1):17-28.

139. Chow K, Go J, Mehdizadeh M, Grant D 1984. Modification of Adipic Acid Crystals: Influence of Growth in the Presence of Fatty Acid Additives on Crystal Properties. International Journal of Pharmaceutics 20(1-2):3-24.

140. Davey R, Fila W, Garside J 1986. The Influence of Biuret on the Growth Kinetics of Urea Crystals from Aqueous Solutions. Journal of Crystal Growth 79(1-3, Part 2):607-613.

141. Lee E, Byrn S, Carvajal M 2006. Additive-Induced Metastable Single Crystal of Mefenamic Acid. Pharmaceutical Research 23(10):2375-2380.

142. Qu H, Louhi-Kultanen M, Kallas J 2007. Additive Effects on the Solvent-Mediated Anhydrate/Hydrate Phase Transformation in a Mixed Solvent. Crystal Growth & Design 7:724-729.

143. Grant D, York P 1986. A Disruption Index for Quantifying the Solid State Disorder Induced by Additives or Impurities. II. Evaluation from Heat of Solution. International Journal of Pharmaceutics 28(2-3):103-112.

144. Scholl J, Lindenberg C, Vicum L, Brozio J, Mazzotti M 2007. Precipitation of Alpha L-Glutamic Acid: Determination of Growth Kinetics. Faraday Discussions 136:247-264.

145. Noyes AA, Whitney WR 1897. The Rate of Solution of Solid Substances in Their Own Solutions. Journal of the American Chemical Society 19(12):930-934.

146. Nernst W 1904. Theorie Der Reaktionsgeschwindigkeit in Heterogenen Systemen. Zeitschrift für physikalische Chemie 47(1):52-55.

147. Brunner E 1904. Reaction Velocity in Heterogeneous Systems. Zeitschrift für physikalische Chemie 47:56-102.

148. Mooney KG, Mintun MA, Himmelstein KJ, Stella VJ 1981. Dissolution Kinetics of Carboxylic-Acids. 1. Effect of pH under Unbuffered Conditions. Journal of Pharmaceutical Sciences 70(1):13-22.

149. Higuchi T, Connors K 1965. Phase-Solubility Techniques. Advances in Analytical Chemistry & Instrumentation 4(2):117–212.

150. Higuchi WI, Hiestand EN 1963. Dissolution Rates of Finely Divided Drug Powders I. Effect of a Distribution of Particle Sizes in a Diffusion-Controlled Process. Journal of Pharmaceutical Sciences 52(1):67-71.

151. De Almeida L, Simões S, Brito P, Portugal A, Figueiredo M 1997. Modeling Dissolution of Sparingly Soluble Multisized Powders. Journal of Pharmaceutical Sciences 86(6):726-732.

152. Galli C 2006. Experimental Determination of the Diffusion Boundary Layer Width of Micron and Submicron Particles. International Journal of Pharmaceutics 313(1-2):114-122.

153. Saleki-Gerhardt A, Ahlneck C, Zografi G 1994. Assessment of Disorder in Crystalline Solids. International Journal of Pharmaceutics 101(3):237-247.

154. Ahmed H, Buckton G, Rawlins DA 1996. The Use of Isothermal Microcalorimetry in the Study of Small Degrees of Amorphous Content of a Hydrophobic Powder. International Journal of Pharmaceutics 130(2):195-201.

155. Urakami K, Shono Y, Higashi A, Umemoto K, Godo M 2002. A Novel Method for Estimation of Transition Temperature for Polymorphic Pairs in Pharmaceuticals Using Heat of Solution and Solubility Data. Chemical & Pharmaceutical Bulletin 50(2):263-267.

156. Yu X, Zipp GL, Davidson Iii GWR 1994. The Effect of Temperature and pH on the Solubility of Quinolone Compounds: Estimation of Heat of Fusion. Pharmaceutical Research 11(4):522-527.

157. Hoffman JD 1958. Thermodynamic Driving Force in Nucleation and Growth Processes. The Journal of Chemical Physics 29(5):1192-1193.

158. Ozturk SS, Palsson BO, Dressman JB 1988. Dissolution of Ionizable Drugs in Buffered and Unbuffered Solutions. Pharmaceutical Research 5(5):272-282.

159. Sheng JJ, Sirois PJ, Dressman JB, Amidon GL 2008. Particle Diffusional Layer Thickness in a Usp Dissolution Apparatus II: A Combined Function of Particle Size and Paddle Speed. Journal of Pharmaceutical Sciences 97(11):4815-4829.

160. Hixson AW, Crowell JH 1931. Dependence of Reaction Velocity Upon Surface and Agitation. Industrial & Engineering Chemistry 23(8):923-931.

161. Hintz RJ, Johnson KC 1989. The Effect of Particle Size Distribution on Dissolution Rate and Oral Absorption. International Journal of Pharmaceutics 51(1):9-17.

162. Simöes S, Pereira de Almeida L, Figueiredo M 1996. Testing the Applicability of Classical Diffusional Models to Polydisperse Systems. International Journal of Pharmaceutics 139(1-2):169-176.

163. Moreno E, Zahradnik R, Glazman A, Hwu R 1977. Precipitation of Hydroxyapatite from Dilute Solutions Upon Seeding. Calcified Tissue International 24(1):47-57.

164. Raghavan SL, Schuessel K, Davis A, Hadgraft J 2003. Formation and Stabilisation of Triclosan Colloidal Suspensions Using Supersaturated Systems. International Journal of Pharmaceutics 261(1-2):153-158.

165. Donald RO 1960. Simultaneous Mass Transfer and Equilibrium Chemical Reaction. AIChE Journal 6(2):233-239.

166. Patel DD, Anderson BD 2013. Maintenance of Supersaturation II: Indomethacin Crystal Growth Kinetics Versus Degree of Supersaturation. Journal of Pharmaceutical Sciences 102(5):1544-1553.

167. Higuchi WI, Parrott EL, Wurster DE, Higuchi T 1958. Investigation of Drug Release from Solids .2. Theoretical and Experimental Study of Influences of Bases and Buffers on Rates of Dissolution of Acidic Solids. Journal of the American Pharmaceutical Association 47(5):376-383.

168. Mooney KG, Rodriguez-gaxiola M, Mintun M, Himmelstein KJ, Stella VJ 1981. Dissolution Kinetics of Phenylbutazone. Journal of Pharmaceutical Sciences 70(12):1358-1365.

169. Yin L, Hillmyer MA 2013. Preparation and Performance of Hydroxypropyl Methylcellulose Esters of Substituted Succinates for in Vitro Supersaturation of a Crystalline Hydrophobic Drug. Molecular Pharmaceutics 11(1):175-185.

170. Kistenmacher TJ, Marsh RE 1972. Crystal and Molecular Structure of an Antiinflammatory Agent, Indomethacin, 1-(P-Chlorobenzoyl)-5-Methoxy-2-Methylindole-3-Acetic Acid. Journal of the American Chemical Society 94(4):1340-1345.

171. Frisch HL, Hellman MY, Lundberg JL 1959. Adsorption of Polymers: Polystyrene on Carbon. Journal of Polymer Science 38(134):441-449.

172. Wurster DE, Burke GM, Berg MJ, Veng-Pedersen P, Schottelius DD 1988. Phenobarbital Adsorption from Simulated Intestinal Fluid, U.S.P., and Simulated Gastric Fluid, U.S.P., by Two Activated Charcoals. Pharmaceutical Research 5(3):183-186.

173. Perkel R, Ullman R 1961. The Adsorption of Polydimethylsiloxanes from Solution. Journal of Polymer Science 54(159):127-148.

174. Cohen Stuart MA, Fleer GJ, Bijsterbosch BH 1982. The Adsorption of Poly(Vinyl Pyrrolidone) onto Silica. I. Adsorbed Amount. Journal of Colloid and Interface Science 90(2):310-320.

175. Hild A, Se´quaris J-M, Narres H-D, Schwuger M 1997. Adsorption of Polyvinylpyrrolidone on Kaolinite. Colloids and Surfaces A: Physicochemical and Engineering Aspects 123–124(0):515-522.

176. Kellaway IW, Najib NM 1980. The Adsorption of Hydrophilic Polymers at the Polystyrene-Water Interface. International Journal of Pharmaceutics 6(3–4):285-294.

177. Law SL, Kayes JB 1983. Adsorption of Non-Ionic Water-Soluble Cellulose Polymers at the Solid-Water Interface and Their Effect on Suspension Stability. International Journal of Pharmaceutics 15(3):251-260.

178. Limousin G, Gaudet JP, Charlet L, Szenknect S, Barthès V, Krimissa M 2007. Sorption Isotherms: A Review on Physical Bases, Modeling and Measurement. Applied Geochemistry 22(2):249-275.

179. Fleer GJ, Scheutjens JMHM, Stuart MAC 1988. Theoretical Progress in Polymer Adsorption, Steric Stabilization and Flocculation. Colloids and Surfaces 31:1-29.

180. Somasundaran P, Krishnakumar S 1997. Adsorption of Surfactants and Polymers at the Solid-Liquid Interface. Colloids and Surfaces. A, Physicochemical and Engineering Aspects 123–124:491-513.

181. Kawaguchi M, Takahashi A 1992. Polymer Adsorption at Solid-Liquid Interfaces. Advances in Colloid and Interface Science 37(3–4):219-317.

182. Kramarenko EY, Winkler RG, Khalatur PG, Khokhlov AR, Reineker P 1996. Molecular Dynamics Simulation Study of Adsorption of Polymer Chains with Variable Degree of Rigidity. I. Static Properties. The Journal of Chemical Physics 104(12):4806-4813.

183. Wen H, Morris KR, Park K 2005. Study on the Interactions between Polyvinylpyrrolidone (PVP) and Acetaminophen Crystals: Partial Dissolution Pattern Change. Journal of Pharmaceutical Sciences 94(10):2166-2174.

184. Cohen Stuart MA, Fleer GJ, Scheutjens JMHM 1984. Displacement of Polymers. I. Theory. Segmental Adsorption Energy from Polymer Desorption in Binary Solvents. Journal of Colloid and Interface Science 97(2):515-525.

185. Taylor LS, Zografi G 1998. Sugar–Polymer Hydrogen Bond Interactions in Lyophilized Amorphous Mixtures. Journal of Pharmaceutical Sciences 87(12):1615-1621.

186. Taylor L, Zografi G 1997. Spectroscopic Characterization of Interactions between PVP and Indomethacin in Amorphous Molecular Dispersions. Pharmaceutical Research 14(12):1691-1698.

187. Lyklema J, Fleer GJ 1987. Electrical Contributions to the Effect of Macromolecules on Colloid Stability. Colloids and Surfaces 25(2–4):357-368.

188. Smith JN, Meadows J, Williams PA 1996. Adsorption of Polyvinylpyrrolidone onto Polystyrene Latices and the Effect on Colloid Stability. Langmuir 12(16):3773-3778.

189. Day JC, Robb ID 1980. Conformation of Adsorbed Poly(Vinyl Pyrrolidinone) Studied by Infra-Red Spectrometry. Polymer 21(4):408-412.

190. Cohen Stuart MA, Fleer GJ, Bijsterbosch BH 1982. Adsorption of Poly(Vinyl Pyrrolidone) on Silica. II. The Fraction of Bound Segments, Measured by a Variety of Techniques. Journal of Colloid and Interface Science 90(2):321-334.

191. Esumi K, Takamine K, Ono M, Osada T, Ichikawa S 1993. The Interaction of Poly(Vinylpyrrolidone) and Solid Particles in Ethanol. Journal of Colloid and Interface Science 161(2):321-324.

192. Séquaris JM, Hild A, Narres HD, Schwuger MJ 2000. Polyvinylpyrrolidone Adsorption on Na-Montmorillonite. Effect of the Polymer Interfacial Conformation on the Colloidal Behavior and Binding of Chemicals. Journal of Colloid and Interface Science 230(1):73-83.

193. Sato T, Kohnosu S 1994. Effect of Polyvinylpyrrolidone on the Physical Properties of Titanium Dioxide Suspensions. Colloids and Surfaces A: Physicochemical and Engineering Aspects 88(2–3):197-205.

194. Goodwin DJ, Sepassi S, King SM, Holland SJ, Martini LG, Lawrence MJ 2013. Characterization of Polymer Adsorption onto Drug Nanoparticles Using Depletion Measurements and Small-Angle Neutron Scattering. Molecular Pharmaceutics 10(11):4146-4158.

195. Chen X, Morris KR, Griesser UJ, Byrn SR, Stowell JG 2002. Reactivity Differences of Indomethacin Solid Forms with Ammonia Gas. Journal of the American Chemical Society 124(50):15012-15019.

196. Xie S, Poornachary SK, Chow PS, Tan RBH 2010. Direct Precipitation of Micron-Size Salbutamol Sulfate: New Insights into the Action of Surfactants and Polymeric Additives. Crystal Growth & Design 10(8):3363-3371.

197. Stuart MAC, Waajen FHWH, Cosgrove T, Vincent B, Crowley TL 1984. Hydrodynamic Thickness of Adsorbed Polymer Layers. Macromolecules 17(9):1825-1830.

Vita

Dhaval Patel

Education:

Master of Science (Pharmaceutical Sciences) 2002
St. John's University, NY.
Thesis: Highly Swellable and Biodegradable PEG-Dextran Hydrogel as an Oral Controlled Drug Delivery System.

Bachelors in Pharmacy 1999
Maharaja Sayajirao University, Vadodara, India

Professional Experience:

Bristol-Myers Squibb Inc., New Brunswick, NJ 2011-Present
Senior Research Investigator I-Research Investigator II

University of Kentucky, Lexington, KY 2006-2011
Research Assistant-Teaching Assistant

GlaxoSmithKline Inc., Research Triangle Park, NC 2001-2006
Scientist-Associate Scientist

Forest Laboratories Inc., Inwood, NY 2001-2001
Research Scientist-Summer Intern

St. John's University, Jamaica, NY 1999-2001
Research Assistant-Teaching Assistant

Honors & Awards:

2010 Selected for 2010 The Globalization of Pharmaceutics Education Network (GPEN) Annual Meeting Oral Symposium
2010 Drug Development Division Representative, AAPS Student Chapter, University of Kentucky
2009 Boehringer-Ingelheim Research Fellowship
2009 College of Pharmacy Representative, Graduate Student Congress, University of Kentucky
2008 University of Kentucky Graduate School Fellowship
2008 Magna cum Laude, The National Scholars Honor Society
2008 Graduate Program Committee Representative, AAPS Student Chapter, University of Kentucky
2003 Bronze Award, GlaxoSmithKline Recognition for Excellence in Science Award
2001 National Dean's Award (US)
1993 National Merit Scholarship, Govt. of India

1993 Top Ten Students of Vadodara (Baroda) City, Gujarat State Board Secondary Examination, India

Publications:

Dhaval Patel and Bradley Anderson. Adsorption of Polyvinylpyrrolidone and Its Impact on Maintenance of Aqueous Supersaturation of Indomethacin via Crystal Growth Inhibition. ***Journal of Pharmaceutical Sciences***, 2015, E-Published (In Press).

Ajit S Narang, Sherif Badawy, Qingmei Ye, **Dhaval Patel**, Maria Vincent, Krishnaswamy Raghavan, Yande Huang, Aaron Yamniuk, Balvinder Vig, John Crison, George Derbin, Yan Xu, Antonio Ramirez, Michael Galella, Frank A Rinaldi. Role of Self-Association and Supersaturation in Oral Absorption of a Poorly Soluble Weakly Basic Drug. ***Pharmaceutical Research***, 2015, 32 (8): 2579-2594.

Dhaval Patel and Bradley Anderson. Effect of Precipitation Inhibitors on Indomethacin Supersaturation Maintenance: Mechanisms and Modeling. ***Molecular Pharmaceutics***, 2014, 11 (5): 1489-1499.

Dhaval Patel and Bradley Anderson. Maintenance of Supersaturation II: Indomethacin Crystal Growth Kinetics Versus Degree of Supersaturation. ***Journal of Pharmaceutical Sciences***, 2013, 102 (5): 1544–1553.

Neil R Mathias, Yan Xu, **Dhaval Patel**, Michael Grass, Brett Caldwell, Casey Jager, Jim Mullin, Luke Hansen, John Crison, Amy Saari, Christoph Gesenberg, John Morrison, Balvinder Vig, Krishnaswamy Raghavan. Assessing the Risk of pH-Dependent Absorption for New Molecular Entities: A Novel In Vitro Dissolution Test, Physicochemical Analysis, and Risk Assessment Strategy. ***Molecular Pharmaceutics***, 2013, 10 (11): 4063-4073.

Dhaval Patel, Vijay Joguparthi, Zeren Wang, and Bradley Anderson. Maintenance of Supersaturation I: Indomethacin Crystal Growth Kinetic Modeling Using an Online Second Derivative Ultraviolet Spectroscopic Method, ***Journal of Pharmaceutical Sciences***, 2011, 100(7):2623-2641.